

**THE GEOCHEMICAL EVOLUTION OF TWO HIGH ARCTIC LAKES
AND THE RECURRENCE OF ELEVATED BOTTOM WATER
CONDUCTIVITY**

by

Maia Rose Somers

A thesis submitted to the Department of Geography and Planning

In conformity with the requirements for

the degree of Master of Science

Queen's University

Kingston, Ontario, Canada

(February 28, 2023)

Copyright ©Maia Rose Somers, 2023

Abstract

This study investigates the long-term physical and chemical changes in High Arctic lakes to understand the source of seasonally recurring elevated bottom water conductivity (EBWC) (in the bottom 0.5-2.0 m of the lake). To achieve this, two separate investigations were carried out on two cold-monomictic lakes at the Cape Bounty Arctic Watershed Observatory (CBAWO), Nunavut, Canada. More specifically, these studies aim to: (1) investigate and compare the water column chemistry of these lakes to identify the source of emerging lake bottom groundwater signatures; and (2) delineate seasonal changes in physical processes in one of these lakes to determine mechanisms driving the occurrence of EBWC. The first study focused on the chemical analysis of major dissolved ions collected at fixed water column depths. Dissolved ions reveal that both lakes have experienced an unprecedented decadal (2006-2019) shift in water column geochemistry, with ionic ratios transitioning to increasing SO_4^{2-} ion enrichments observed in catchment rivers. In contrast, the ionic composition of EBWC (<30 m depth) is distinctly different from the rapidly changing water column chemistry, suggesting a separate source of water with a geochemical signature more similar to relic late-glacial marine water. These results suggest that lake bottom sediment porewater is the primary source of EBWC. The second study continued the investigation of EBWC through seasonal analysis of a 2.5-year continuous time series of specific conductivity (SpC), temperature, and density anomaly collected in the deepest region of West Lake (unofficial name) at the CBAWO (32 m depth). The SpC record indicates that under-ice accumulation of EBWC not only occurs in late winter but in early winter, immediately following the complete formation of surficial lake ice. The mechanisms generating EBWC are controlled by patterns in lake ice phenology and occur when the lake is ice covered. These mechanisms include late winter (before the onset of ice melt), radiatively driven convection, and subtle early winter and water column circulation driven by bottom sediment heat flux (following ice-on). Therefore, EBWC occurs through the diffusion of sediment pore-water accumulating in the lake bottom through the downward movement of dense currents driven by under-ice processes.

Co-Authorship

This thesis is presented in manuscript style in accordance with the style outlined by the School of Graduate Studies and Research. I am the primary author responsible for analysis and writing of all manuscripts in this thesis. S.F. Lamoureux and C.R. Omelon provided guidance and revisions on all chapters.

Various field crews collected water column profiles and water samples from lakes at Cape Bounty between 2006 and 2019. M. J. Lafrenière provided data collected from Cape Bounty rivers between 2006 and 2017. I compiled and analyzed all major ion geochemical data for Chapter 3. A. Normandeau collected swath bathymetric sonars in the field and provided bathymetric lake data displayed in Chapter 3. Lake bottom mooring data presented in Chapter 4 was collected by S.F. Lamoureux.

Acknowledgements

I would like to thank my supervisors Dr. Christopher Omelon, and Dr. Scott Lamoureux. I certainly would not be here without your guidance, edits, and support throughout this project. I am very grateful to have had the opportunity to gain access to the knowledge and passion you both have on the Arctic. Thank you for allowing me the time and space to complete this process in my own way.

Thank you to my committee members, Dr. John Smol, Dr. Neal Scott, and Dr. Paul Treitz for your input and suggestions which helped shape this thesis. This project would not have been possible without the funding assistance from NSERC, NSTP, PCSP, and ArcticNet. Additional thanks to all those who have completed field work on lakes and rivers at Cape Bounty. Without your data collection, hard work and planning, I would not have had access to the data that propelled this project into existence and kept it progressing forward.

To my family, thank you for your unwavering support, encouragement, and giving me the opportunity to grow up surrounded by nature. To Erin you are my hero, thank you for encouraging me to follow my dreams. Destiny and Skylar, thank you for always checking in with a daily dose of laughter and cheering me on through each step in this process. Most importantly, to Ben, your logic, joy, and cooking keep me moving forward every day.

Table of Contents

Abstract.....	ii
Co-Authorship.....	iii
Acknowledgements.....	iv
List of Figures.....	ix
List of Tables.....	xi
List of Abbreviations.....	xii
Chapter 1 Introduction.....	1
1.1 Research Objectives.....	2
1.2 Study Area.....	2
1.3 References.....	6
Chapter 2 Literature Review.....	10
2.1 Hydrology in Cold Regions.....	10
2.2 Polar Lakes.....	12
2.2.1 Water Balance in Polar Lakes.....	13
2.2.2 The Physics of Polar Lakes.....	14
2.2.3 Ice Phenology of Polar Lakes.....	16
2.2.3.1 Formation of Ice on Polar Lakes.....	16
2.2.3.2 Ice Melt on Polar Lakes.....	18
2.2.4 Hydrodynamics of Polar Lakes.....	18
2.2.4.1 Physical Classifications of Lakes.....	19
2.2.4.2 Hydrodynamics of Cold Monomictic Lakes.....	19
2.3 Groundwater in Polar Regions.....	24
2.3.1 Permafrost Distribution and Structure.....	24
2.3.2 Groundwater Classifications in Permafrost.....	27
2.3.3 Groundwater in Continuous Permafrost Regions.....	28
2.3.4 Taliks.....	29
2.3.4.1 Talik Classification.....	29
2.3.5 Taliks and Polar Lakes.....	30
2.4 Sampling and Measurement Methods.....	31
2.4.1 Methods in Polar Lakes.....	31
2.4.2 Methods for Groundwater Associated with Polar Lakes.....	34

2.5 The Coastal High Arctic Setting	35
2.5.1 Coastal High Arctic Lake Formation	35
2.5.2 Groundwater Associated with Coastal High Arctic Lakes.....	38
2.6 The Importance of Studying High Arctic lakes	38
2.7 References.....	40
Chapter 3 Investigating multi-year (2006-2019) ionic concentrations to characterize groundwater signatures occurring in two coastal High Arctic lakes.....	
3.1 Abstract.....	53
3.2 Introduction.....	53
3.3 Study Area and Background	55
3.3.1 Climate and Permafrost.....	55
3.3.2 Geology.....	57
3.3.3 Hydrology	57
3.4 Methods.....	58
3.4.1 Water Column.....	58
3.4.2 River Flux	62
3.5 Results.....	62
3.5.1 Water Column Profiles.....	62
3.5.2 Water Column Ion Concentrations and Ratios.....	64
3.5.3 Temporal Trends in Ion Concentrations	67
3.5.4 River Ion Concentration Temporal Trends	72
3.6 Discussion.....	74
3.6.1 Processes Related to Overall Water Column Trends	75
3.6.2 Processes and Origins of Elevated Bottom Water Conductivity.....	80
3.6.2.1 Sediment Pore Water Diffusion	82
3.6.2.2 Talik Porewater Migration	83
3.6.2.3 Sub-permafrost and intra-permafrost zone groundwater inputs.....	85
3.6.2.4 The most probable source and mechanism generating the EBWC	86
3.6.3 Environmental Change.....	88
3.7 Conclusions.....	89
3.8 References.....	91
Chapter 4 Investigating the physico-chemical response to seasonal changes in a High Arctic monomictic lake at Cape Bounty Arctic Watershed Observatory, Melville Island, Nunavut	
	98

4.1 Abstract.....	98
4.2 Introduction.....	99
4.3 Study Area	101
4.4 Methods.....	104
4.4.1 Ice Phenology.....	104
4.4.2 Lake Mooring.....	105
4.3.5 Wavelet Analysis	107
4.5 Results.....	108
4.5.1 Surface Ice Phenology	108
4.5.2 Hydrometeorology	110
4.5.2.1 Air Temperature and Precipitation.....	110
4.5.2.2 West River Discharge and Suspended Sediment Load	112
4.5.3 Water Column Conditions	112
4.5.4 Lake Mooring Patterns.....	116
4.5.4.1 Bottom Specific Conductivity.....	117
4.5.4.2 Bottom Temperature	118
4.5.4.3 Bottom Density Anomaly	119
4.5.4.4 Wavelet Analysis of Bottom Data.....	119
4.6 Discussion	124
4.6.1 Phase 1: Late Winter	126
4.6.2 Phase 2: Spring-Summer.....	130
4.6.3 Phase 3: Early Winter	131
4.6.4 Phase 4: Mid-Winter	135
4.7 Conclusion	138
4.8 References.....	140
Chapter 5 Conclusions and Future Work.....	146
5.1 Conclusions.....	146
5.2 Impact of Lake Size and Morphology on Biology.....	147
5.3 Future Work.....	149
5.4 References.....	150
Appendix A Water Column Casts.....	152
Appendix B Lake Phenology	153
Appendix C Linked Data	154

Appendix D Active Layer Data 155

List of Figures

Figure 2.1: Cold region hydrology.....	11
Figure 2.2: The relationship between temperature and density.	15
Figure 2.3: Potential hydrologic interactions occurring across various permafrost landscapes	25
Figure 2.4 The typical cryotic structure of the thermal regime from the surface to depth in a permafrost landscape unimpeded by features that may impact temperature at depth	27
Figure 2.5: A water column profile displaying the chemical data collected from the surface to the lake bottom.	33
Figure 2.6: Postulated evolutionary sequence for coastal high latitude landscapes, embayments, and lakes	37
Figure 3.1: The study area map of the Cape Bounty Arctic Watershed Observatory (CBAWO) on Melville Island in the Canadian Arctic Archipelago	56
Figure 3.2: Typical specific conductivity profiles and sampling depths in East and West lakes.	61
Figure 3.3: May and August 2018 Water column casts collected SpC from West and East lakes	63
Figure 3.4 Ratios of sulphate to chloride dissolved ion concentrations through the water column.....	66
Figure 3.5: 2006-2019 mean annual ion concentrations of the column and bottom water	68
Figure 3.6: 2006-2019 mean annual ion concentration ratios of bottom water to column water	69
Figure 3.7: Ratio:ratio trend analysis for ion concentrations over time in the CBAWO lakes.....	71
Figure 3.8: Total annual flux (Mg) of major anions (Cl^- , SO_4^{2-}) and cations (Na^+ , Mg^{2+} , Ca^{2+} , K^+) for West River and East rivers.....	73
Figure 3.9: Percentages of dissolved ion concentrations in lakes and rivers across the Canadian High Arctic	77

Figure 3.10: Displaying mean annual $\text{SO}_4^{2-}:\text{Cl}^-$ ratios at the CBAWO.....	79
Figure 3.11: Three possible mechanisms for compositional differences in elevated conductivity bottom water (EBWC) of West Lake at the CBAWO	81
Figure 4.1: Study area maps of West Lake at the CBAWO.....	103
Figure 4.2: The CTD mooring sampling design in West Lake	106
Figure 4.3: Temporal trends in surface ice phenology and active layer freeze up near West Lake between 2012 and 2019.....	109
Figure 4.4: Terrestrial and lake data collected at the CBAWO during the study period	113
Figure 4.5: Profiles of temperature and specific conductivity from mid-lake station in West Lake.	115
Figure 4.6: Annual patterns in the lake bottom specific conductivity, temperature, and density collected by a lake-bottom mooring.....	116
Figure 4.7: The wavelet power spectrum for the West Lake bottom specific conductivity, temperature, and density anomaly	121
Figure 4.8: Wavelet power spectrum for 2017 lake bottom SpC data displaying oscillations found in Phase 1 and Phase 3	122
Figure 4.9: The cross-coherence spectrum of solar radiation and lake bottom specific conductivity	123
Figure 4.10: Four phases defined in lake bottom mooring data.....	125
Figure 4.11: The mechanisms driving the occurrence of elevated bottom water conductivity in West Lake	129
Figure 4.12: The stationary lake bottom mooring and EBWC	134

List of Tables

Table 3.1: Characteristics of East and West Lakes at CBAWO.	58
Table 3.2: CTD measurements and water column sampling dates for lake water column profiles.	60
Table 3.3: Ion concentrations from vertical casts collected in May and August 2018 from middle stations in West and East Lakes at CBAWO.	65
Table 4.1: Air temperature and rainfall data from West Met meteorological station	111

List of Abbreviations

ALD	Active layer detachment
asl	Above sea level
B:C	Bottom to column water ratios
BP	Before Present
CAA	Canadian Arctic Archipelago
CBAWO	Cape Bounty Arctic Watershed Observatory
CMWC	Convectively mixed water column
CTD	Conductivity, temperature, depth instrument used in limnology and oceanography
DO	Dissolved oxygen
EBWC	Elevated bottom water conductivity
ICS	Ion Chromatography System
IIS	Innuitian Ice Sheet
LGM	Last glacial maximum
LIS	Laurentide ice sheet
Main Met	Main meteorological station at Cape Bounty Arctic Watershed Observatory
RBR	Richard Branker Research Inc.
RDC	Radiatively Driven Convection
SpC	Specific conductivity
SSC	Suspended sediment concentration
UNESCO	United Nations Educational, Scientific and Cultural Organization
West Met	West meteorological Station at Cape Bounty Arctic Watershed Observatory

Chapter 1

Introduction

There is an abundance of lakes in the High Arctic contributing to the hydrology of cold regions. Arctic lakes are studied for many scientific reasons, including paleolimnology and paleoecology, biogeochemical cycling, water quality and security, and, more recently, their response to climate change (Bégin et al., 2021; Lafrenière & Lamoureux, 2013; Lyons & Finlay, 2008; Smol & Douglas, 2007). A notable feature of High Arctic lakes is the persistent presence of ice cover resulting from long periods of extreme cold and little to no solar energy inputs. This polar climate also results in the development of thick continuous permafrost in the region, which is generally viewed as an impermeable barrier to deeper water movement, effectively reducing groundwater recharge, flow rates, storage capacity, and interaction with surface waters (French, 2018). However, recent studies provide evidence that, in some geologic settings, it is possible for groundwater-surface water connections to occur in landscapes underlain by thick continuous permafrost in the Canadian Arctic Archipelago (CAA) (Grasby et al., 2014; Omelon et al., 2006; Pollard et al., 1999; Pollard, 2005). Evidence for groundwater seepage has also been found to occur in lakes underlain by continuous permafrost in Western Greenland (Johansson et al., 2015), and in the CAA on Little Cornwallis Island (Ouellet et al., 1989) and Melville Island (Dugan et al., 2012; Harasyn, 2017), the latter identifying the presence of elevated bottom water conductivity (EBWC) and laying the foundational work for the material presented in this thesis.

While continuous permafrost dominates many aspects of High Arctic settings, lakes present a compelling example of external features that influence the thermal regime of frozen ground. If lakes are sufficiently large, unfrozen zones, known as taliks, can form to provide subsurface pathways for water migration, creating a hydrologic connection between surface water and groundwater (French, 2018). Due to a warming climate, current and future permafrost thaw will likely increase groundwater connectivity with surface waters such as rivers or lakes (Lecher, 2017).

High Arctic lakes are also highly sensitive to changes in climate because their physical and chemical properties are largely controlled by ice cover and the surrounding permafrost (Adrian et al., 2009; Sharma et al., 2021). Understanding the connections between the hydrologic cycle of High Arctic lakes and the cryosphere will become increasingly important to understand how water quality may change and subsequently impact water resources in the future as climate warming continues. However, much of the hydrologic research in the High Arctic has focused on surface water dynamics, with lesser attention to groundwater (Cochand et al., 2019). Recent studies have shown a reduction in shallow permafrost resulting from the increased depth of seasonally thawed ground due to warming temperatures (Lafrenière & Lamoureux, 2019; Lamhonwah et al., 2017). Thawing permafrost has been shown to increase the concentrations of nutrients and ions in underflows due to increasing the interactions between surface water and groundwater (Lamontagne-Hallé et al., 2018). It is predicted that these interactions will likely contribute to changes in the physical and chemical water column properties of downstream lakes (Lafrenière & Lamoureux, 2019; Roberts et al., 2017; Walvoord et al., 2012).

1.1 Research Objectives

This research builds upon previous work by developing a deeper understanding of the interactions between High Arctic lakes and groundwater, examining physical and chemical patterns within lakes, and determining the mechanisms that govern them. More specifically, the goals of this study are to:

- (1) Investigate and compare the water column chemistry in two High Arctic lakes to understand the source of emerging lake bottom groundwater signatures; and
- (2) Delineate seasonal changes in the physical processes of a High Arctic lake to determine the mechanism(s) driving the occurrence of EBWC.

1.2 Study Area

The lakes chosen for this study, East Lake and West Lake (unofficial names), are situated within paired watersheds located at the Cape Bounty Arctic Watershed Observatory (CBAWO) (74°50'N,

109°30'W). The CBAWO, located in the Canadian High Arctic on the south-central coast of Melville Island, Nunavut, is characterized by polar semi-desert conditions with very cold, dry winters and cool summers. Mean annual temperatures are -14.8°C ($\pm 1.3^{\circ}\text{C}$) (Beel et al., 2021). Only in June, July, and August are mean monthly air temperatures above 0°C . Annual precipitation is low, with the majority occurring as snowfall.

The CBAWO comprises hilly terrain with gentle slopes and up to 100 m of relief. During the late Wisconsinan glacial period, the area was covered by the Laurentide Ice Sheet (LIS) during the Last Glacial Maximum (LGM) (England et al., 2006) dated 19000-22000 BP (before present) from marine sediments (Yokoyama et al., 2000). The lake basins are morphologically similar, and are located approximately 5 m above sea level, and would have been located below the Holocene sea level during deglaciation. The retreat of LIS delivered a flux of meltwater to the oceans, which increased sea levels, submerging an estimated 116-123 m of land below sea level (Peltier, 2002). Sediment records indicate both lake basins are Holocene in origin and similar in terms of sediment accumulation. Lake bottom sediments extend 2-8 m below the lake bottom and consist of glacio-marine massive muds gradually transitioning upwards to laminated sediments (Normandeau et al., 2016). The transition from marine to terrestrial influence resulted from isostatic rebound which caused the gradual emergence of the lake basins from the sea estimated by to occur between 4197-1763 yr. BP (Cuyen et al., 2011).

The lakes at the CBAWO are currently situated within a landscape shaped by the periglacial processes of the Holocene. East and West lakes are approximately 1.0 km^2 and 30 m deep, with morphologically similar lake basins. West Lake has a surface area of 1.4 km^2 , a mean depth of 15.3 m, and a maximum depth of 34 m. East Lake is slightly larger, with a surface area of 1.6 km^2 , a mean depth of 13.3 m, and a maximum depth of 31 m (Stewart & Lamoureux, 2011). Both lakes are ice-covered for 9-11 months of the year, with a maximum ice thickness of 1.8-2.0 m. Seasonal inflows and outflows are active during the melt season, with snowmelt and runoff beginning in June that diminishes after several weeks.

The geology of the area consists of Devonian-aged shallow-marine shales and deltaic quartzose sandstones of the Weatherall Formation and fluvial-deltaic terrigenous quartz sandstone and siltstone of the Hecla Bay Formation (Harrison, 1995). These two units are separated by a geologic boundary located directly beneath a lithologic unconformity (~290° strike) dipping 15° to the southwest (Harasyn, 2017). This bedrock is overlain by pre-late Wisconsinan glacial till with both lacustrine and oceanic sources (England et al., 2009). The area is underlain by continuous permafrost extending 500+ meters below the surface, thinning out near the shoreline (Judge, 1973). At the surface, active layer thaw begins in June, and the uppermost portion of the ground thaws to depths between 0.5 to 1.0 m to the top of the permafrost. The mean annual near-surface permafrost measured at a depth of seven metres from a borehole located at the CBAWO campsite 50 m from the shore of West Lake, and collected at two-hour intervals continuously between June 2012 and July 2019 was -11.1 °C.

Previous studies on the lakes at the CBAWO have detected the presence of EBWC compared to the overlying column water (Dugan, 2010; Harasyn, 2017). EBWC is more commonly present in West Lake compared to East Lake and occurs in the deepest regions of the water column (the bottom 2.0-1.5 metres), specifically in late-winter (i.e., May-June) and is periodically flushed out in years with sufficiently high suspended sediment concentration (SSC) in river inflows during the melt season (Harasyn, 2017; Lewis et al., 2018). Through a preliminary analysis of the physical and chemical composition of the CBAWO lakes, Harasyn (2017) proposed groundwater as the source of EBWC.

This study builds upon these previous investigations in two ways: first, through the analysis of over a decade of lake and river geochemistry data, delineating temporal changes between the composition (i.e., ionic ratios of major dissolved ions) of bottom and column waters in both lakes, it can be concluded that EBWC is sourced not from groundwater but from lake sediment pore waters; second, the examination of time series data collected from a bottom mooring in West Lake resulted in the identification of the different physical processes responsible for annual occurrences of EBWC. Combined, this work provides new knowledge about the chemical evolution of these lakes as well as mechanisms driving lake water

circulation and enhances our understanding of the interactions between surface water, groundwater, and terrestrial processes in a High Arctic setting.

1.3 References

- Adrian, R., O'Reilly, C. M., Zagarese, H., Baines, S. B., Hessen, D. O., Keller, W., Livingstone, D. M., Sommaruga, R., Straile, D., van Donk, E., Weyhenmeyer, G. A., & Winder, M. (2009). Lakes as sentinels of climate change. *Limnology and Oceanography*, *54*(6 PART 2), 2283–2297.
https://doi.org/10.4319/lo.2009.54.6_part_2.2283
- Beel, C. R., Heslop, J. K., Orwin, J. F., Pope, M. A., Schevers, A. J., Hung, J. K. Y., Lafrenière, M. J., & Lamoureux, S. F. (2021). Emerging dominance of summer rainfall driving High Arctic terrestrial-aquatic connectivity. *Nature Communications*, *12*(1448). <https://doi.org/10.1038/s41467-021-21759-3>
- Bégin, P. N., Tanabe, Y., Rautio, M., Wauthy, M., Laurion, I., Uchida, M., Culley, A. I., Warwick, &, & Vincent, F. (2021). Water column gradients beneath the summer ice of a High Arctic freshwater lake as indicators of sensitivity to climate change. *Scientific Reports*, *11*, 2868.
<https://doi.org/10.1038/s41598-021-82234-z>
- Cochand, M., Molson, J., & Lemieux, J. M. (2019). Groundwater hydrogeochemistry in permafrost regions. *Permafrost and Periglacial Processes*, *30*(2), 90–103. <https://doi.org/10.1002/ppp.1998>
- Dugan, H.A. (2010). *Long-term development and recent dynamics of High Arctic coastal basins*. MSc Thesis, Dept. of Geography and Planning, Queen's University, Kingston, ON.
- Dugan, H. A., Gleeson, T., Lamoureux, S. F., & Novakowski, K. (2012). Tracing groundwater discharge in a High Arctic lake using radon-222. *Environmental Earth Sciences*, *66*, 1385–1392.
<https://link.springer.com/article/10.1007/s12665-011-1348-6>
- England, J., Atkinson, N., Bednarski, J., Dyke, A. S., Hodgson, D. A., & Ó Cofaigh, C. (2006). The Inuitian Ice Sheet: configuration, dynamics and chronology. *Quaternary Science Reviews*, *25*(7–8), 689–703. <https://doi.org/10.1016/J.QUASCIREV.2005.08.007>
- England, J. H., Furze, M. F. A., & Doupe, J. P. (2009). Revision of the NW Laurentide Ice Sheet: implications for paleoclimate, the northeast extremity of Beringia, and Arctic Ocean sedimentation. *Quaternary Science Reviews*, *28*, 1573–1596.

- French, H. M. (2018). *The Periglacial Environment* (4th ed.). John Wiley & Sons Ltd.
<https://doi.org/10.2307/j.ctt1w6tb9v.3>
- Grasby, S. E., Proemse, B. C., & Beauchamp, B. (2014). Deep groundwater circulation through the High Arctic cryosphere forms Mars-like gullies. *Geology*, *42*(8), 651–654.
<https://doi.org/10.1130/G35599.1>
- Harasyn, M. L. (2017). *Detecting the Presence of Localized Groundwater Inputs into High Arctic Lakes*. BSc Thesis, Dept. of Geography and Planning, Queen's University, Kingston, ON.
- Harrison, J. C. (1995). *Melville Island's Salt-Based Fold Belt, Arctic Canada*. Geological Survey of Canada.
- Johansson, E., Gustafsson, L. G., Berglund, S., Lindborg, T., Selroos, J. O., Claesson Liljedahl, L., & Destouni, G. (2015). Data evaluation and numerical modeling of hydrological interactions between active layer, lake and talik in a permafrost catchment, Western Greenland. *Journal of Hydrology*, *527*, 688–703. <https://doi.org/10.1016/j.jhydrol.2015.05.026>
- Judge, A. (1973). The prediction of permafrost thickness. *Canadian Geotechnical Journal*, *10*(1), 313–321.
- Lafrenière, M. J., & Lamoureux, S. F. (2013). Thermal perturbation and rainfall runoff have greater impact on seasonal solute loads than physical disturbance of the active layer. *Permafrost and Periglacial Processes*, *24*(3), 241–251. <https://doi.org/10.1002/ppp.1784>
- Lafrenière, M. J., & Lamoureux, S. F. (2019). Effects of changing permafrost conditions on hydrological processes and fluvial fluxes. *Earth-Science Reviews*, *191*, 212–223.
<https://doi.org/10.1016/j.earscirev.2019.02.018>
- Lamhonwah, D., Lafrenière, M. J., Lamoureux, S. F., & Wolfe, B. B. (2017). Multi-year impacts of permafrost disturbance and thermal perturbation on High Arctic stream chemistry. *Arctic Science*, *3*(2), 254–276. <https://doi.org/10.1139/as-2016-0024>
- Lamontagne-Hallé, P., McKenzie, J. M., Kurylyk, B. L., & Zipper, S. C. (2018). Changing groundwater discharge dynamics in permafrost regions. *Environmental Research Letters*, *13*(8).
<https://doi.org/10.1088/1748-9326/aad404>

- Lecher, A. L. (2017). Groundwater discharge in the Arctic: A review of studies and implications for biogeochemistry. *Hydrology*, 4(3), 1–16. <https://doi.org/10.3390/hydrology4030041>
- Lewis, T., Lamoureux, S. F., Normandeau, A., & Dugan, H. A. (2018). Hyperpycnal flows control the persistence and flushing of hypoxic high conductivity bottom water in a High Arctic lake. *Arctic Science*, 4, 25–41. <https://doi.org/10.1139/as-2017-0022>
- Lyons, W. B., & Finlay, J. C. (2008). Biogeochemical processes in high latitude lakes and rivers. In W. F. Vincent & J. Laybourn-Parry (Eds.), *Polar Lakes and Rivers : Limnology of Arctic and Antarctic Aquatic Ecosystems* (pp. 119–136). Oxford University Press.
- Normandeau, A., Lamoureux, S. F., Lajeunesse, P., & Francus, P. (2016). Sediment dynamics in paired High Arctic lakes revealed from high-resolution swath bathymetry and acoustic stratigraphy surveys. *Journal of Geophysical Research: Earth Surface*, 121, 1676–1696. <https://doi.org/10.1002/2013JF002871>.
- Omelon, C. R., Pollard, W. H., & Andersen, D. T. (2006). A geochemical evaluation of perennial spring activity and associated mineral precipitates at Expedition Fjord, Axel Heiberg Island, Canadian High Arctic. *Applied Geochemistry*, 21(1), 1–15. <https://doi.org/10.1016/j.apgeochem.2005.08.004>
- Ouellet, M., Dickman, M., Bisson, M., & Pagé, P. (1989). Physico-chemical characteristics and origin of hypersaline meromictic Lake Garrow in the Canadian high Arctic. *Hydrobiologia*, 172(1), 215–234. <https://doi.org/10.1007/BF00031624>
- Peltier, W. R. (2002). Global glacial isostatic adjustment: Palaeogeodetic and space-geodetic tests of the ICE-4G (VM2) model. *Journal of Quaternary Science*, 17(5–6), 491–510. <https://doi.org/10.1002/jqs.713>
- Pollard, W. H. (2005). Icing processes associated with high Arctic perennial springs, Axel Heiberg Island, Nunavut, Canada. *Permafrost and Periglacial Processes*, 16(1), 51–68. <https://doi.org/10.1002/ppp.515>
- Pollard, W., Omelon, C., Andersen, D., & McKay, C. (1999). Perennial spring occurrence in the Expedition Fjord area of western Axel Heiberg Island, Canadian High Arctic. *Canadian Journal of Earth Sciences*, 36, 105–120.

- Roberts, K. E., Lamoureux, S. F., Kyser, T. K., Muir, D. C. G., Lafrenière, M. J., Iqaluk, D., Pieńkowski, A. J., & Normandeau, A. (2017). Climate and permafrost effects on the chemistry and ecosystems of High Arctic Lakes. *Scientific Reports*, 7(1), 1–8. <https://doi.org/10.1038/s41598-017-13658-9>
- Sharma, S., Richardson, D. C., Woolway, R. I., Imrit, M. A., Bouffard, D., Blagrove, K., Daly, J., Filazzola, A., Granin, N., Korhonen, J., Magnuson, J., Marszelewski, W., Matsuzaki, S. I. S., Perry, W., Robertson, D. M., Rudstam, L. G., Weyhenmeyer, G. A., & Yao, H. (2021). Loss of ice cover, shifting phenology, and more extreme events in Northern Hemisphere lakes. *Journal of Geophysical Research: Biogeosciences*, 126(10). <https://doi.org/10.1029/2021JG006348>
- Smol, J. P., & Douglas, M. S. V. (2007). From controversy to consensus: Making the case for recent climate change in the Arctic using lake sediments. *Frontiers in Ecology and the Environment*, 5(9), 466–474. <https://doi.org/10.1890/060162>
- Stewart, K. A., & Lamoureux, S. F. (2011). Connections between river runoff and limnological conditions in adjacent High Arctic lakes: Cape Bounty, Melville Island, Nunavut. *Arctic*, 64(2), 169–182.
- Walvoord, M. A., Voss, C. I., & Wellman, T. P. (2012). Influence of permafrost distribution on groundwater flow in the context of climate-driven permafrost thaw: Example from Yukon Flats basin, Alaska, United States. *Water Resources Research*, 48(7). <https://doi.org/10.1029/2011WR011595>
- Woo, M. (2012). Cold lakes. In *Permafrost Hydrology* (pp. 305–346). Springer-Verlag Berlin Heidelberg. https://doi.org/10.1007/978-3-642-23462-0_7
- Yokoyama, Y., Lambeck, K., & Deckker, P. D. (2000). Timing of last glacial maximum from observed sea level minima. *Nature*, 406, 713–716.

Chapter 2

Literature Review

2.1 Hydrology in Cold Regions

The hydrologic cycle, which considers the movement and storage of water on Earth, includes atmospheric, surface, and subsurface components. In the High Arctic, this cycle is impacted by a climate characterized by a weak diurnal but strong seasonal pattern (French, 2018). Most notable is solar radiation, with long periods of little to no energy inputs, extremely cold temperatures, and precipitation as snowfall during winter. This results in effectively halting the hydrologic cycle as the ground and all but larger surface water bodies freeze completely.

The above setting contrasts with the short summer season, characterized by 24-hour sunlight and air temperatures above 0°C. Melting snow initially travels as overland flow due to the underlying frozen ground, with progressive warming resulting in activation of the larger hydrologic cycle observed as initiation of river flow, lakes becoming ice free, precipitation as rainfall, ground thawing, and movement of water along surficial and shallow subsurface pathways. Beyond this strong seasonality in the hydrologic cycle is the presence of permafrost, which redefines hydrology in cold regions by acting as an aquitard, primarily controlling the flux, flow paths, and distribution of water (Woo, 2012b) (Figure 2.1). Where permafrost is extensive and continuous, hydrologic activity in summer is restricted to only the seasonally thawed shallow subsurface settings (Yang et al., 2021).

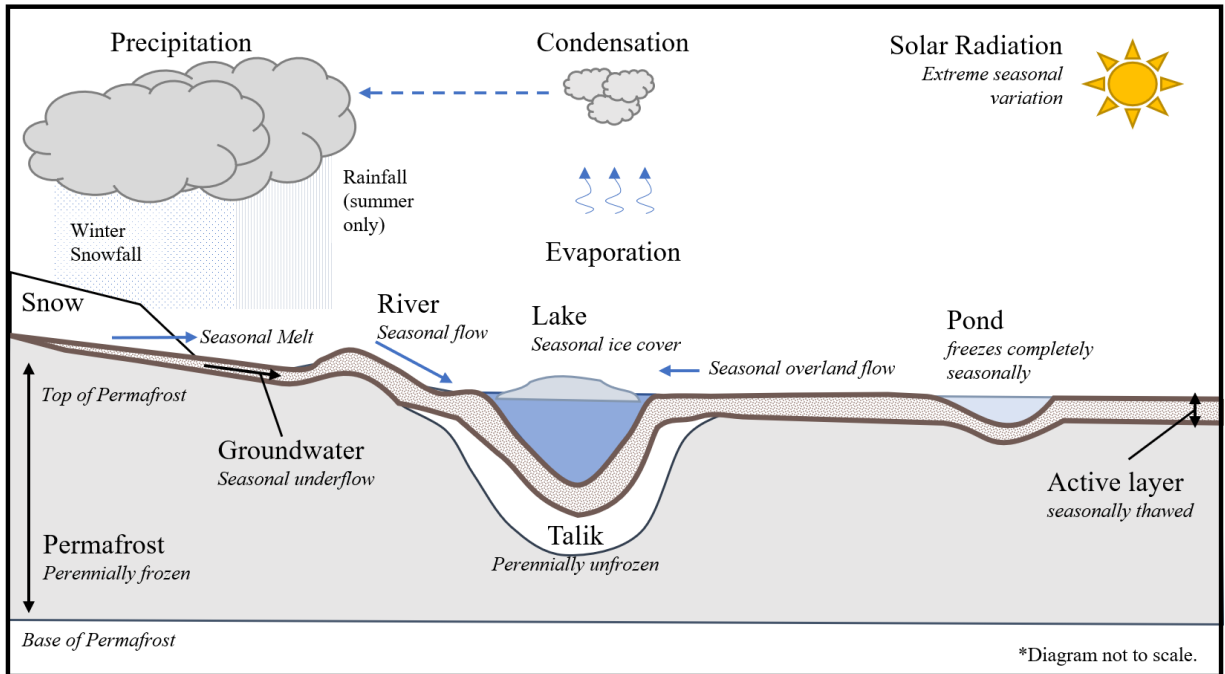


Figure 2.1: Cold region hydrology (modified from Woo, 2012c).

It is widely understood that warming temperatures are altering hydrologic regimes in polar regions, which includes higher rates of summer rainfall, deepening of seasonal thaw, degradation of permafrost, and increasing subsurface water storage (Lafrenière & Lamoureux, 2019; Walvoord & Kurylyk, 2016). In a terrestrial catchment, these thermal, physical, and hydrologic disturbances will result in runoff with increased delivery of nutrient and suspended sediment loads to lakes (Lafrenière & Lamoureux, 2019). Lakes are sensitive integrators of their catchment, reflecting seasonal changes in the catchment through the hydrologic response of their water column (Lafrenière & Lamoureux, 2019; Roberts et al., 2017; Vincent, 2009).

This review explores hydrology in continuous permafrost regions (i.e., the High Arctic) with a focus on polar lakes. Emphasis is placed on the lakes and their connections to the seasonality of the hydrologic cycle in the High Arctic. It first addresses the physics, ice phenology and hydrodynamics of High Arctic lakes, followed by a discussion on the influence of lakes on permafrost and the potential for

groundwater-surface water connections in permafrost regions. The review concludes with a brief overview of the physiographic origin of coastal High Arctic lakes and the importance of studying them.

2.2 Polar Lakes

The dominant surface water reservoirs in terrestrial cold region settings are lakes. A distinguishing feature of polar lakes is the persistent presence and thickness of ice cover (Boehrer & Schultze, 2009; Kirillin et al., 2012). Prolonged ice cover on polar lakes brings long periods without significant exchanges between the atmosphere and the water column. In the significant absence of atmospheric exchanges, specific hydrodynamic conditions become dominant under ice, resulting in unique physical and chemical conditions through the water column compared to temperate lakes (cf. Section 2.2.4) (Kirillin et al., 2012). Although ice covered lakes appear to be quiescent bodies of water, their water properties (i.e., the physical and chemical structure of the water column) can vary from the surface to the lake bottom (Boehrer & Schultze, 2008). The hydrodynamics of ice-covered lakes is a neglected area of research in modern limnology (Kirillin et al., 2012). However, foundational studies have shown under-ice processes are not static, demonstrating dynamic seasonal changes (Mortimer & Mackereth, 1958; Rahm, 1985; Welch & Bergmann, 1985). Improved monitoring capabilities now allow more studies to record water column properties throughout the ice-covered period, improving our scientific understanding of seasonal changes within these lakes (Bégin et al., 2020; Bégin et al., 2021; Cortés & MacIntyre, 2020; Jansen et al., 2021; Kirillin et al., 2012, 2018; MacIntyre et al., 2018; Rizk et al., 2014; Terzhevik et al., 2009; Yang et al., 2017; Zdrovennova et al., 2021b). Furthermore, the presence or absence of ice cover in High Arctic lakes is becoming critical to furthering our understanding of how internal lake processes are linked to seasonal and annual climate trends (Brown & Duguay, 2010a; Surdu et al., 2016; Woolway et al., 2020).

2.2.1 Water Balance in Polar Lakes

The water levels in any lake (dH) (i.e., lake volume) are determined by the positive or negative total hydrologic inputs (T_I) or outputs (T_O) as well as the water surface area (A_L). According to the equation of continuity, these three factors determine the water balance in a lake at the most basic level (Szesztay, 1974):

$$dH = \frac{T_I - T_O}{A_L}$$

Potential inputs into a water body include precipitation, surface inflows (i.e., rivers), and groundwater seepage, whereas outputs occur through surface outflows, evaporation, and subsurface drainage (Bengtsson, 2012b).

The water balance of polar lakes is different from temperate lakes due to strong seasonality; polar lakes are influenced by the cold climate and large fluctuations in seasonal energy balance (French, 2018). Consequently, polar lakes exhibit long periods of ice cover, reducing the interactions between surface water and the atmosphere. Surface inputs in temperate lakes are also very different from polar lakes, where ~ 80% of precipitation falls as snow at high latitudes (Woo et al., 2008).

In most temperate lakes, the most dominant form of surficial inflow is from rivers transporting runoff year-round (Bengtsson, 2012b). In contrast, water is stored in polar regions as snow and ice for most of the year, released from rivers only during the melt season accounting for the majority of annual inputs into High Arctic lakes (Woo, 2012a). Continuous permafrost hinders deep percolation of snowmelt and rainfall during the melt season, causing more lateral inflow from the catchment compared to lakes in non-permafrost regions (Woo, 2012a).

In addition to surficial meltwater, groundwater can be released as runoff through unfrozen pathways in seasonally thawed ground (known as the active layer). Permafrost prevents groundwater from percolating deeper into sediments allowing it to connect with surface water as runoff into rivers and lakes. Previous work has suggested that groundwater could potentially have a significant influence on the chemistry of lakes in polar regions (Harasyn, 2017) (cf. Chapter 3).

2.2.2 The Physics of Polar Lakes

Temperature plays a significant role in water column circulation, especially in ice-covered lakes as it is a major determinant of density differences in the lake (Bertilsson et al., 2013; Cortés & MacIntyre, 2020). The effect of temperature on density is non-linear (Figure 2.2), with maximum density occurring at approximately 4°C (T_{MD}) in freshwater (Boehrer & Schultze, 2009). As the temperature of water moves closer to the T_{MD} , water will sink, causing convection in the lake and potentially initiating mixing of the water column (Boehrer & Schultze, 2009).

Physical and chemical conditions within a lake will often change over the course of a year, generally with variations in climate (Vincent et al., 2008). These changes are typically driven by ice cover, solar radiation, temperature, wind, cloud coverage, and lake morphometry (Brown & Duguay, 2010a). Unlike lakes at temperate latitudes that exhibit large seasonal temperature fluctuations, lakes in polar climates experience a narrow seasonal temperature range (Bengtsson, 2012a). Polar lake temperatures are generally much closer to the T_{MD} , which drastically impacts the annual cycling of water in the lake by limiting the number of temperature-driven buoyancy differences annually through the water column. For example, many High Arctic lakes only turnover once each year during the melt season where colder winter water temperatures warm from close to 0 °C closer to the T_{MD} ; in some cases, lake water never exceeds 4°C during the melt season, meaning temperatures will cool away from T_{MD} , resulting in no autumn overturn (Woo, 2012a).

In ice-covered lakes, external heat sources such as solar radiation or residual heat stored in littoral sediments are known to generate density-driven currents created by subtle changes in temperature within a water body (Kirillin et al., 2012; Welch & Bergmann, 1985; Zdrovennova et al., 2021b). Complete turnover results in the redistribution of oxygen and nutrients in the water column, affecting biogeochemical cycling within lakes (Boehrer & Schultze, 2008). However, if water density is impacted by impurities such as solutes or sediment, it may stratify, separating the chemically or physically denser water from the rest of the water column (Boehrer et al., 2010). If stratification is strong a gradient (i.e.,

salinity) may occur between the monolimnion and the water column and the lake may never fully turnover, permanently separating the bottom and column water in a lake (Boehrer & Schultze, 2008; Woo, 2012a).

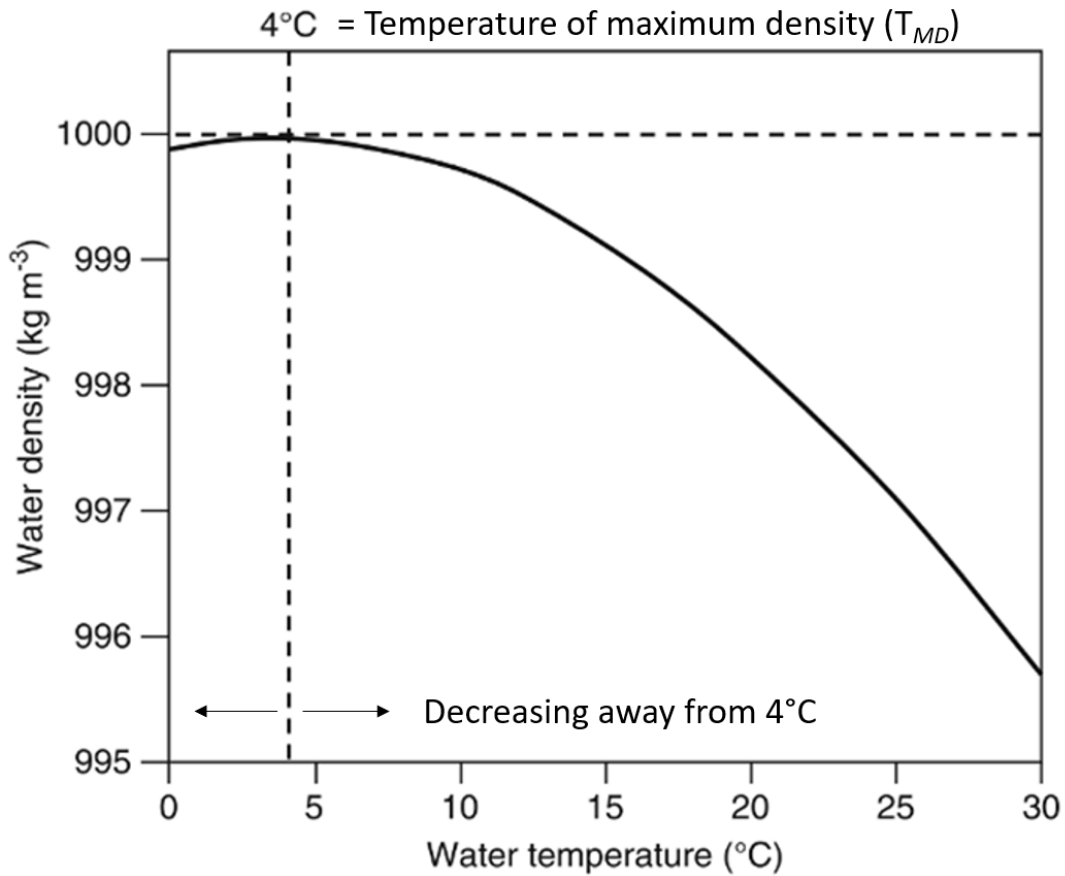


Figure 2.2: Displaying the relationship between temperature and density of freshwater. The temperature of maximum density (T_{MD}) is attained at approximately 4°C (or 3.98°C). Density decreases as temperatures move further above or below the T_{MD} (modified from Woo, 2012a).

2.2.3 Ice Phenology of Polar Lakes

Ice phenology studies the timing and duration of ice occurrence on a lake. The two major ice phenology definitions are ice-on (i.e., ice start due to freeze-up) and ice-off (i.e., ice-end due to ice melt and breakup). Ice-on is the first day the lake is fully ice covered (following the preceding ice-off period), whereas ice-off is the first day the lake is completely ice-free (following the prior ice-covered period). Air temperature is the dominant control on lake ice phenology; however, wind, solar radiation, relative humidity, and snowfall are also driving variables (Livingstone et al., 2010; Mishra et al., 2011). Many studies on lake ice phenology in the Northern Hemisphere have found that the duration of ice cover on lakes is strongly correlated to latitude and temperature, where the duration of ice cover becomes increasingly longer with increasing latitude (Adrian et al., 2009; Assel & Hérche, 1998; Magnuson et al., 2000; Wang et al., 2021; Williams & Stefan, 2006). Since lakes in polar regions are primarily ice dominated, they have been classified based on their ice characteristics as: (1) lakes with perennial ice cover; (2) lakes that intermittently retain their ice cover for less than one year; and (3) lakes with several months of ice-free conditions (Veillette et al., 2010).

Ice phenology is important because seasonal freeze-thaw cycles often mark sharp transition points in the seasonal limnology of the water column (e.g., water column turnover) (Vincent et al., 2008). Ice cover acts as a barrier that strongly affects heat and moisture exchanges with the atmosphere and annual cycles of water circulation within lakes (Woo, 2012a). This influences polar lake ecosystems by directly affecting solar energy supply, heat content of the water, light attenuation, wind-driven kinetic energy transfer, gas exchange to and from the atmosphere, the fate of inflowing materials, and the duration of stratification and mixing (Vincent et al., 2008).

2.2.3.1 Formation of Ice on Polar Lakes

The ice-on date is the date preceding the last ice-off date, where the lake surface is completely ice-covered (Kirillin et al., 2012). Ice formation on lakes generally occurs when air temperatures drop consistently below 0 °C (Arp et al., 2013; Woo, 2012a). However, there is a lag between cooling air

temperatures and the initial formation of lake ice. Summer heat gained in the water column needs to be sufficiently released into the atmosphere before freezing begins. The larger the lake, the more heat is retained and the longer it will take for the ice to form (Woo, 2012a). The depth of a lake impacts the amount of time it will take for the ice to form on the surface, where each additional meter corresponds to an additional day of delay in freezing (Kirillin et al., 2012; Leppäranta, 2010). This release of heat occurs through intense radiative and convective heat loss from the warmer lake surface to the colder atmosphere. When heat lost at the ice surface exceeds heat gained (i.e., incoming solar radiation), the lake surface can cool and form ice (Devik, 1944; Duguay et al., 2006; Kirillin et al., 2012; Leppäranta, 2010).

Conditions during ice formation determine the quality of the ice on the lake surface, as well as snow coverage, and will impact the amount of solar radiation that can penetrate the ice surface throughout the ice-covered period (Kirillin et al., 2012). Ice formation generally forms vertically and can occur on calm or turbulent water. Ice formation on calm water will create a sheet of ice across the surface of a lake. Thin sheets of ice will appear black; however, if snow is present during ice formation, the frazils (~1 mm diameter circular ice plates) will form in ice and reflect light in different directions, appearing white at the surface. Ice first develops along the shores and expands outwards to more turbulent areas. In turbulent areas, ice initially forms as frazils, which congregate, forming larger ice called frazil flocs, to frazil balls, slush, and eventually frazil floes (Woo, 2012a).

Once a lake is entirely ice-covered, surficial ice will thicken as long as latent heat can continue to conduct through the ice surface (above and below) to the atmosphere (Leppäranta, 2010). The thickness of the ice is associated with snow cover, seasonal thermodynamics within the ice, and heat fluxes from the upper and lower ice surface (Brown & Duguay, 2010b; Kirillin et al., 2012). High Arctic lakes are generally ice-covered for ~10 months, where ice usually reaches a thickness of two metres or greater (Arp et al., 2015). In the High Arctic, once the ice has formed, the probability of melt-freeze events during the cold season is low due to the lack of solar radiation inputs over winter (daily irradiance drops to zero during two or more months of winter darkness) (Woo, 2012a). The lack of seasonal irradiance during

Arctic winters results in extreme seasonal fluctuations in the energy supply delivered to the lake and thus drastic seasonal differences in solar-dependent processes such as melting and water column heating (Vincent et al., 2008).

2.2.3.2 Ice Melt on Polar Lakes

Heat transfer at both the ice-air and ice-water interfaces drives ice melt, which initiates at the ice-air interface where warming temperatures cause melting on the ice surface to form meltwater pools and channels. Weakening of the ice sheet first occurs along the shoreline of a lake where the water is shallower and warmer forming a moat around the ice sheet (Arp et al., 2013). The inflow of warmer river and runoff waters flowing from the surrounding basin can further accelerate ice decay and moat formation (Woo, 2012a). The formation of a moat eventually separates the main body of ice from the land surface, creating a mobile ice pan. Eventually, the solid ice sheet weakens, separating into elongated, hexagonal crystals known as candle ice (Woo, 2012a). The ice pan breaks up, melting as it travels across the surface.

In High Arctic lakes, it is common that ice does not melt completely and will float on the water surface over the entire summer (Mueller et al., 2009). However, the timing and extent of ice melt is changing in the Northern Hemisphere (Sharma et al., 2021). For example, Ward Hunt Lake, a freshwater lake in the Canadian High Arctic is experiencing a decrease in mid-summer ice (Bégin et al., 2021). The decrease in year-round ice cover is changing light and gas exchanges with the atmosphere, shifting water column hydrodynamics and ultimately biogeochemical cycles in the lake that results in markedly different ecosystem regimes (Bégin et al., 2021; Bégin, et al., 2020).

2.2.4 Hydrodynamics of Polar Lakes

Lake hydrodynamics are the response of a waterbody to external forcing such as weather (e.g., wind, solar radiation, air temperature; Boegman, 2019). Changes in the energy balance (i.e., temperature) in a lake will impact the water density, which can cause instabilities in the water column (i.e., regions in the water column warming or cooling to T_{MD}) and initiate mixing or create stratified layers (Boehrer &

Schultze, 2008). Physical perturbations in density by wind, boundary flows, or convection can generate a range of motions creating turbulence in the water column (Bohrer & Schultze, 2008). These changes usually occur during the spring and fall seasons, when air temperature regimes shift and ice forms or thaws at the surface (Block et al., 2019).

2.2.4.1 Physical Classifications of Lakes

Lakes are often classified based on the annual cycles of mixing in their water columns as they drastically impact the properties and processes in a water body. Amictic lakes are only found in very cold regions (typically Antarctica) and never overturn due to perennial ice cover, preventing interactions with seasonal changes at the surface (for example, Lake Vanda and Lake Fryxell in Antarctica; Green & Lyons, 2009). In contrast, most lakes will overturn fully or partially at least once annually. Holomictic lakes overturn at least once each year, completely homogenizing their water column, where meromictic lakes only partially overturn, leaving the deepest stratum of the water column perennially isolated due to the development of salinity gradients (Wetzel, 2001). Holomictic lakes are subdivided using various categories and are broadly defined as: monomictic lakes (overturn once annually), dimictic lakes (overturn twice annually), polymictic (mix several times each year), and oligomictic lakes (Lewis, 1983; Wetzel, 2001). Typically, dimictic lakes are found in temperate regions where overturn occurs in the spring and fall seasons and polymictic and oligomictic are located within equatorial regions (Wetzel, 2001). Both meromictic and monomictic lakes are found in the High Arctic, however, this review is focuses specifically on cold-monomictic lakes.

2.2.4.2 Hydrodynamics of Cold Monomictic Lakes

In the High Arctic cold monomictic lakes are common, as persistent cold and prolonged ice cover ensure temperatures never exceed 4°C (Wetzel, 2001). Cold monomictic lakes overturn once each year during the melt season when cold winter water temperatures (close to zero degrees) warm to 4°C (closer to the T_{MD}) (Lewis, 1983). Four annual hydrodynamic phases in cold monomictic lakes have been

outlined: (1) early winter, (2) mid-winter, (3) late winter, and (4) the melt season. These phases are outlined below (Jansen et al., 2021; Kirillin et al., 2012).

2.2.4.2.1 Early Winter

Early winter begins when air temperatures begin to cool below 0°C and ice forms on the lake surface (Jansen et al., 2021). During ice formation, conductive heat loss occurs through a lake, dramatically cooling the temperature of the entire water column until ice forms. In dimictic lakes, decreasing air temperatures in autumn leads to overturn of the water column until T_{MD} is reached (Salonen et al., 2014). Monomictic lakes do not overturn at this time as the water is cooling at temperatures already at, or below the T_{MD} (Woo, 2012a). During this time conductive heat loss is common in polar lakes, where relatively calm conditions and a tremendous loss of heat maintains near 0°C at the sediment-water interface eventually causing the static growth of ice at the lake surface (Kirillin et al., 2012; Woo, 2012a).

Once the lake freezes over completely, the release of sediment stored heat (summer heat) warms near bottom lake temperatures (Golosov & Kirillin, 2010; Huttula et al., 2010; Jansen et al., 2021; Kirillin et al., 2012; Rahm, 1985). Sediments can store a considerable amount of heat collected through convection of warmer water to the lake bottom during the melt season (Cortés & MacIntyre, 2020; Jansen et al., 2021). Where heat is transferred from sediments to the water column along the slopes of the lake, the water becomes denser, and density currents are formed. Density currents flow downslope to deeper locations in the lake. Flows have been detected as soon as ice cover forms and can last for an extended period, dissipating into mid-winter (Rizk et al., 2014). These density currents can form an organized circulation pattern with the downslope flow of warmer, denser water, and the upwards compensating vertical flow of the lake interior (Likens & Ragotzkie, 1965). Downslope flow velocities revealed by tracer experiments have been found to be on the order of 10^{-4} m s⁻¹ with upward vertical velocities of 10^{-6} m s⁻¹ (Likens & Ragotzkie, 1965; Welch & Bergmann, 1985). Upward flows balance out downward gravity currents and sometimes become two-layered, separating the water column into two convective cells (Rahm, 1985; Welch & Bergmann, 1985). Winter under-ice circulation is known to be ubiquitous in

the Arctic and has been documented by more recent studies (Cortés & MacIntyre, 2020; Jansen et al., 2021; Kirillin et al., 2012). Respiration produced by the oxidation of organic matter at the sediment-water interface has also been suspected to contribute to these winter under-ice density flows by producing solutes (MacIntyre et al., 2018; Mortimer & Mackereth, 1958). Early winter circulations have important consequences for the vertical transport of substances (i.e., dissolved oxygen) to deeper areas of a water body; however, where high concentrations of solutes occur at the sediment water interface, circulation may not penetrate (i.e., stratification), and anoxic zones may form (Terzhevik et al., 2009).

2.2.4.2.2 Mid-Winter

The heat stored in sediments is limited, and eventually circulation slows. Upward velocities of early winter dissipate from 10^{-5} m s^{-1} to 10^{-6} m s^{-1} by mid-winter (Likens & Ragotzkie, 1965; MacIntyre et al., 2018; Malm, 1998). The number of circulation cycles will vary from year-to-year depending on the amount of heat stored in the sediments (Kirillin et al., 2012), and the size and number of circulation cells will vary over the course of a winter season (Rahm, 1985; Terzhevik et al., 2009). Apart from the seasonal heat exchanges at the sediment-water interface, many additional factors can drive under-ice circulation and water column properties including biological, chemical, thermal, or physical external forcing (Boehrer & Schultze, 2008). Some examples include subsurface inflows and groundwater seepage, seiches (standing waves produced by oscillations within a waterbody), fluxes of dissolved ions, the extent of stratification in the water column, and the morphology of the lake bottom (Bertilsson et al., 2013; Jansen et al., 2021). The contribution of internal waves (i.e., seiches, gyres etc.) can also completely change the circulation pattern of thermally driven circulation in a lake (Petrov et al., 2007). These internal waves can be caused by wind-induced oscillations of the ice on the lake, or gyres made possible by the deflection of density driven flows by Earth's rotation (i.e., Coriolis forcing) (Jansen et al., 2021).

Although mid-winter circulation slows, there is still some circulation of the water column that is correlated with the distribution and accumulation of dissolved ions throughout the water column. Solute

can occur under ice in the lake through groundwater seepage, salt exclusion during ice formation (i.e., cryo-concentration), and microbial respiration at the sediment-water interface (MacIntyre et al., 2018; Mortimer & Mackereth, 1958; Ouellet et al., 1989; Welch & Bergmann, 1985). The fate of solutes may vary with circulation or stay in place at the ice-water interface. Mid-winter tracer experiments have demonstrated that they may be incorporated into horizontal convective circulation, sinking downslope, and accumulating in the deepest depressions at the lake bottom (Welch & Bergmann, 1985). When this occurs a denser, warmer region in the lake bottom forms due to high concentrations of dissolved ions.

2.2.4.2.3 Late Winter

Ice cover shields the water column from interactions with the atmosphere preventing particulate inputs, gas exchange at the surface and wind-induced mixing (Boehrer & Schultze, 2008). However, when solar radiation is closer to its peak, short-wave radiation can penetrate the ice surface and heat the water column (Bengtsson, 1996; Kirillin et al., 2012; Matthews & Heaney, 1987). The intensity of solar radiation warming a lake surface varies with the angular height of the sun and, therefore, with the time of day, season, and latitude (U.S. Geological Survey (USGS), 2018). The supply and spectral composition of solar radiation penetrating the water column depends on the incident radiation and the nature of the overlying snow and ice cover (Vincent et al., 2008). If solar radiation can penetrate the ice, it will warm the water in the lake. In ice-covered cold monomictic lakes, solar radiation increases the temperature of water from near 0 °C to T_{MD} in which denser water sinks, creating instabilities and convection within the water column (Cortés & MacIntyre, 2020; Jansen et al., 2021; Kirillin et al., 2012; Yang et al., 2017).

Solar driven convection in ice covered lakes and is known as radiatively-driven convection (RDC) (Farmer, 1975; Jansen et al., 2021). Convection will be vertical unless lakes have extensive shallow regions, where horizontal convection will develop from a warmer, denser gradient between offshore and onshore waters (Farmer, 1975). The depth and temperature of vertical convection increases over time, where the final depth of convection is inversely correlated with earlier deep-water temperatures (Farmer, 1975; Forrest et al., 2008; Salonen et al., 2014). In some cases, RDC will be delayed or may not

occur if: (1) lakes are snow covered; (2) near-surface density gradients are caused by rapid ice melt; or (3) stratification in the water column has been enhanced by solutes overcoming density changes at the surface (Cortés & MacIntyre, 2020; Jansen et al., 2021; Pieters & Lawrence, 2009).

Ultimately, RDC in late winter leads to much faster warming than the over-winter heat fluxes from lake bottom sediments (Bengtsson, 1996; Salonen et al., 2014). Although lakes are still ice-covered and the landscape is still frozen when it begins, RDC is the initial transition between the relatively quiescent winter to the active melt season in polar lakes. RDC has been linked to lake stratification, with decreasing dissolved oxygen and increasing density and dissolved ion concentrations at the lake bottom (cf. Chapter 4) (Cortés & MacIntyre, 2020; Jansen et al., 2021).

2.2.4.2.4 Melt Season

During the melt season ice-covered lakes begin to melt allowing the water column to interact with the atmosphere and the surrounding landscape (Vincent et al., 2008; Woo, 2012a). With initial melting on the lake surface and the input of flowing rivers and runoff (i.e., snow melt), a moat forms around the main ice pan that exposes the nearshore areas to direct incoming solar radiation (Woo, 2012a). With sufficient ice melt the lake ice detaches from the land surface allowing fresher and colder snowmelt to enter the water column as a dense plume (Jansen et al., 2021). Where river water is denser than the water column, it has the potential to displace or flush the heat and solutes accumulated at the bottom of the lake (Lewis et al., 2018).

As melting of the ice pan continues, atmospheric influences such as wind have more of an intense impact on the physical properties of a lake. For example, wind can accelerate the breakup of ice melting on the lake surface, pushing ice blocks into one another and along the shoreline (Kirillin et al., 2012; Woo, 2012a). With additional melting the water exposed at the surface increases and air temperature has a greater influence on the surface water temperature, accelerating warming of the water column. In cold lakes, water warming from 0°C becomes denser, sinking and displacing colder bottom water. This can eventually result in complete turnover of the water column. In a monomictic lake, this is the only period

of mixing in the lake because summer water temperatures rarely increase above 4 °C so there is no density-driven overturn in the fall (Woo, 2012a).

2.3 Groundwater in Polar Regions

Groundwater is normally stored in aquifers within the pore spaces or fractures of sediments and rocks. Lakes in temperate regions typically interact with aquifers through inflow or recharge depending upon subsurface hydrostatic pressure. If hydrostatic pressure is adequate, it will force groundwater to travel slowly through the subsurface in the direction of least pressure, such as to the surface through lakebed sediments (Woo, 2012b). Just as in temperate climates there are both groundwater and surface water components to the hydrologic cycle in polar regions, however, permafrost (cf. Section 2.3.1) prevents groundwater from travelling freely in the subsurface in polar regions. Permafrost acts as an aquitard that effectively restricts groundwater movement. However, lakes can warm the permafrost beneath them, creating unfrozen areas known as taliks (cf. Section 2.3.4). It is here that there is a possibility for groundwater to migrate to the surface in continuous permafrost areas. To understand how groundwater might interact with lakes in the High Arctic, permafrost structure and its effect on hydrology in cold regions must first be understood.

2.3.1 Permafrost Distribution and Structure

Permafrost is ground that is cryotic, remaining at, or below 0°C, for at least two consecutive years (Woo, 2012c). Permafrost can vary in thickness from a few centimeters to hundreds of meters (French, 2018). The extent of permafrost in an area varies largely with latitude and climate, but it is also controlled on a local scale by the thermal properties of soil and rock, abundance of vegetation and snow cover, topography, aspect, fire, and surface water bodies such as lakes (Woo, 2012c).

There are 4 categories of permafrost classified by the extent of coverage and thickness (Figure 2.3). The thinnest permafrost covers < 10% (isolated) to 50% (sporadic) of the ground, usually occurring in regions with organic-rich sediments. Discontinuous permafrost covers 50 – 90 % of the landscape and

is perforated with unfrozen zones due to local characteristics that impact ground surface temperature (i.e., water bodies, topography, microclimate, vegetation, and snow cover). Finally, continuous permafrost covers 90% to 100% of the subsurface and is present everywhere except beneath large surface water bodies (Woo, 2012c).

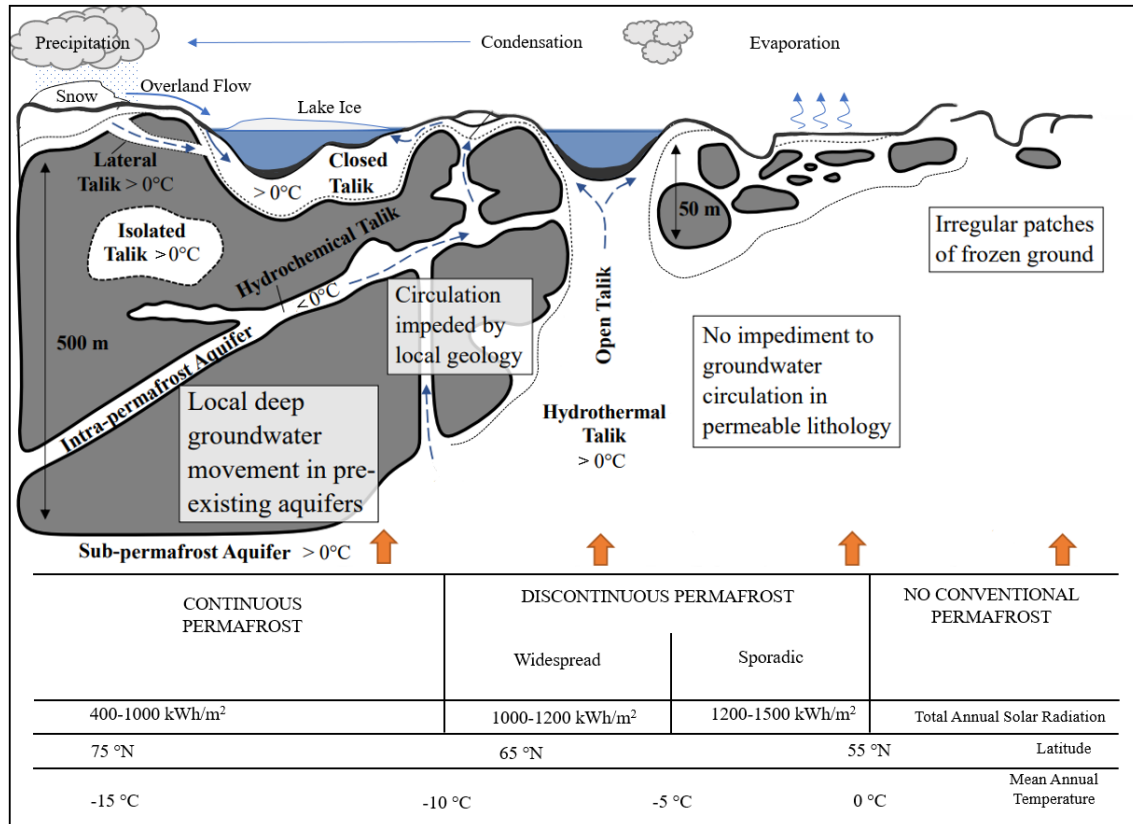


Figure 2.3: A demonstration of potential hydrologic interactions occurring across landscapes underlain by various permafrost distributions (from left to right: continuous, discontinuous, sporadic, and irregular permafrost). Latitude corresponds to permafrost distribution and associated mean annual temperatures and total annual solar radiation. Potential talik geometry (i.e., open, closed talik) and pathways for the movement of groundwater to the surface through the frozen ground are also shown. Additionally, locations of supra-permafrost, intra-permafrost, and sub-permafrost aquifers are displayed. (Modified from French, 2018).

Permafrost is complex because it can exist in both a solid and liquid state at temperatures at, or below 0°C, and unfrozen zones (both above or below 0°C) can be found below, within, or above the permafrost (Woo, 2012c). Regions within permafrost are defined based on temperature (Figure 2.4). At the surface, above the permafrost, is the active layer that freezes and thaws seasonally with changes in local air temperatures (Woo, 2012c). During the thaw season, the active layer thaws from the top down until it reaches the maximum thaw depth for the season. The maximum thaw depth marks the transition zone between the active layer and permafrost, separating thawed and frozen sediments (Walvoord & Kurylyk, 2016). The transition zone is unfrozen but remains below 0°C due to freezing-point depression of water, induced by dissolved ions, adsorption, and capillary forces. From the base of the active layer, permafrost extends vertically to the permafrost base. The thickness of the permafrost is mainly dependent on the balance between the internal heat gain (i.e., geothermal flux or proximity to a waterbody) and the heat lost at the surface (dependent on the air temperature) (French, 2018). Similar to the transition zone, an unfrozen zone called the cryopeg occurs at the base of permafrost (Walvoord & Kurylyk, 2016; Woo, 2012c) (Figure 2.4).

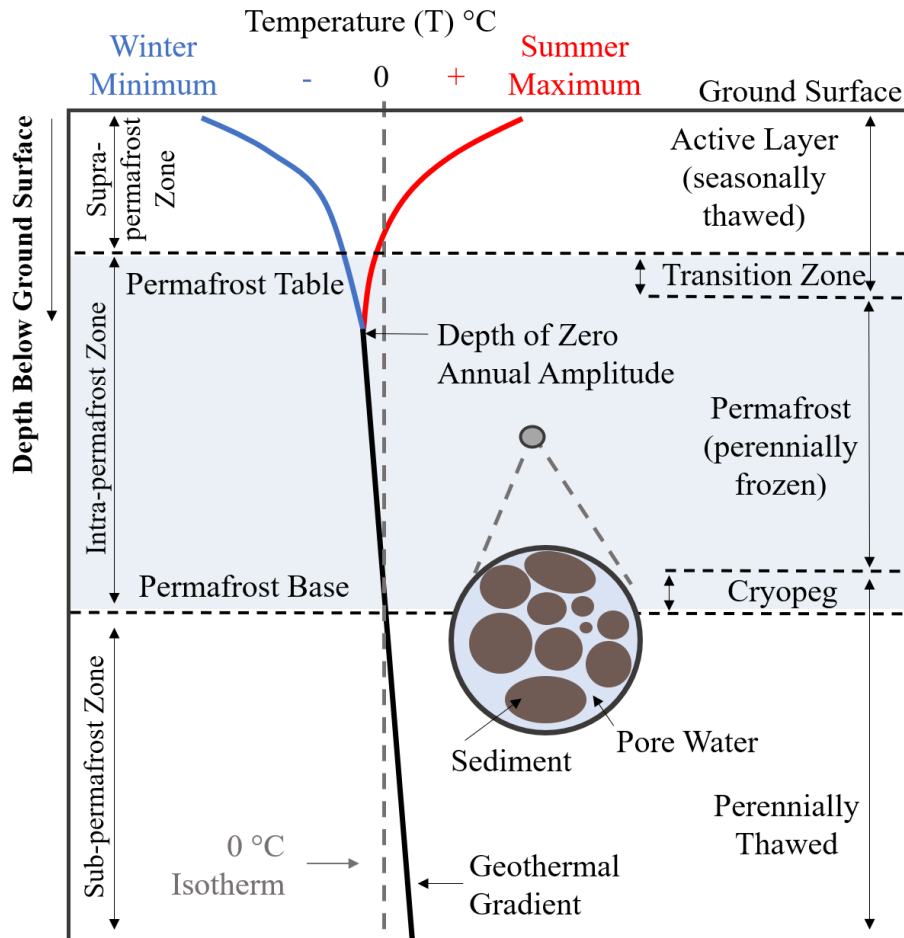


Figure 2.4 A schematic displaying the typical cryotic structure of the thermal regime from the surface to depth in a permafrost landscape unimpeded by features that may impact temperature at depth (Modified from Woolvord and Kyurylyk, 2016)

2.3.2 Groundwater Classifications in Permafrost

The distribution of permafrost and ice content largely influences water flux, flow patterns, and groundwater distribution through the frozen ground (Figure 2.3). Groundwater can flow within soils and sediments above permafrost in the supra-(above) permafrost zone, which often makes contact with the surface due to the seasonally thawed active layer. Groundwater flows seasonally or perennially (i.e., in the transition zone), connecting shallow groundwater to surface water bodies (e.g., lakes, rivers) (Woo, 2012b). Groundwater can also be found within and below the permafrost. Intra-permafrost groundwater is stored in aquifers within the permafrost, and sub-permafrost groundwater is stored below the permafrost

(Woo, 2012b). Intra- or sub-permafrost groundwater often contain high concentrations of dissolved solids, varying as a function of bedrock composition and the length of residence time (i.e., increased rock-(mineral) water interactions) (Cochand et al., 2019).

2.3.3 Groundwater in Continuous Permafrost Regions

Studies in discontinuous permafrost areas with seasonally active groundwater-surface water connections indicate that permafrost distribution and active layer structures can substantially impact groundwater flow paths (Liao & Zhuang, 2017). In contrast, sub-permafrost groundwater discharge in the High Arctic is rare due to thick continuous permafrost extending deep into the subsurface (Woo, 2012b). While much hydrologic research conducted in the High Arctic has focused on the surface water dynamics (Cochand et al., 2019), groundwater may flow all year round if there are appropriate conduits to concentrate flow and heat to prevent freezing (Utting et al., 2013). One example of groundwater activity in continuous permafrost is found on Axel Heiberg Island, where highly mineralized fluids discharge perennially the surface at constant temperatures (2.0 to 6.5 °C) despite a mean average annual temperature of -15 °C (Omelon et al., 2006; Pollard et al., 1999; Pollard, 2005; Zentilli et al., 2019). In this case, the presence of evaporites and the high discharge temperatures suggest the source of these springs to be likely sub-permafrost (Zentilli et al., 2019). Another occurrence of groundwater documented on Ellesmere Island, where perennial springs (flowing at 9.0 °C) also demonstrate how groundwater originating from depth reaches the surface through a highly permeable pathway within the local geology (Grasby et al., 2014). Sub-permafrost groundwater has also been suspected to be seeping into lakes on the coast of Melville Island in two separate studies (Dugan et al., 2012; Harasyn et al., 2017). In both studies geochemical signatures collected from the lake bottom were indicative of sub- or intra-permafrost groundwater seepage into the lake. Finally, modelling by Scheidegger et al. (2012) suggests that glacial meltwater-fed spring systems in areas with continuous permafrost can persist for millennia after having been exposed from underneath glaciers, suggesting that flow channels in permafrost can persist over time (Scheidegger et al., 2012). Findings such as these indicate that groundwater is present beneath and within

thick continuous permafrost and is more mobile than previously thought. This highlights an increasing need for hydrogeochemical characterization of sub-permafrost groundwater in the context of geology and geochemistry to understand groundwater dynamics and flow paths, particularly in the CAA (Cochand et al., 2019; Henkemans et al., 2018; Lecher, 2017; Walvoord & Kurylyk, 2016).

2.3.4 Taliks

Taliks are thawed zones in permafrost which form due to thermal or chemical influence (French, 2018). Examples include heat transferred from a landscape feature (thermal influence) or freezing depression by the introduction of dissolved ions (chemical influence). Groundwater may flow perennially in taliks if there are appropriate conduits to concentrate flow and heat to prevent freezing, or saline fluids to depress freezing and stay liquid at temperatures below 0 °C (French, 2018; Utting et al., 2013).

2.3.4.1 Talik Classification

There are multiple classifications of taliks determined by their location in permafrost, mechanisms of formation, and relation to groundwater (French, 2018; Walvoord et al., 2012; Woo, 2012b). Taliks are classified by their connections between the permafrost and the surface, and include: open (or through talik), lateral, isolated, or closed taliks (Figure 2.3). Taliks are further distinguished by the processes that form them, which determine if they are cryotic (unfrozen below 0 °C, or chemical) or non-cryotic (unfrozen above 0 °C, or thermal). Hydrothermal taliks form when heat is supplied to permafrost by an external source, warming the temperature of the adjacent ground (such as a lake, river, or groundwater, or geothermal heat) (French, 2018; Woo, 2012a). Hydrochemical taliks form when mineralized (i.e., saline) groundwater depresses the freezing temperatures of permafrost allowing water to remain liquid at temperatures below 0 °C (French, 2018; Woo, 2012a). For example, Bing & Ma, (2011) found that at low water content, NaCl salinities on the order of 2000 mg/L can depress freezing point of water by 3°C compared to dilute water.

2.3.5 Taliks and Polar Lakes

The high heat capacity of lake water prevents heat loss from underlying sediments, warming the permafrost below (French, 2018; Johnston & Brown, 1964). This situation requires that the water body be deep enough to prevent freezing to the bottom in winter and that the lake bottom water remains unfrozen for a year or more, which prevents lake bottom sediments from freezing and insulates the ground below (Burn, 2005). These conditions promote the formation of a talik beneath a lake (Arp et al., 2015; Wellman et al., 2013). There is limited information about taliks beneath lakes in continuous permafrost settings (French, 2018); however, they have been investigated beneath lakes in the continuous permafrost zones of the Mackenzie Delta Region (Burn, 2005) and Western Greenland (Johansson et al., 2015), and are suspected to be associated with monomictic freshwater lakes on Melville Island (Dugan et al., 2012; Dugan & Lamoureux, 2011; Harasyn et al., 2017) and Cornwallis Island (Ouellet et al., 1989; Welch & Bergmann, 1985).

The geometry of a taliks associated with lakes depends on the size and depth of the water body, the water temperature, ice thickness, snow cover, and compaction of bottom sediments (French, 2018). Where lakes are sufficiently large and deep (i.e., where the lake width is more than twice the depth of the permafrost), unfrozen zones extend through the entire permafrost thickness, connecting sub-permafrost groundwater to surface water (French, 2018). Taliks can also exist adjacent to the sides of a lake, extending laterally away from the lake slopes allowing for groundwater seepage into porous littoral sediments (Dugan et al., 2012; Lecher, 2017). Groundwater seepage in lakes has the potential to moderate water-level fluctuations, supply nutrients and inorganic ions to lakes (Hayashi & Rosenberry, 2002), and even alter the chemical signature of a lake (Ouellet et al., 1989). However, further research is required to quantify the contribution of groundwater seepage in High Arctic lakes.

2.4 Sampling and Measurement Methods

2.4.1 Methods in Polar Lakes

Baseline measurements are necessary to understand and monitor the water quality in a lake over time (USGS, 2018) and *in-situ* sampling methods are essential to measuring the physical and chemical properties through the water column of a lake. The most common approaches for quantitatively evaluating the characteristics of a lake are by measuring relevant physical and chemical parameters including light and water clarity, temperature and stratification, conductivity, turbidity, pH, dissolved oxygen, nutrients (e.g., phosphorus and nitrogen) and photosynthetic pigments (e.g., Chlorophyll *a*) (USGS, 2018). Abrupt transitions in processes such as under ice circulation, hyperycnal flows, and potential sites of groundwater seepage have been correlated to the seasonal dates of freeze-up and breakup of ice on lakes in continuous permafrost regions (Bégin et al., 2021a; Cortés & MacIntyre, 2020; Dugan et al., 2012; Harasyn et al., 2017; Lewis et al., 2018). Using a combination of measurement strategies, such as individual sensor deployment from the surface through the water column and placing moorings at specific depths, can provide both spatial and temporal information about lake properties (Bégin et al., 2020a; Bégin et al., 2020b; Cortés & MacIntyre, 2020; Saber et al., 2019; Vincent et al., 2008). In turn, these properties can help to infer the magnitude and timing of dynamic processes that operate within a given water body during specific times of year.

Common techniques for assessing the chemistry of the water column include water column profiling (i.e., multiple depths, recording measurements at a single point in time from multiple depths), and moored loggers (i.e., fixed depth, recording measurements from the same location many times) (Figure 2.5). Water column profiles are normally measured by repeatedly deploying sensors from the lake surface to the bottom of the lake with a rope or cable. These profiles are typically collected during late spring or summer when research locations are accessible, whereas late fall and winter data collection is uncommon due to the remote nature of many High Arctic lakes that are difficult to access during this time (Block et al., 2019; Cochand et al., 2019). Ice cover provides a stable platform for carrying out repeated

water column casts via holes drilled in the ice (Harasyn et al., 2017; Lewis et al., 2018), whereas moored loggers stationed at targeted lake depths provide a continuous record of lake water column properties over an extended time period (Bégin et al., 2020b). Multiple fixed loggers moored at different depths in the lake can record the changes in a single variable over time, revealing changes and patterns in the chemical structure of the lake such as stratification and mixing regimes (Bégin et al., 2020a; Cortés & MacIntyre, 2020; Vincent et al., 2008). Such long-term records of altered circulation patterns or water column properties in lakes are critical to determining the effects of warming Arctic temperatures (Boehrer et al., 2010; Mueller et al., 2009).

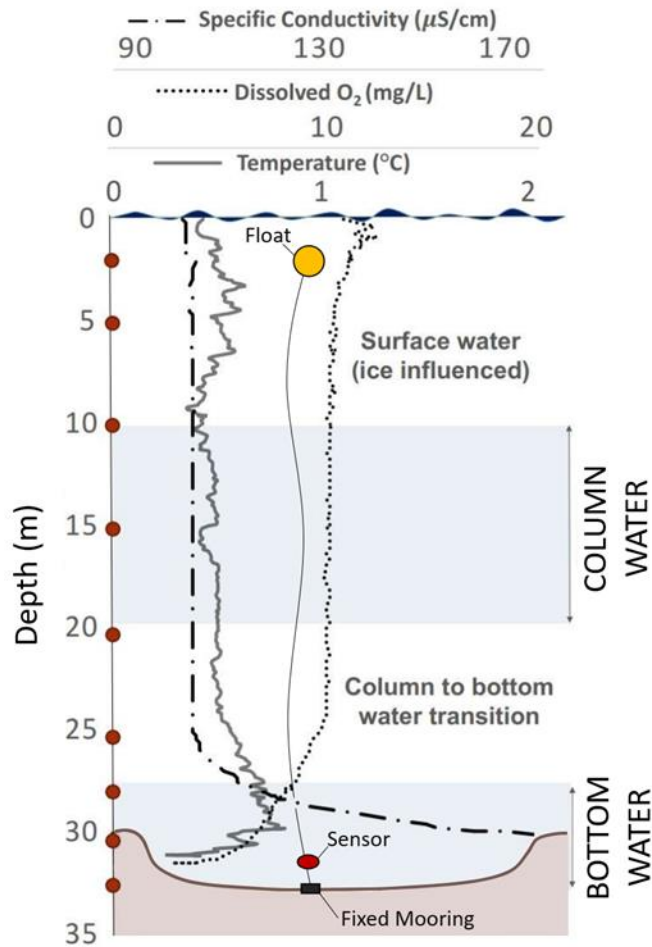


Figure 2.5: A water column profile displaying the chemical data collected from the surface to the lake bottom (32 meters depth). Red dots mark the depth that water samples were collected by water column profiling. This cast was collected from the ice surface of West Lake (unofficial name) at Cape Bounty Arctic Watershed Observatory, Nunavut (74°50'N, 109°30'W) on May 31, 2016 (Harasyn et al., 2017). The differences in the chemistry (Specific Conductivity, Dissolved Oxygen, and Temperature) between the bottom water and the column water are highlighted (shaded in blue). A fixed mooring is also depicted at 32 metres depth.

2.4.2 Methods for Groundwater Associated with Polar Lakes

Lakes have a warming effect on the permafrost around them which can create taliks and facilitate pathway for groundwater flow into lakes. Groundwater seepage can be quantified using a variety of methods including watershed-scale studies, lake-water budgets, lake-water and chemical budgets, monitoring wells and flow net-analysis, groundwater flow modelling, tracer studies, thermal methods, and biological indicators (Dugan et al., 2012; Harvey et al., 1997; Johansson et al., 2015; Judge, 1973; Jutebring Sterte et al., 2018; Paquette et al., 2017; Rautio & Korkka-Niemi, 2011). Such methods rely upon indirect measurements, making it difficult to detect and quantify groundwater inputs especially where exchanges are small. Alternative methods include sampling groundwater discharge using a seepage meter that directly measures the flux of groundwater into a waterbody (Rosenberry et al., 2015; Rosenberry & Morin, 2004). Seepage meters operate by collecting water at the site of seepage through a plastic bag (volume chamber) which is attached to an open-ended cylinder (Rosenberry & Morin, 2004). Although this is a common method, it is often impractical in larger lakes and remote areas such as the High Arctic (Harvey et al., 1997).

Where direct quantification is not possible, chemical characterization of groundwater provides an understanding of potential sources and how this water may impact the composition of surface water (Harasyn et al., 2017; Ouellet et al., 1989). Groundwater and surface water often differ in chemical and physical properties; for example, groundwater typically has higher total dissolved solids than surface water, leading to greater ionic strengths and higher electrical conductivities (Harvey et al., 1997). Water column variations in dissolved ion concentrations, specific conductivity, temperature and dissolved oxygen can all be indicative of groundwater occurrence in lakes (Kalbus et al., 2006). High groundwater input into a lake potentially changing water column chemistry, water balance, and mixing regimes, making characterization important to the hydrological monitoring of water bodies (Henkemans et al., 2018).

2.5 The Coastal High Arctic Setting

In the CAA, permafrost may be thinner near coastlines due to the warming effect from the sea. Permafrost extent is continuously in flux; during the Holocene marine transgression period after the retreat of the Laurentide Ice Sheet (LIS) (11.3 and 11.7 ka (i.e., 10^3 years; Dyke & Prest, 1987), permafrost would have receded due to the effects of sea level rise (Van Hove et al., 2006). When permafrost is submerged beneath sea water it can create unfrozen conditions allowing salt water to intrude landward (Guimond et al., 2021; Keating et al., 2018). Isostatic rebound caused the sea level to retreat following sea level retreat by isostatic rebound, permafrost would have aggraded inland, freezing intruded seawater that was in pores of the unfrozen, previously submerged sediments. This resulted in a situation whereby late-glacial marine-sourced groundwater is a potential source of high conductivity waters through migration of trapped sea water beneath coastal lakes (Dugan et al., 2012; Harasyn et al., 2017; Ouellet et al., 1989; Van Hove et al., 2006).

2.5.1 Coastal High Arctic Lake Formation

Lakes are widespread in high latitude regions of the northern hemisphere, with many located along or near coastlines, especially in the CAA (Woo, 2012a). Many of these coastal High Arctic lakes originated from glacial processes that shaped the landscape through erosion and re-distribution of sediment and mineral deposits (Van Hove et al., 2006). More specifically, these lakes formed in deep depressions scoured by the movement and melt of glacial ice blocks during glacial retreat (Woo, 2012a). Many lakes in the CAA continue to be influenced by glacial and periglacial processes from the most recent retreat of the LIS and Innuitian Ice Sheet (IIS), which formed during the Last Glacial Maximum (LGM) and reached its maximum extent during the Late Wisconsinan (Dyke et al., 2002; England et al., 2006; Stokes, 2017). The LGM is defined as the maximum extent of the ice sheets during the last glaciation dating between 19000 – 22000 BP (Yokoyama et al., 2000). The LGM occurred during a period of low global sea level (130-135 m lower than present) and relative climate stability (Clark & Mix, 2000). However, the retreat of ice sheets and the melting of coastal ice shelves increased the flow of

meltwater to the oceans. In turn, these events increased sea levels that resulted in submergence of the land (Church et al., 2001).

Many coastal lakes along the shorelines of the CAA today were once below sea level but emerged with the resurgence of the land through isostatic rebound of 80 – 150 m asl in response to glacial influence (England, 1999; Nixon, 2012; Stokes, 2017). This resulted in the gradual isolation of the glacially-formed basins from the coastal marine landscape to produce a series of saline lakes. Over time, these lakes will transition to either hypersaline lakes or to freshwater lakes depending on whether they experience a negative or positive water balance (Figure 2.6). Saline lakes will become hypersaline if there is a negative water balance or freshen if the water balance is positive (Van Hove et al., 2006). This emphasizes the importance of understanding how present-day conditions of a lake directly result from the changes in the surrounding landscape over time. For example, researchers were only able to understand the source of hypersaline waters in Sophia Lake and Garrow Lake through a thorough understanding of their geological history (Ouellet et al., 1989; K. M. Stewart & Platford, 1986). The origin of each lake plays a role in defining the present-day water balance, especially in regions underlain by thick continuous permafrost.

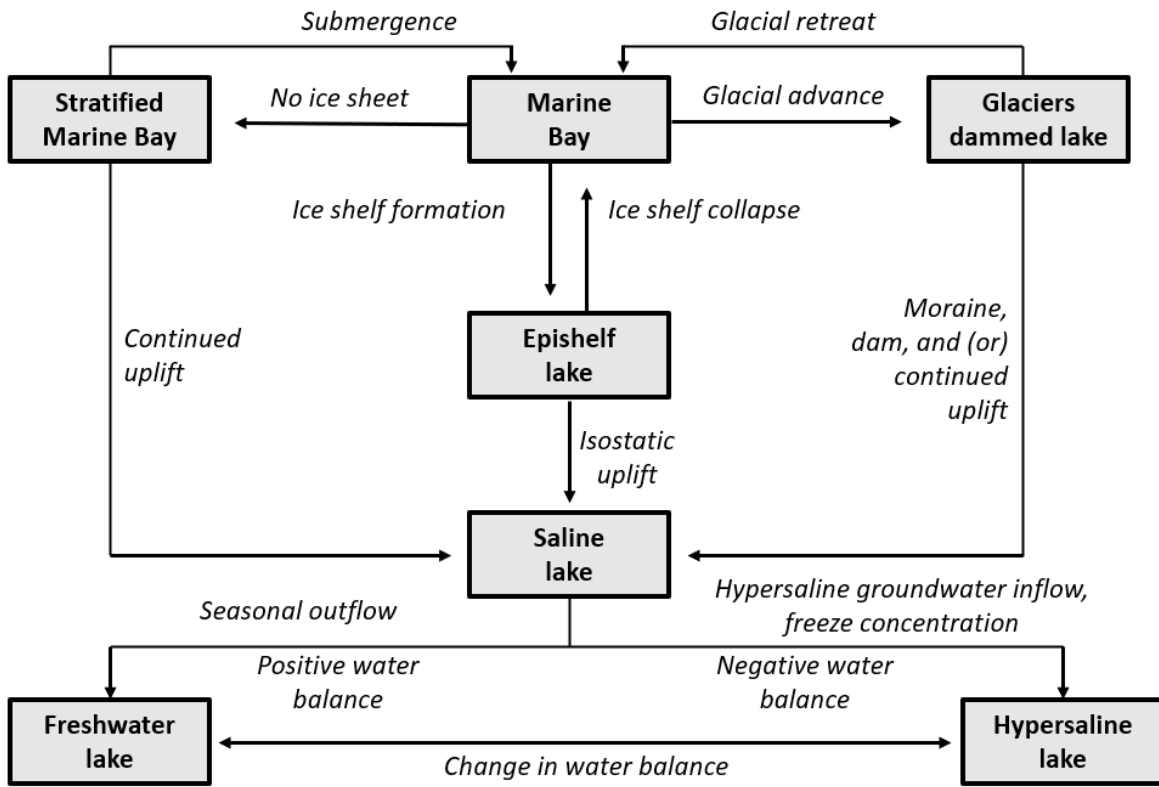


Figure 2.6: Postulated evolutionary sequence for coastal high latitude landscapes, embayments, and lakes (modified from Van Hove et al., 2006).

2.5.2 Groundwater Associated with Coastal High Arctic Lakes

Geochemical signatures indicative of groundwater have been found in the deepest regions of coastal High Arctic lakes (Besonen et al., 2008; Dugan & Lamoureux, 2011; Ouellet et al., 1989) and recent work on monomictic High Arctic lakes have revealed evidence for potential groundwater seepage following the nival period, when discharge is controlled largely by snowmelt (Harasyn et al., 2017; Roberts et al., 2017).

Dugan et al. (2012) detected elevated levels of radon-222 in the bottom water of a High Arctic lake near Shellabear Point on Melville Island. As radon-222 is elevated in groundwater compared to surface water, this suggested that subsurface flow may be discharging into the lake. This raised numerous questions about groundwater activity in the Arctic, and suggested additional sampling be completed during a melt season to improve understanding of groundwater origin and flow characteristics (Dugan et al., 2012). Recent work on two other High Arctic lakes along the south-central coast of Cape Bounty on Melville Island has identified geochemical signatures indicative of groundwater in the bottom water (Harasyn et al., 2017). Elevated specific conductivity in conjunction with distinctly different ratios of dissolved ions were found in localized depressions at the bottom of the lakes (Harasyn et al., 2017). Although these signatures were indicative of groundwater seepage, this study did not find sufficient evidence to quantify or confirm the source of these signatures.

2.6 The Importance of Studying High Arctic lakes

Lacustrine systems are highly sensitive integrators of their terrestrial surroundings and respond rapidly to changes in their catchments (Adrian et al., 2009; Hassol, 2004; Mueller et al., 2009; Williamson et al., 2009). High Arctic lakes are particularly sensitive to climate change (Vincent, 2009). Recent studies have found that physical processes such as increased suspended sediment concentration delivery and duration of ice-covered periods in High Arctic lakes change in response to warming temperatures (Kirillin et al., 2012; Lewis et al., 2018; Zdrovennova, et al., 2021a). Climate change can also alter the chemical composition of lakes by affecting landscape properties within the catchment. In

addition, climate change can impact lake properties such as ice cover, stratification, and mixing, and altering the physical structure and biogeochemical interactions of lake ecosystems (Vincent, 2009).

High Arctic lakes are unique as they are hydrologically bound by continuous permafrost and long periods of ice cover. Climate warming has triggered changes in annual freeze-thaw patterns (ice phenology) across lakes in the Northern Hemisphere (Wang et al., 2021). In the High Arctic, there has been a notable decrease in ice cover duration in many lakes, demonstrating a widespread shift in lake ice phenology across the CAA (Brown & Duguay, 2010b; Sharma et al., 2019; Surdu et al., 2016; Woolway et al., 2020). For example, perennially frozen lakes are now shifting to seasonal ice regimes, and seasonally frozen lakes are facing shortened ice-covered seasons by 25-40 days (Surdu et al., 2016). In addition, extreme warming events are shifting lake systems to more irregular freeze-thaw patterns, resulting in unstable water column conditions from year-to-year (Bégin et al., 2020b; Duguay et al., 2006; Mueller et al., 2009; Surdu et al., 2016; M. Woo, 2012a). Changing water column conditions can impact water quality and biogeochemical cycling critical to lake ecosystems in the High Arctic (Hamilton et al., 2001; Klanten et al., 2021). This sensitivity to changes in ice cover underpins the need for studies detailing under-ice water column processes. As temperatures warm and permafrost increasingly thaws across the High Arctic, changes in lakes can provide useful indicators of changes in the surrounding landscape. Therefore, studies focusing on the phenology and limnology of ice-covered High Arctic lakes provide essential opportunities to capture not only how hydrologic patterns are changing within lakes but also infer their response to landscape changes with climate warming.

2.7 References

- Adrian, R., O'Reilly, C. M., Zagarese, H., Baines, S. B., Hessen, D. O., Keller, W., Livingstone, D. M., Sommaruga, R., Straile, D., van Donk, E., Weyhenmeyer, G. A., & Winder, M. (2009). Lakes as sentinels of climate change. *Limnology and Oceanography*, *54*(6 PART 2), 2283–2297.
https://doi.org/10.4319/lo.2009.54.6_part_2.2283
- Arp, C. D., Jones, B. M., & Grosse, G. (2013). Recent lake ice-out phenology within and among lake districts of Alaska, U.S.A. *Limnology and Oceanography*, *58*(6), 2013–2028.
<https://doi.org/doi:10.4319/lo.2013.58.6.2013>
- Arp, C. D., Jones, B. M., Liljedahl, A. K., Hinkel, K. M., & Welker, J. A. (2015). Depth, ice thickness, and ice-out timing cause divergent hydrologic responses among Arctic lakes. *Water Resources Research*, *51*, 9379–9401. <https://doi.org/10.1002/2015WR017362>
- Assel, R. A., & Herche, L. R. (1998). Ice-on, ice-off, and ice duration for lakes and rivers with long-term records. *Ice in Surface Waters: Proceedings of the 14th International Symposium on Ice, New York, 27-31 July 1998. Volume 1, July*, 147–151.
- Bégin, P. N., Rautio, M., Tanabe, Y., Uchida, M., Culley, A. I., & Vincent, W. F. (2020a). The littoral zone of polar lakes: Inshore-offshore contrasts in an ice-covered high arctic lake. *Arctic Science*, *7*(1), 158–181. <https://doi.org/10.1139/as-2020-0026>
- Bégin, P. N., Tanabe, Y., Kumagai, M., Culley, A. I., Paquette, M., Sarrazin, D., Uchida, M., & Vincent, W. F. (2020b). Extreme warming and regime shift toward amplified variability in a far northern lake. *Limnology and Oceanography*, *July*. <https://doi.org/10.1002/lno.11546>
- Bégin, P. N., Tanabe, Y., Rautio, M., Wauthy, M., Laurion, I., Uchida, M., Culley, A. I., Warwick, & Vincent, F. (2021). Water column gradients beneath the summer ice of a High Arctic freshwater lake as indicators of sensitivity to climate change. *Scientific Reports*, *11*, 2868.
<https://doi.org/10.1038/s41598-021-82234-z>
- Bengtsson, L. (1996). Mixing in ice-covered lakes. *Hydrobiologia*, *322*(1–3), 91–97.
<https://doi.org/10.1007/BF00031811>
- Bengtsson, L. (2012a). Ice covered lakes. In L. Bengtsson, R. W. Herschy, & R. W. Fairbridge (Eds.), *Encyclopedia of Lakes and Reservoirs*. Springer. https://doi.org/10.1007/978-1-4020-4410-6_31

- Bengtsson, L. (2012b). Water balance of lakes. In L. Bengtsson, R. W. Herschy, & R. W. Fairbridge (Eds.), *Encyclopedia of Lakes and Reservoirs*. (pp. 869–872). Springer.
https://doi.org/10.1007/978-1-4020-4410-6_244
- Bertilsson, S., Burgin, A., Carey, C. C., Fey, S. B., Grossart, H. P., Grubisic, L. M., Jones, I. D., Kirillin, G., Lennon, J. T., Shade, A., & Smyth, R. L. (2013). The under-ice microbiome of seasonally frozen lakes. *Limnology and Oceanography*, *58*(6), 1998–2012.
<https://doi.org/10.4319/lo.2013.58.6.1998>
- Besonen, M. R., Patridge, W., Bradley, R. S., Francus, P., Stoner, J. S., & Abbott, M. B. (2008). A record of climate over the last millennium based on varved lake sediments from the Canadian High Arctic. *Holocene*, *18*(1), 169–180. <https://doi.org/10.1177/0959683607085607>
- Bing, H., & Ma, W. (2011). Laboratory investigation of the freezing point of saline soil. *Cold Regions Science and Technology*, *67*(1–2), 79–88. <https://doi.org/10.1016/j.coldregions.2011.02.008>
- Block, B. D., Denfeld, B. A., Stockwell, J. D., Flaim, G., Grossart, H. P. F., Knoll, L. B., Maier, D. B., North, R. L., Rautio, M., Rusak, J. A., Sadro, S., Weyhenmeyer, G. A., Bramburger, A. J., Branstrator, D. K., Salonen, K., & Hampton, S. E. (2019). The unique methodological challenges of winter limnology. *Limnology and Oceanography: Methods*, *17*(1), 42–57.
<https://doi.org/10.1002/lom3.10295>
- Boegman, L. (2019). Hydrodynamics of Lakes. In *Encyclopedia of Water*. Wiley.
<https://doi.org/10.1002/9781119300762.wsts0231>
- Boehrer, B., Herzsprung, P., Schultze, M., & Millero, F. J. (2010). Calculating density of water in geochemical lake stratification models. *Limnology and Oceanography: Methods*, *8*, 567–574.
<https://doi.org/10.4319/lom.2010.8.567>
- Boehrer, B., & Schultze, M. (2008). Stratification of lakes. *Reviews of Geophysics*, *46*(2), 1–27.
<https://doi.org/10.1029/2006RG000210>
- Boehrer, B., & Schultze, M. (2009). Density stratification and stability. *Reviews of Geophysics*, *46*(2), 583–593. <https://doi.org/10.1029/2006RG000210>
- Brown, L. C., & Duguay, C. R. (2010a). The response and role of ice cover in lake-climate interactions. *Progress in Physical Geography*, *34*(5), 671–704. <https://doi.org/10.1177/0309133310375653>

- Brown, L. C., & Duguay, C. R. (2010b). The response and role of ice cover in lake-climate interactions. *Progress in Physical Geography*, 34(5), 671–704. <https://doi.org/10.1177/0309133310375653>
- Burn, C. R. (2005). Lake-bottom thermal regimes, western Arctic Coast, Canada. *Permafrost and Periglacial Processes*, 16(4), 355–367. <https://doi.org/10.1002/ppp.542>
- Church, J. A., Gregory, J. M., Huybrechts, P., Kuhn, M., Lambeck, K., Nhuan, M. T., Qin, D., Woodworth, P. L., Anisimov, O. A., Bryan, F. O., Cazenave, A., Dixon, K. W., Fitzharris, B. B., Flato, G. M., Ganopolski, A., Gorniz, V., Lowe, J. A., Noda, A., Oberhuber, J. M., ... Zwally, H. J. (2001). Changes in sea level. In J.T. Houghton, Y. Ding, D.J. Griggs, M. Noguer, P.J. Van der Linden, X. Dai, , K. Maskell (eds.), *Climate Change 2001: The Scientific Basis: Contribution of working group I to the third assessment report of the Intergovernmental Panel on Climate Change*. Cambridge University Press. 639–693. https://doi.org/10.1007/978-3-642-69317-5_7
- Clark, P. U., & Mix, A. C. (2000). Ice sheets by volume. *Nature*, 406, 689–690. <https://doi.org/10.1038/35021176>
- Cochand, M., Molson, J., & Lemieux, J. M. (2019). Groundwater hydrogeochemistry in permafrost regions. *Permafrost and Periglacial Processes*, 30(2), 90–103. <https://doi.org/10.1002/ppp.1998>
- Cortés, A., & MacIntyre, S. (2020). Mixing processes in small arctic lakes during spring. *Limnology and Oceanography*, 65(2), 260–288. <https://doi.org/10.1002/lno.11296>
- Devik, O. (1944). Ice formation in lakes and rivers. *The Royal Geographical Society*, 103(5), 193–203. <https://about.jstor.org/terms>
- Dugan, H. A., Gleeson, T., Lamoureux, S. F., & Novakowski, K. (2012). Tracing groundwater discharge in a High Arctic lake using radon-222. *Environmental Earth Sciences*, 66, 1385–1392. <https://link.springer.com/article/10.1007/s12665-011-1348-6>
- Dugan, H. A., & Lamoureux, S. F. (2011). The chemical development of a hypersaline coastal basin in the High Arctic. *Limnology and Oceanography*, 56(2), 495–507. <https://doi.org/10.4319/lo.2011.56.2.0495>
- Duguay, C. R., Prowse, T. D., Bonsal, B. R., Brown, R. D., Lacroix, M. P., & Ménard, P. (2006). Recent trends in Canadian lake ice cover. *Hydrological Processes*, 20(4), 781–801. <https://doi.org/10.1002/hyp.6131>

- Dyke, A. S., Andrews, J. T., Clark, P. U., England, J. H., Miller, G. H., Shaw, J., & Veillette, J. J. (2002). The Laurentide and Innuitian ice sheets during the Last Glacial Maximum. *Quaternary Science Reviews*, 21(1–3), 9–31. [https://doi.org/10.1016/S0277-3791\(01\)00095-6](https://doi.org/10.1016/S0277-3791(01)00095-6)
- Dyke, A. S., & Prest, V. K. (1987). Late Wisconsinan and Holocene history of the Laurentide Ice Sheet. *Géographie Physique et Quaternaire*, 41(2), 237–263. <https://doi.org/10.7202/032681ar>
- England, J. (1999). Coalescent Greenland and Innuitian ice during the Last Glacial Maximum: Revising the Quaternary of the Canadian High Arctic. *Quaternary Science Reviews*, 18(3), 421–456. [https://doi.org/10.1016/S0277-3791\(98\)00070-5](https://doi.org/10.1016/S0277-3791(98)00070-5)
- England, J., Atkinson, N., Bednarski, J., Dyke, A. S., Hodgson, D. A., & Ó Cofaigh, C. (2006). The Innuitian Ice Sheet: configuration, dynamics and chronology. *Quaternary Science Reviews*, 25(7–8), 689–703. <https://doi.org/10.1016/J.QUASCIREV.2005.08.007>
- Farmer, D. M. (1975). Penetrative convection in the absence of mean shear. *Quarterly Journal of the Royal Meteorological Society*, 101(430), 869–891. <https://doi.org/10.1002/qj.49710143011>
- Forrest, A. L., Laval, B. E., Pieters, R., & Lim, D. S. S. (2008). Convectively driven transport in temperate lakes. *Limnology and Oceanography*, 53(5 PART 2), 2321–2332. https://doi.org/10.4319/lo.2008.53.5_part_2.2321
- French, H. M. (2018). *The Periglacial Environment* (4th ed.). John Wiley & Sons Ltd. <https://doi.org/10.2307/j.ctt1w6tb9v.3>
- Golosov, S., & Kirillin, G. (2010). A parameterized model of heat storage by lake sediments. *Environmental Modelling and Software*, 25(6), 793–801. <https://doi.org/10.1016/j.envsoft.2010.01.002>
- Grasby, S. E., Proemse, B. C., & Beauchamp, B. (2014). Deep groundwater circulation through the High Arctic cryosphere forms Mars-like gullies. *Geology*, 42(8), 651–654. <https://doi.org/10.1130/G35599.1>
- Green, W. J., & Lyons, W. B. (2009). The saline lakes of the McMurdo Dry Valleys, Antarctica. *Aquatic Geochemistry*, 15(1–2), 321–348. <https://doi.org/10.1007/s10498-008-9052-1>

- Guimond, J. A., Mohammed, A. A., Walvoord, M. A., Bense, V. F., & Kurylyk, B. L. (2021). Saltwater intrusion intensifies coastal permafrost thaw. *Geophysical Research Letters*, 48(19).
<https://doi.org/10.1029/2021GL094776>
- Hamilton, P. B., Gajewski, K., Atkinson, D. E., & Lean, D. R. S. (2001). Physical and chemical limnology of 204 lakes from the Canadian Arctic Archipelago. *Hydrobiologia*, 457, 133–148.
<https://doi.org/10.1023/A:1012275316543>
- Harasyn, M. L., Lamoureux, S., & Normandeau, A. (2017, October 1-4). *Detecting the presence of localized ground water inputs into High Arctic lakes* [Paper presentation]. GeoOttawa 2017 – 70th Canadian Geotechnical Conference and the 12th CGS/IAH-CNC Groundwater Conference Ottawa, CA.
- Harvey, F. E., Lee, R., Rudolph, D. L., & Frape, S. K. (1997). Locating groundwater discharge in large lakes using bottom sediment electrical conductivity mapping. *Water Resources Research*, 33(11), 2609–2615.
- Hassol, S. J. (2004). Impacts of a warming Arctic. In *Arctic Climate Impact Assessment*. Cambridge University Press. <http://www.acia.uaf.edu>
- Hayashi, M., & Rosenberry, D. O. (2002). Effects of ground water exchange on the hydrology and ecology of surface water. In *Ground Water* (Vol. 40, Issue 3, pp. 309–316). National Ground Water Association. <https://doi.org/10.1111/j.1745-6584.2002.tb02659.x>
- Henkemans, E., Frape, S. K., Ruskeeniemi, T., Anderson, N. J., & Hobbs, M. (2018). A landscape-isotopic approach to the geochemical characterization of lakes in the Kangerlussuaq region, west Greenland. *Arctic, Antarctic, and Alpine Research*, 50(1).
<https://doi.org/10.1080/15230430.2017.1420863>
- Huttula, T., Pulkkanen, M., Arkhipov, B., Leppäranta, M., Solbakov, V., Shirasawa, K., & Salonen, K. (2010). Modelling circulation in an ice-covered lake. *Estonian Journal of Earth Sciences*, 59(4), 298–309. <https://doi.org/10.3176/earth.2010.4.06>
- Jansen, J., MacIntyre, S., Barrett, D. C., Chin, Y. P., Cortés, A., Forrest, A. L., Hrycik, A. R., Martin, R., McMeans, B. C., Rautio, M., & Schwefel, R. (2021). Winter limnology: How do hydrodynamics and biogeochemistry shape ecosystems under ice? *Journal of Geophysical Research: Biogeosciences*, 126(6). <https://doi.org/10.1029/2020JG006237>

- Johansson, E., Gustafsson, L. G., Berglund, S., Lindborg, T., Selroos, J. O., Claesson Liljedahl, L., & Destouni, G. (2015). Data evaluation and numerical modeling of hydrological interactions between active layer, lake and talik in a permafrost catchment, Western Greenland. *Journal of Hydrology*, 527, 688–703. <https://doi.org/10.1016/j.jhydrol.2015.05.026>
- Johnston, G., & Brown, R. (1964). Some observations on permafrost distribution at a lake in the Mackenzie Delta, N. W.T., Canada. *Arctic Institute of North America*, 17(3), 145–216.
- Judge, A. (1973). The predictions of permafrost thickness. *Canadian Geotechnical Journal*, 10(1), 313–321.
- Jutebring Sterte, E., Johansson, E., Sjöberg, Y., Huseby Karlsen, R., & Laudon, H. (2018). Groundwater-surface water interactions across scales in a boreal landscape investigated using a numerical modelling approach. *Journal of Hydrology*, 560, 184–201. <https://doi.org/10.1016/j.jhydrol.2018.03.011>
- Kalbus, E., Reinstorf, F., & Schirmer, M. (2006). Measuring methods for groundwater - surface water interactions: A review. In *Hydrology and Earth System Sciences* (Vol. 10, Issue 6). <https://doi.org/10.5194/hess-10-873-2006>
- Keating, K., Binley, A., Bense, V., van Dam, R. L., & Christiansen, H. H. (2018). Combined geophysical measurements provide evidence for unfrozen water in permafrost in the Adventdalen Valley in Svalbard. *Geophysical Research Letters*, 45(15), 7606–7614. <https://doi.org/10.1029/2017GL076508>
- Kirillin, G., Aslamov, I., Leppäranta, M., & Lindgren, E. (2018). Turbulent mixing and heat fluxes under lake ice: the role of seiche oscillations. *Hydrology and Earth System Sciences. Discuss.* <https://doi.org/10.5194/hess-2018-376>
- Kirillin, G., Leppäranta, M., Terzhevik, A., Granin, N., Bernhardt, J., Engelhardt, C., Efremova, T., Golosov, S., Palshin, N., Sherstyankin, P., Zdorovenova, G., & Zdorovenov, R. (2012). Physics of seasonally ice-covered lakes: A review. *Aquatic Sciences*, 74(4), 659–682. <https://doi.org/10.1007/s00027-012-0279-y>
- Klanten, Y., Triglav, K., Marois, C., & Antoniadou, D. (2021). Under-ice limnology of coastal valley lakes at the edge of the Arctic Ocean. *Arctic Science*, 7(4), 813–831. <https://cdnsicepub.com/doi/full/10.1139/as-2020-0038>

- Lafrenière, M. J., & Lamoureux, S. F. (2019). Effects of changing permafrost conditions on hydrological processes and fluvial fluxes. *Earth-Science Reviews*, *191*, 212–223.
<https://doi.org/10.1016/j.earscirev.2019.02.018>
- Lecher, A. L. (2017). Groundwater discharge in the Arctic: a review of studies and implications for biogeochemistry. *Hydrology*, *4*(3), 1–16. <https://doi.org/10.3390/hydrology4030041>
- Leppäranta, M. (2010). Modelling the formation and decay of lake ice. In *The Impact of Climate Change on European Lakes* (pp. 63–83). Springer Netherlands. https://doi.org/10.1007/978-90-481-2945-4_5
- Lewis, T., Lamoureux, S. F., Normandeau, A., & Dugan, H. A. (2018). Hyperpycnal flows control the persistence and flushing of hypoxic high conductivity bottom water in a High Arctic lake. *Arctic Science*, *4*, 25–41. <https://doi.org/10.1139/as-2017-0022>
- Lewis, W.M. (1983). A revised classification of lakes based on mixing. *Canadian Journal of Fisheries and Aquatic Sciences*, *40*, 1779–1787.
- Liao, C., & Zhuang, Q. (2017). Quantifying the role of permafrost distribution in groundwater and surface water interactions using a three-dimensional hydrological model. *Arctic, Antarctic, and Alpine Research*, *49*(1), 81–100. <https://doi.org/10.1657/AAAR0016-022>
- Likens, G., & Ragotzkie, R. (1965). Vertical water motions in a small ice-covered lake. *Journal of Geophysical Research*, *70*(10). 2333–2344.
- Livingstone, D. M., Adrian, R., Blenckner, T., George, G., & Weyhenmeyer, G. A. (2010). Lake Ice Phenology. In *The Impact of Climate Change on European Lakes* (pp. 51–61). Springer Netherlands. https://doi.org/10.1007/978-90-481-2945-4_4
- MacIntyre, S., Cortés, A., & Sadro, S. (2018). Sediment respiration drives circulation and production of CO₂ in ice-covered Alaskan arctic lakes. *Limnology and Oceanography Letters*, *3*(3), 302–310.
<https://doi.org/10.1002/lol2.10083>
- Magnuson, J. J., Wynne, R. H., Benson, B. J., & Robertson, D. M. (2000). Lake and river ice as a powerful indicator of past and present climates. *Verhandlungen des Internationalen Verein Limnologie*, *1922-2010*, *27*(5), 2749–2756. <https://doi.org/10.1080/03680770.1998.11898166>

- Malm, J. (1998). Bottom buoyancy layer in an ice-covered lake. *Water Resources Research*, 34(11), 2981–2993. <https://doi.org/10.1029/98WR01904>
- Matthews, P. C., & Heaney, S. I. (1987). Solar heating and its influence on mixing in ice-covered lakes. *Freshwater Biology*, 18(1), 135–149. <https://doi.org/10.1111/j.1365-2427.1987.tb01302.x>
- Mishra, V., Cherkauer, K. A., Bowling, L. C., & Huber, M. (2011). Lake Ice phenology of small lakes: Impacts of climate variability in the Great Lakes region. *Global and Planetary Change*, 76(3–4), 166–185. <https://doi.org/10.1016/j.gloplacha.2011.01.004>
- Mortimer, C. H., & Mackereth, F. J. H. (1958). Convection and its consequences in ice-covered lakes. *Verhandlungen des Internationalen Verein Limnologie*, 13(2), 923–932. <https://doi.org/10.1080/03680770.1956.11895490>
- Mueller, D. R., van Hove, P., Antoniadou, D., Jeffries, M. O., & Vincent, W. F. (2009). High Arctic lakes as sentinel ecosystems: cascading regime shifts in climate, ice cover, and mixing. *Limnology and Oceanography*, 54(6 part 2), 2371–2385. https://doi.org/10.4319/lo.2009.54.6_part_2.2371
- Nixon, F. C. (2012). *The glacial, sea level, and sea ice histories of Melville and Eglinton islands, western Canadian High Arctic: Last Glacial Maximum to present*. University of Alberta.
- Omelon, C. R., Pollard, W. H., & Andersen, D. T. (2006). A geochemical evaluation of perennial spring activity and associated mineral precipitates at Expedition Fjord, Axel Heiberg Island, Canadian High Arctic. *Applied Geochemistry*, 21(1), 1–15. <https://doi.org/10.1016/j.apgeochem.2005.08.004>
- Ouellet, M., Dickman, M., Bisson, M., & Pagé, P. (1989). Physico-chemical characteristics and origin of hypersaline meromictic Lake Garro in the Canadian high Arctic. *Hydrobiologia*, 172(1), 215–234. <https://doi.org/10.1007/BF00031624>
- Paquette, M., Fortier, D., & Vincent, W. F. (2017). Water tracks in the High Arctic: a hydrological network dominated by rapid subsurface flow through patterned ground. *Arctic Science*, 3(2), 334–353. <https://doi.org/10.1139/as-2016-0014>
- Petrov, M. P., Terzhevik, A. Y., Zdorovenov, R. E., & Zdorovenova, G. E. (2007). Motion of water in an ice-covered shallow lake. *Water Resources*, 34(2), 113–122. <https://doi.org/10.1134/S0097807807020017>

- Pieters, R., & Lawrence, G. A. (2009). Effect of salt exclusion from lake ice on seasonal circulation. *Limnology and Oceanography*, *54*(2), 401–412. <https://doi.org/10.4319/lo.2009.54.2.0401>
- Pollard, W. H. (2005). Icing processes associated with High Arctic perennial springs, Axel Heiberg Island, Nunavut, Canada. *Permafrost and Periglacial Processes*, *16*(1), 51–68. <https://doi.org/10.1002/ppp.515>
- Pollard, W., Omelon, C., Andersen, D., & McKay, C. (1999). Perennial spring occurrence in the Expedition Fiord area of western Axel Heiberg Island, Canadian High Arctic. *Canadian Journal of Earth Sciences*, *36*, 105–120.
- Rahm, L. (1985). The thermally forced circulation in a small, ice-covered lake. *American Society of Limnology and Oceanography*, *30*(5), 1122–1128.
- Rautio, A., & Korkka-Niemi, K. (2011). Characterization of groundwater-lake water interactions at Pyhäjärvi, a lake in SW Finland. *Boreal Environment Research*, *16*(5), 363–380.
- Rizk, W., Kirillin, G., & Leppä Ranta, M. (2014). Basin-scale circulation and heat fluxes in ice-covered lakes. *Limnology and Oceanography*, *59*(2), 445–464. <https://doi.org/10.4319/lo.2014.59.02.0445>
- Roberts, K. E., Lamoureux, S. F., Kyser, T. K., Muir, D. C. G., Lafrenière, M. J., Iqaluk, D., Pieńkowski, A. J., & Normandeau, A. (2017). Climate and permafrost effects on the chemistry and ecosystems of High Arctic Lakes. *Scientific Reports*, *7*(1), 1–8. <https://doi.org/10.1038/s41598-017-13658-9>
- Rosenberry, D. O., Lewandowski, J., Meinikmann, K., & Nützmänn, G. (2015). Groundwater - the disregarded component in lake water and nutrient budgets. Part 1: Effects of groundwater on hydrology. *Hydrological Processes*, *29*(13), 2895–2921. <https://doi.org/10.1002/hyp.10403>
- Rosenberry, D. O., & Morin, R. H. (2004). Use of an electromagnetic seepage meter to investigate temporal variability in lake seepage. *Ground Water*, *42*(1). <https://doi.org/10.1111/j.1745-6584.2004.tb02451.x>
- Saber, A., James, D. E., & Hayes, D. F. (2019). Estimation of water quality profiles in deep lakes based on easily measurable constituents at the water surface using artificial neural networks coupled with stationary wavelet transform. *Science of the Total Environment*, *694*, 133690. <https://doi.org/10.1016/j.scitotenv.2019.133690>

- Salonen, K., Pulkkanen, M., Salmi, P., & Griffiths, R. W. (2014). Interannual variability of circulation under spring ice in a boreal lake. *Limnology and Oceanography*, *59*(6), 2121–2132.
<https://doi.org/10.4319/lo.2014.59.6.2121>
- Scheidegger, J. M., Bense, V. F., & Grasby, S. E. (2012). Transient nature of Arctic spring systems driven by subglacial meltwater. *Geophysical Research Letters*, *39*(12).
<https://doi.org/10.1029/2012GL051445>
- Sharma, S., Blagrove, K., Magnuson, J. J., O'Reilly, C. M., Oliver, S., Batt, R. D., Magee, M. R., Straile, D., Weyhenmeyer, G. A., Winslow, L., & Woolway, R. I. (2019). Widespread loss of lake ice around the Northern Hemisphere in a warming world. *Nature Climate Change*, *9*(3), 227–231.
<https://doi.org/10.1038/s41558-018-0393-5>
- Sharma, S., Richardson, D. C., Woolway, R. I., Imrit, M. A., Bouffard, D., Blagrove, K., Daly, J., Filazzola, A., Granin, N., Korhonen, J., Magnuson, J., Marszelewski, W., Matsuzaki, S. I. S., Perry, W., Robertson, D. M., Rudstam, L. G., Weyhenmeyer, G. A., & Yao, H. (2021). Loss of ice cover, shifting phenology, and more extreme events in northern hemisphere lakes. *Journal of Geophysical Research: Biogeosciences*, *126*(10). <https://doi.org/10.1029/2021JG006348>
- Stewart, K. M., & Platford, R. F. (1986). Hypersaline gradients in two Canadian High Arctic lakes. *Canadian Journal of Fisheries and Aquatic Sciences*, *43*(9), 1795–1803.
<https://doi.org/10.1139/f86-223>
- Stokes, C. R. (2017). Deglaciation of the Laurentide ice sheet from the last glacial maximum. *Geographical Research Letters*, *43*(2), 377–428. <https://doi.org/10.18172/cig.3237>
- Surdu, C. M., Duguay, C. R., & Prieto, D. F. (2016). Evidence of recent changes in the ice regime of lakes in the Canadian High Arctic from spaceborne satellite observations. *Cryosphere*, *10*(3), 941–960. <https://doi.org/10.5194/tc-10-941-2016>
- Szesztay, K. (1974). Water balance and water level fluctuations of lakes. *Hydrological Sciences Bulletin*, *19*(1), 73–84. <https://doi.org/10.1080/02626667409493872>
- Terzhevik, A., Golosov, S., Palshin, N., Mitrokhov, A., Zdrovennov, R., Zdrovennova, G., Kirillin, G., Shipunova, E., & Zverev, I. (2009). Some features of the thermal and dissolved oxygen structure in boreal, shallow ice-covered Lake Vendyurskoe, Russia. *Aquatic Ecology*, *43*(3), 617–627.
<https://doi.org/10.1007/s10452-009-9288-x>

- U.S. Geological Survey. (2018). Lakes and Reservoirs-Guidelines for Study Design and Sampling. In *U.S. Geological Survey Techniques and Methods, book 9* (1st ed.).
<https://pubs.er.usgs.gov/publication/tm9A10>
- Utting, N., Lauriol, B., Mochnacz, N., Aeschbach-Hertig, W., & Clark, I. (2013). Noble gas and isotope geochemistry in western Canadian Arctic watersheds: Tracing groundwater recharge in permafrost terrain. *Hydrogeology Journal*, 21(1), 79–91. <https://doi.org/10.1007/s10040-012-0913-8>
- Van Hove, P., Belzile, C., Gibson, J. A. E., & Vincent, W. F. (2006). Coupled landscape-lake evolution in High Arctic Canada. *Canadian Journal of Earth Sciences*, 43(5), 533–546.
<https://doi.org/10.1139/E06-003>
- Veillette, J., Martineau, M. J., Antoniades, D., Sarrazin, D., & Vincent, W. F. (2010). Effects of loss of perennial lake ice on mixing and phytoplankton dynamics: Insights from High Arctic Canada. *Annals of Glaciology*, 51(56), 56–70. <https://doi.org/10.3189/172756411795931921>
- Vincent, W. F. (2009). Effects of climate change on lakes. In G. E. Likens (Ed.), *Biogeochemistry of Inland Waters: A Derivative of Encyclopedia of Inland Waters*. Elsevier.
- Vincent, W. F., Macintyre, S., Spigel, R. H., & Laurion, I. (2008). The physical limnology of high-latitude lakes. In W. F. Vincent & J. Laybourn-Parrym (Eds.), *Polar Lakes and Rivers: Limnology of Arctic and Antarctic Aquatic Ecosystems* (pp. 65–81). Oxford University Press.
<https://doi.org/10.1093/acprof:oso/9780199213887.003.0004>
- Walvoord, M. A., & Kurylyk, B. L. (2016). Hydrologic impacts of thawing permafrost-a review. *Vadose Zone Journal*, 15(6), 20. <https://doi.org/10.2136/vzj2016.01.0010>
- Walvoord, M. A., Voss, C. I., & Wellman, T. P. (2012). Influence of permafrost distribution on groundwater flow in the context of climate-driven permafrost thaw: Example from Yukon Flats basin, Alaska, United States. *Water Resources Research*, 48(7).
<https://doi.org/10.1029/2011WR011595>
- Wang, X., Qiu, Y., Zhang, Y., Lemmetyinen, J., Cheng, B., Liang, W., & Leppäranta, M. (2021). A lake ice phenology dataset for the Northern Hemisphere based on passive microwave remote sensing. *Big Earth Data*. <https://doi.org/10.1080/20964471.2021.1992916>

- Welch, H. E., & Bergmann, M. A. (1985). Water circulation in small Arctic lakes in winter. *Canadian Journal of Fisheries and Aquatic Sciences*, 42, 506–520. <https://doi.org/10.1139/f85-068>
- Wellman, T. P., Voss, C. I., & Walvoord, M. A. (2013). Impacts of climate, lake size, and supra- and sub-permafrost groundwater flow on lake-talik evolution, Yukon Flats, Alaska (USA). *Hydrogeology Journal*, 21(1). <https://doi.org/10.1007/s10040-012-0941-4>
- Wetzel, R. G. (2001). Fate of Heat. In *Limnology: Lake and River Ecosystems* (3rd ed.). Academic Press. <https://doi.org/10.1016/B978-0-08-057439-4.50010-1>.
- Williams, S. G., & Stefan, H. G. (2006). Modeling of lake ice characteristics in North America using climate, geography, and lake bathymetry. *Journal of Cold Regions Engineering*, 20(4), 140–167. [https://doi.org/10.1061/\(asce\)0887-381x\(2006\)20:4\(140\)](https://doi.org/10.1061/(asce)0887-381x(2006)20:4(140))
- Williamson, C. E., Saros, J. E., Vincent, W. F., & Smol, J. P. (2009). Lakes and reservoirs as sentinels, integrators, and regulators of climate change. *Limnology and Oceanography*, 54, 2273–2282. https://doi.org/10.4319/lo.2009.54.6_part_2.2273
- Woo, M.K. (2012a). Cold lakes. In *Permafrost Hydrology* (pp. 305–346). Springer Berlin Heidelberg. https://doi.org/10.1007/978-3-642-23462-0_7
- Woo, M.K. (2012b). Groundwater. In *Permafrost Hydrology* (pp. 73–118). Springer Berlin Heidelberg. https://doi.org/10.1007/978-3-642-23462-0_3
- Woo, M.K. (2012c). Introduction. In *Permafrost Hydrology* (pp. 1–34). Springer Berlin Heidelberg. https://doi.org/10.1007/978-3-642-23462-0_1
- Woo, M. K., Kane, D. L., Carey, S. K., & Yang, D. (2008). Progress in permafrost hydrology in the new millennium. *Permafrost and Periglacial Processes*, 19(2), 237–254. <https://doi.org/10.1002/ppp>
- Woo, M., & Woo, M. (2012). Moisture and Heat. In *Permafrost Hydrology* (pp. 35–72). Springer Berlin Heidelberg. https://doi.org/10.1007/978-3-642-23462-0_2
- Woolway, R. I., Kraemer, B. M., Lenters, J. D., Merchant, C. J., O'Reilly, C. M., & Sharma, S. (2020). Global lake responses to climate change. *Nature Reviews Earth & Environment*, 1(8), 388–403. <https://doi.org/10.1038/s43017-020-0067-5>

- Yang, B., Wells, M. G., McMeans, B. C., Dugan, H. A., Rusak, J. A., Weyhenmeyer, G. A., Brentrup, J. A., Hrycik, A. R., Laas, A., Pilla, R. M., Austin, J. A., Blanchfield, P. J., Carey, C. C., Guzzo, M. M., Lottig, N. R., MacKay, M. D., Middel, T. A., Pierson, D. C., Wang, J., & Young, J. D. (2021). A new thermal categorization of ice-covered lakes. *Geophysical Research Letters*, *48*(3), 1–11. <https://doi.org/10.1029/2020GL091374>
- Yang, B., Young, J., Brown, L., & Wells, M. (2017). High-frequency observations of temperature and dissolved oxygen reveal under-ice convection in a large lake. *Geophysical Research Letters*, *44*(24), 12,218–12,226. <https://doi.org/10.1002/2017GL075373>
- Yokoyama, Y., Lambeck, K., & Deckker, P. de. (2000). Timing of last glacial maximum from observed sea level minima. *Nature*, *406*, 713–716.
- Zdrovennova, G., Palshin, N., Golosov, S., Efremova, T., Belashev, B., Bogdanov, S., Fedorova, I., Zverev, I., Zdrovennov, R., & Terzhevik, A. (2021a). Dissolved oxygen in a shallow ice-covered lake in winter: Effect of changes in light, thermal and ice regimes. *Water (Switzerland)*, *13*(17). <https://doi.org/10.3390/w13172435>
- Zdrovennova, G., Terzhevik, A., Palshin, N., Efremova, T., Bogdanov, S., & Zdrovennov, R. (2021b). Seasonal change in heat flux at the water-bottom sediment boundary in a small lake. *Journal of Physics: Conference Series*, *2131*(3). <https://doi.org/10.1088/1742-6596/2131/3/032080>
- Zentilli, M., Omelon, C. R., Hanley, J., & LeFort, D. (2019). Paleo-hydrothermal predecessor to perennial spring activity in thick permafrost in the Canadian High Arctic, and its relation to deep salt structures: Expedition Fiord, Axel Heiberg Island, Nunavut. *Geofluids*, *2019*, 1–33. <https://doi.org/10.1155/2019/9502904>

Chapter 3

Investigating multi-year (2006-2019) ionic concentrations to characterize groundwater signatures occurring in two coastal High Arctic lakes

3.1 Abstract

Over a 10–15-year timescale, two lakes at the Cape Bounty Arctic Watershed Observatory (CBAWO), Melville Island, Nunavut, Canada have demonstrated a dramatic decadal shift in water column geochemistry. The shift, determined through analysis of geochemical data collected between 2006 and 2019, shows that water column geochemistry has transitioned away from ionic ratios similar to marine sources to ratios more akin to those observed in the catchment rivers. Since 2012 (the warmest year on record at the CBAWO) SO_4^{2-} in both lakes is becoming disproportionately enriched compared to other major dissolved ions. Additionally, lake water column specific conductivity and dissolved ion concentration profiles indicate the presence of elevated bottom water conductivity (EBWC) in the bottom <0.5-2.0 m of the lakes in late winter, which becomes less evident (or absent) by summer due to seasonal lake turnover. Ratios of mean major dissolved ion concentrations of bottom water to overlying column water (B:C) indicate that the ionic composition of the EBWC is distinctly different from the water column. Moreover, ionic ratios reveal bottom water SO_4^{2-} enrichments lag those in the overlying water column, suggesting a separate source for this water. Observed rapid enrichments of SO_4^{2-} in the lakes indicate notable landscape changes in the catchments of this High Arctic hydrologic setting. It is suggested that EBWC may be derived from slow, sub-lacustrine ion-rich sediment pore water diffusion.

3.2 Introduction

High Arctic freshwater lakes are strongly influenced by persistent ice cover and permafrost conditions, making them highly sensitive to small changes in climate (Adrian et al., 2009; Van Hove et al., 2006; Vincent, 2009; Vincent et al., 2008). Studies indicate that rapid climate change is increasing

near-surface permafrost thaw and altering subsurface hydrologic pathways across cold regions (Hassol, 2004; Kokelj et al., 2009; Lawrence & Slater, 2005). Additionally, increases in later season rainfall events are changing the timing and magnitude of surface hydrologic fluxes (Beel et al., 2021; Lewis et al., 2012). Increasing thermal perturbations in permafrost combined with this late season rainfall results in the mobilization of soluble ions preserved in the deep active layer and shallow permafrost, shifting the chemical composition of waterbodies downstream (Lamoureux & Lafrenière, 2017; Roberts et al., 2017). These changes will significantly impact freshwater lakes by delivering previously immobile soluble ions to surface waters, altering water quality in Arctic catchments. These increasing air temperatures are transitioning the Arctic towards a more groundwater-dominated system due to increases in permafrost thaw, which could impact the distribution, thickness and other hydrogeologic properties of permafrost (Lecher, 2017). Therefore, there is a need to better understand how thaw alters both subsurface flow dynamics and surface water geochemistry as well as the potential for increased groundwater-surface water interactions, and to characterize hydrogeochemical properties of groundwater environments as permafrost evolves (Cochand et al., 2019; Lamoureux & Lafrenière, 2017).

Lakes in the High Arctic present a compelling example of a surface feature that can strongly influence the thermal regime of permafrost. Surface water bodies such as lakes warm the surrounding permafrost to form taliks, unfrozen ground that can facilitate the exchange of waters between surface and subsurface environments (French, 2018; Woo, 2012a). In High Arctic lakes, evidence of sub-permafrost groundwater entering surface waters via the presence of taliks has been increasingly identified (Dugan & Lamoureux, 2011; Harasyn et al., 2017; Ouellet et al., 1989; Roberts et al., 2017; Stewart & Platford, 1986). Evidence of groundwater seepage into lakes has also been identified in lake bottoms through measured increases in electrical conductivity in bottom waters, which have higher dissolved solutes than the overlying water column (Biddanda et al., 2006; Harvey et al., 1997; Rautio & Korkka-Niemi, 2011).

This study builds upon the work of Harasyn et al., (2017) by examining the geochemistry of two cold, monomictic High Arctic lakes at the Cape Bounty Arctic Watershed Observatory (CBAWO),

Melville Island, Nunavut Canada. The CBAWO lakes are situated just one kilometer apart from each other with similar morphological characteristics and geological settings, and are mainly composed of freshwater, however lower water column properties were indicative of groundwater (increased temperature, specific conductivity (SpC), and lower dissolved oxygen (DO)) in only one lake, with no measurable change in the other (Harasyn et al., 2017). Despite this, both lakes exhibit ionic ratios similar to marine water in the deepest areas, greatly differing in composition from the ratios in the water column. In addition, SO_4^{2-} concentrations in the water column have been found to be high in comparison to the bottom water (Roberts et al., 2017). As the coastal landscape where the lakes reside was recently submerged after the LGM, marine signatures are expected for these coastal lakes. However, it is still unknown how these distinct geochemical compositions have varied over time within the water column. Using major dissolved ion geochemical data collected from both water column and bottom water regions between 2006-2019, this study investigates the multi-year geochemical evolution of the CBAWO lakes. If the composition of the ambient water column evolves in a manner that is distinctly different from the geochemical signatures of the bottom water, it is hypothesized that groundwater seepage is altering the composition in the bottom few meters of these lakes.

3.3 Study Area and Background

3.3.1 Climate and Permafrost

This research was conducted on East and West Lakes (unofficial name) at CBAWO (74°55'N, 109°35'W), located on the south-central coast of Melville Island, Nunavut, in the Canadian High Arctic (Figure 3.1). The CBAWO is situated in a polar semi-desert climate with a mean annual air temperature of -14.8°C ($\pm 1.3^\circ\text{C}$), receiving no more than 160 mm of precipitation annually (Beel et al., 2021; Roberts et al., 2017). Only in June, July, and August do mean monthly air temperatures rise above 0°C and the uppermost portion of the ground thaws (active layer) to depths between 0.5 to 1.0 meters below the surface. Below the active layer, mean annual temperatures of the permafrost (7 m depth) were -11.1 °C

between June 2012 and July 2019 from a borehole located 50 m from the shore of West Lake. Continuous permafrost reaches depths of 500+ meters in the region (Judge, 1973).

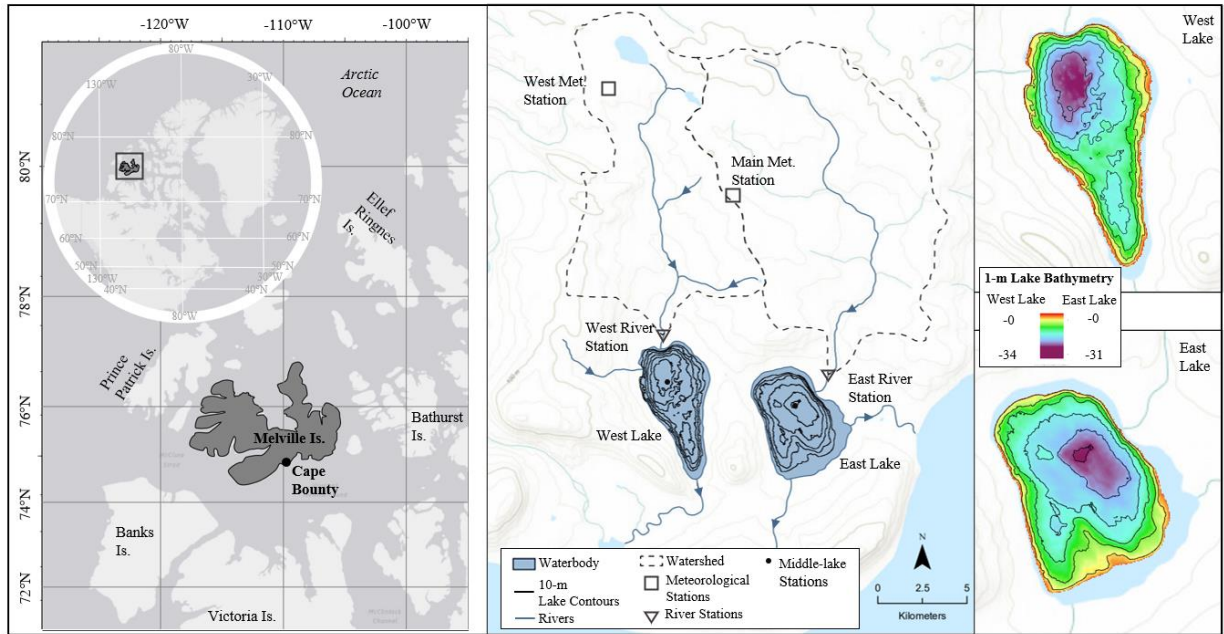


Figure 3.1: The study area map of the Cape Bounty Arctic Watershed Observatory on Melville Island in the Canadian Arctic Archipelago (left). Locations of East Lake and West Lake with 1 m resolution bathymetry (10 m contour interval) showing lake bottom terrain (right). Middle lake water column sampling stations are marked as circles. West Lake station located at 74°53'41.4"N 109°35'54.9"W. East Lake station located at 74°53'30.2"N 109°32'08.3"W. Base map courtesy of Esri Canada.

3.3.2 Geology

The CBAWO region is underlain by pre-late Wisconsinan glacial till with both lacustrine and oceanic sources (England et al., 2009). Both lakes are hypothesized to be Late Wisconsinan glacial scour basins, which transitioned from marine to terrestrial influence due to isostatic uplift following glacial retreat between 4197-1763 yr. BP (before present) (Cuven et al., 2011). Lake-bottom sediments are laminated silty-clay underlain by massive muds (Cuven et al., 2011). Soils and unconsolidated sediments are underlain by folded Paleozoic bedrock of the Cape Bounty Anticline, where a lithologic unconformity (~290° strike) separates two Devonian-aged Formations, dipping 15° southwest (Harrison, 1995). The bedrock south of the boundary is characterized by shallow-marine shales and deltaic quartzose sandstones of the Weatherall Formation subcropping beneath the south end of the lakes. North of the lithologic boundary, surficial bedrock changes to the Helca Bay Formation that is composed of fluvial-deltaic terrigenous quartz sandstone and siltstone containing minor shale and coals (Harrison, 1995).

3.3.3 Hydrology

Hydrological and limnological records have been collected from East and West lakes since 2003. The lakes are situated in separate drainage catchments (Figure 3.1), each having a main river inflow (East River and West River, unofficial names) during the thaw season (June - September). Runoff generated in both rivers is primarily nival; however, rainfall events have become more common in the region and have been known to produce significant runoff events (Beel et al., 2021). Peak discharge occurs in June and recedes with snowmelt, reaching baseflow in July and August and ceasing completely when the ground begins to freeze again. Outflow from these lakes drains to the south and eventually into the sea.

The lakes are similar in terms of area and volume in which lake dimensions (Table 3.1) have been interpreted through detailed (1-m horizontal) resolution bathymetric surveys (Normandeau et al., 2016). This data was used to locate bathymetric depressions at the bottom of both East and West lakes as targeted sites for sample collection and geochemical analysis to determine their potential as

locations of groundwater inputs (Harasyn et al., 2017). Bathymetric data has also revealed lake bottom sediment deposits resulting from former mass movement events along the slopes of West Lake. Recent events in 2008, 2011 and 2012 have occurred as subaqueous slumps in West Lake, causing an increase in turbidity due to the suspension of fine-grained sediments for prolonged periods in the water column (Dugan, 2010; Roberts et al., 2017), which are thought to impact complete mixing of the water column in spring (Harasyn et al., 2017).

Table 3.1: Characteristics of East and West Lakes at CBAWO.
**Timing of typical ice-off determined from time-lapse camera images.*

	West Lake	East Lake
Lake area (km²)	1.4	1.6
Maximum depth (m)	34	31
Lake volume (km³)	0.02145	0.02086
Watershed area (km²)	8.0	11.6
Ice thickness (m)	2.0 - 2.3	2.0 - 2.3
Typical ice-off *	Late July - Early August	Mid-July

3.4 Methods

3.4.1 Water Column

For this study, lake profiles and water samples collected from 2006-2019 were used to assess the geochemical composition of West and East lakes. Geochemical data has been recorded at CBAWO since 2006 in West Lake and 2008 in East Lake, with limited sampling for years 2011, 2013 and 2015. Temperature (°C), SpC (µS/cm; corrected at 25 °C), and DO (% saturation) measurements through the water column were collected from vertical casts using a Richard Branker Research (RBR) XR-420 CTD [SpC ($\sigma = 1 \mu\text{S/cm}$), temperature ($\sigma = 0.001 \text{ }^\circ\text{C}$), DO (3 %), and depth] instrument (factory calibrated annually). Late winter casts were collected from a fixed station on ice near the middle of both lakes starting in 2006 (Figure 3.1). The CTD was lowered slowly (~30 sec/m, slowed to 50 sec/m for the

bottom 2 m) to capture any subtle changes through the water column. Summer casts which were collected by boat were subject to drift and did not always measure the deepest locations in the lakes. Results from some of these casts have been previously published (Table 3.2; Harasyn et al., 2017; Roberts et al., 2017). Turbidity measurements were also collected but is not considered in this study.

Water column samples analyzed for this study were collected from the same sampling stations (Figure 3.1) using a 400 ml stainless-steel Kemmerer sampler at depth intervals of 2, 10, 15, 20, 25, 27 (East), 30, and 32 m (West). East Lake's maximum depth is 30 m, whereas West Lake's maximum depth is 35 m. Samples were collected each year from May to August between 2006 and 2019, vacuum filtered through 0.45 μm cellulose nitrate filters and stored in the dark without headspace at 4°C in 250 ml polypropylene bottles. Samples were analyzed by ion chromatography at Queen's University using a Dionex (Sunnyvale, CA, USA) chromatograph. Cations (Na^+ , Ca^{2+} , Mg^{2+} , and Li^+ , NH_4^+ , K^+ and Sr^{2+}) were measured isocratically with 16 methanesulfonic acid eluent, and anions (F^- , NO_3^- , Br^- , PO_4^{3-} , SO_4^{2-} and Cl^-) were separated by gradient elution with 16-40 mM potassium hydroxide.

Table 3.2: Showing conductivity, temperature, depth (CTD) measurements and water column sampling dates for lake water column profiles. Sampling between mid-July to early August was not possible due to mobile ice during breakup.

Year	West Lake	East Lake
2006	June-01, June-18, June-21, June-24, June-27, June-30, July-03, July-07, July-10, July-13, July-16, July-19	May-31
2007	June-04, June-10, June-13, June-14, June-16, June-18, June-19, June-21, June-25, June-28, June-30, July-01, July-03, July-04, July-07, July-10, July-12, July-13, July-15	June-04
2008	May-31, June-03, June-09, June-12, June-15, June-18, June-22, June-25, June-26, June-28, July-01, July-04, July-07, July-10, July-13, July-16, July-19, July-22, Aug-6, Aug-8, Aug-11	June-02, June-03, June-10, June-13, June-16, June-19, June-28, July-01, June-22, June-25, July-04, July-13, July-07
2009	May-25, May-30, June-07, June-17, June-18, June-24, June-30, July-06, July-12, July-18, July-20	May-26, July-05, July-07, July-01, July-13, July-19, July-25
2010	June-08, June-21, June-30, June-24, July-06, July-12, July-14	June-10, June-18, June-21, June-26, July-01, July-07, July-10
2011	-	-
2012	June-04, June-25, June-30, July-08	June-05, June-24, June-29
2013	May-19	Aug-01
2014	May 29, June-18, July-03	June-04
2015	July-15, Aug-03, Aug-21	Aug-04, Aug-20
2016	May-30, June-22, Aug-05, Deep: May-31	May-29, June-21
2017	June-10, July-01, July-08, Aug-03	June-09, June-11, July-06, July-31
2018	May-19, Aug-05	May-18, Aug-08
2019	June 19, Aug-04	June-02, Aug-19

Geochemical data of bottom and column waters in both lakes were analyzed as ionic ratios of SO_4^{2-} to anions (Cl^-) and SO_4^{2-} to cations (Na^+ , Ca^{2+} , Mg^{2+}) from 2006 – 2019. For this study, column and bottom water are defined as two distinct regions (Figure 3.2), with column water encompassing 10-20 m depths and bottom water below 30 m (27 m in East Lake). These depths were chosen to determine differences in geochemical signatures between the two regions (Figure 3.2). The top 10 m was not used due to lake ice effects, as was the transition zone between the water column region and bottom water (20-25 m in East Lake, 20-30 m in West Lake) to eliminate data where mixing between the two regions may occur.

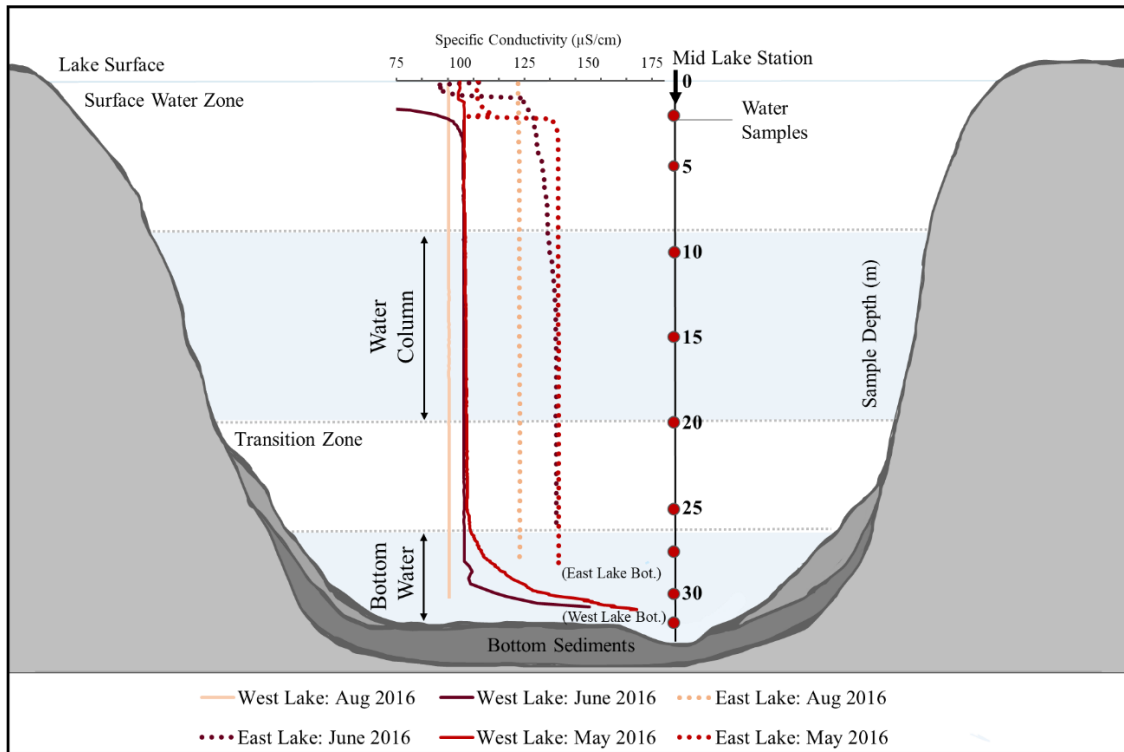


Figure 3.2: Typical specific conductivity profiles (SpC, left) and sampling depths (right) in East and West lakes. Analyses for this work (shaded in blue) focused on the water column (10-20 m) and bottom water regions (<27 m East, <30 m West). SpC profiles display casting data from both lakes in three separate months: May, June, and August. Data used from CTD casts were collected in 2016 at West Lake on May 30, June 22, and August 5, and in East Lake on May 29, June 21, and August 5, 2016. Water samples were collected at two- to five-meter fixed depth intervals (red circles); at 2, 5, 10, 15, 20, 25, 27, 30, and 32 m depths (bottom depths vary for each lake).

Average annual ionic compositions of bottom and column waters were assessed for major dissolved ions (Na^+ , Ca^{2+} , Mg^{2+} , K^+ , SO_4^{2-} , and Cl^-) by calculating mean annual values for all concentrations at each sampled interval in a single year. Average annual ionic ratios were compared temporally within bottom and column waters and between East and West lakes using composition diagrams (Mazor, 2004).

3.4.2 River Flux

In addition to lake waters, river water samples were collected at the CBAWO between 2006 and 2017 to estimate river flux, which represents the delivery (mass) of dissolved ions flowing into a lake per volume of water, or total watershed export by:

$$\text{Major ion}_{flux} (mg) = \left[\frac{1000L}{m^3} \right] * [Q(m^3)] * [\text{major ions } (mgL^{-1})]$$

Annual fluxes displayed in this study at West and East River stations between 2006 and 2017 were calculated using the daily flux of ions in each river (mg; major ion_{flux}). Daily flux was calculated as the product of total daily discharge (Q ; m^3) and daily mean major ions (mg/L) summed for each melt season, and $1000 \text{ L}/m^3$ to convert concentration (mg/L) to mass (mg). To accommodate the large daily flux of ions, milligrams (mg) were converted to megagrams (Mg; $1 \text{ mg} = 10^9 \text{ Mg}$). Total uncertainties for major ion_{flux} are estimated at $\pm 5\text{-}9\%$.

3.5 Results

3.5.1 Water Column Profiles

Water column profiles in May represent the late winter season (May-June) when ice is still present on the surface of the lakes, while August profiles represent the summer season with open water conditions. SpC of both lakes are greatest in late winter (May) compared to summer (August) (Figure 3.3 A). Notable variations in SpC and dissolved ion concentrations occurred in the lakes' bottom two to five meters in late winter (Figure 3.3 A-C). West Lake shows a gradual increase in SpC and Cl^- , Na^+ , and

SO₄²⁻ concentrations compared to East Lake, which shows no notable variation in ion concentrations through the water column of East Lake but a steep increase in late winter SpC in the bottom one meter of the lake. Differences in SpC between bottom water and column water are much more prominent in West Lake (107 μS/cm) compared to East Lake (16 μS/cm). Ionic ratios in West Lake reflect the late winter increase in SpC data, with May bottom water concentrations (mg/L) of all dissolved ions increasing below 30 m (Figure 3.3 B). In contrast, East Lake bottom water ionic ratios do not increase in late winter. Late winter SpC increases in both lake bottom profiles, which decrease to overlying water column values by summer.

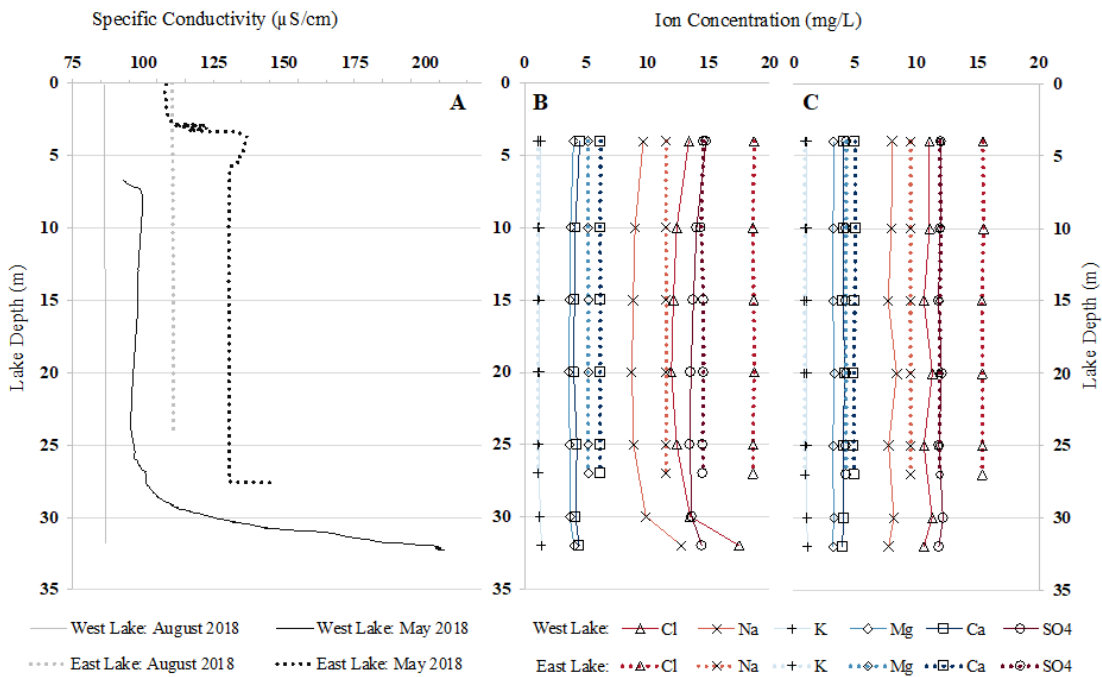


Figure 3.3: Water column casts collected SpC (A) from West Lake (solid lines) and East Lake (dotted lines) at CBAWO in May and August of 2018. May casts are representative of late winter water column conditions, whereas August are representative of summer conditions. Ion concentration profiles of SO₄²⁻, Cl⁻, Na⁺, Ca²⁺, Mg²⁺, and K⁺ display (B) late winter (collected on May-22-2018 in West Lake, and May-23-2018 in East Lake) and (C) summer (collected on the August-5-2018 in West Lake and Aug-8-2018 in East Lake) conditions in the water column of both lakes. Numeric values are displayed in Table 33.

Temperature and DO profiles collected during late winter and summer also demonstrate seasonal variation in the water column of the lakes (Appendix A). In late winter profiles, temperature in both lakes is coldest in proximity to the ice cover (close to 0 °C) in comparison to the water column (close to 2 °C below five meters). Summer temperatures through the water column measure just above 1 °C in West Lake and close to 3 °C in East Lake. DO in both lakes is slightly lower near the surface compared to the bottom water, however there is a greater disparity between DO at the surface and water column of West Lake compared to East Lake. DO in late winter is lowest near the ice surface in both East and West lakes, however, West Lake bottom water is depleted compared to the water column. Whereas in East Lake, DO water column and bottom water are consistent.

3.5.2 Water Column Ion Concentrations and Ratios

Ion concentrations of both lakes are dominated by SO_4^{2-} and Cl^- , and concentrations are generally higher in East Lake than in West Lake (Figure 3.3, Table 3.3). Seasonally, water column ion concentrations in both lakes are greatest in late winter and lower in the summer (Table 3.3). West Lake bottom water shows a gradual increase in SpC towards the lake bottom, increasing from 100 $\mu\text{S}/\text{cm}$ at 25 m depth to values greater than 200 $\mu\text{S}/\text{cm}$ at 32 m depth. The increased dissolved ions in West Lake occur with late winter increases in Cl^- concentrations (Table 3.3). In West Lake, the late-winter (May) water column is primarily dominated by SO_4^{2-} ions ($\text{SO}_4^{2-} > \text{Cl}^- > \text{Na}^+ > \text{Ca}^{2+} > \text{Mg}^{2+} > \text{K}^+$ at 15-m depth), where bottom water concentrations are Cl^- dominant ($\text{Cl}^- > \text{SO}_4^{2-} > \text{Na}^+ > \text{Ca}^{2+} > \text{Mg}^{2+} > \text{K}^+$ at > 30-m depth) (Table 3.3). By August, West Lake's bottom and column water ion composition become fully SO_4^{2-} dominant. In comparison, ion concentrations in East Lake are consistently dominated by Cl^- through the entire water column (both bottom and column water) in both May and August ($\text{Cl}^- > \text{SO}_4^{2-} > \text{Na}^+ > \text{Ca}^{2+} > \text{Mg}^{2+} > \text{K}^+$ at 15-m and > 27-m depth) (Table 3.3). The recorded abrupt increase in bottom water SpC in East Lake does not correspond with ion concentrations and is assumed to reflect the sensor touching the lake bottom sediments.

Table 3.3: Ion concentrations from vertical casts collected in May and August 2018 from middle stations in West and East lakes at CBAWO. Column water values highlighted in blue; bottom water sample values highlighted in orange.

Lake	Date (yyyy-mm-dd)	Depth (m)	Cl ⁻ (mg/L)	SO ₄ ²⁻ (mg/L)	Na ⁺ (mg/L)	K ⁺ (mg/L)	Mg ²⁺ (mg/L)	Ca ²⁺ (mg/L)
West	2018-05-22	4	13.43	14.83	9.70	1.32	4.00	4.51
West	2018-05-22	10	12.44	14.05	9.04	1.22	3.75	4.15
West	2018-05-22	15	12.16	13.79	8.87	1.20	3.68	4.07
West	2018-05-22	20	12.00	13.58	8.77	1.19	3.63	4.02
West	2018-05-22	25	12.44	13.51	8.93	1.18	3.69	4.29
West	2018-05-22	30	13.50	13.66	9.90	1.25	3.68	4.18
West	2018-05-22	32	17.52	14.48	12.81	1.39	4.04	4.46
West	2018-08-05	4	11.07	12.01	8.02	1.06	3.25	4.07
West	2018-08-05	10	11.08	11.96	7.96	1.05	3.23	4.03
West	2018-08-05	15	10.61	11.81	7.70	1.05	3.20	4.03
West	2018-08-05	20	11.31	12.08	8.40	1.07	3.32	4.16
West	2018-08-05	25	10.64	11.85	7.74	1.05	3.20	4.04
West	2018-08-05	30	11.30	12.18	8.17	1.07	3.27	4.10
West	2018-08-05	32	10.60	11.84	7.74	1.10	3.19	3.94
East	2018-05-23	4	18.75	14.61	11.56	1.09	5.20	6.19
East	2018-05-23	10	18.66	14.42	11.54	1.09	5.19	6.17
East	2018-05-23	15	18.72	14.62	11.58	1.10	5.21	6.19
East	2018-05-23	20	18.76	14.63	11.58	1.09	5.20	6.18
East	2018-05-23	25	18.65	14.55	11.55	1.09	5.20	6.18
East	2018-05-23	27	18.67	14.56	11.55	1.09	5.20	6.18
East	2018-08-08	4	15.42	11.93	9.53	0.91	4.29	5.01
East	2018-08-08	10	15.47	11.98	9.53	0.91	4.26	5.05
East	2018-08-08	15	15.35	11.91	9.52	0.90	4.25	4.99
East	2018-08-08	20	15.39	11.91	9.53	0.91	4.27	4.89
East	2018-08-08	25	15.38	11.88	9.52	0.91	4.27	4.89
East	2018-08-08	27	15.37	11.90	9.53	0.91	4.27	4.91

While dissolved ionic concentrations represent the total amount of ions in each sample, ionic ratios compare the concentration of one specific ion in proportion to another, highlighting differences as a function of ion types. For example, the proportions of SO₄²⁻ : Cl⁻ in the water column are clearly different in both lakes (Figure 3.4). In West Lake, ratios decrease from 1.14 in the water column (10-20 m) to a minimum of 0.83 at 32 m bottom water depth in late winter. In contrast, East Lake ratios consistently range from 0.77 to 0.78 through the entire water column to 27 m depth. In summer, the water column ratio in West Lake increases from 1.08 to 1.11 from 5-10 m and then decreases to 1.07 at 20 m

while the bottom water ratio increases slightly to a maximum of 1.12 at 32 m depth. East Lake water column and bottom water are consistent in summer with ratios of 0.77. These ionic ratios highlight the major differences in composition between the two lakes in the bottom and column water. The seasonal trends in SpC and ionic concentrations recur annually, recorded by repeated CTD casts collected at East and West Lakes since 2003 (Harasyn et al., 2017).

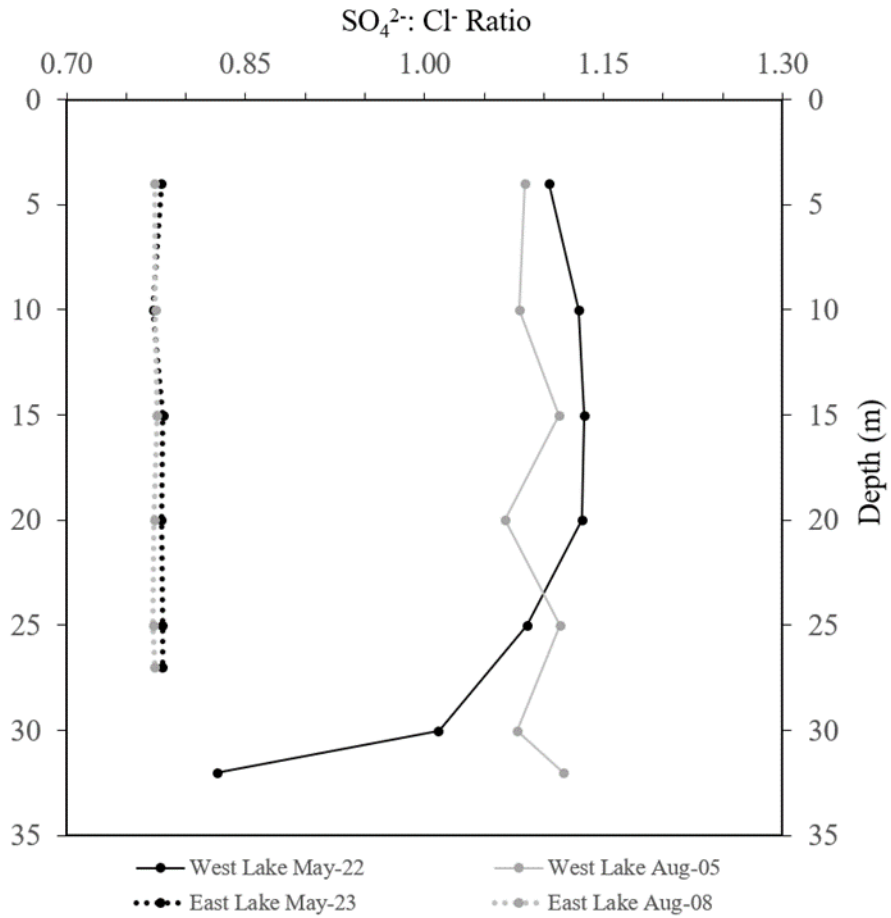


Figure 3.4 Ratios of sulphate (SO_4^{2-}) to chloride (Cl^-) dissolved ion concentrations through the water column of East and West lakes. Water sample collection occurred in May and August 2018 between 2-m and 27-m depth (East) and 32-m (West).

3.5.3 Temporal Trends in Ion Concentrations

Cl⁻ was the dominant anion in both lakes between 2006-2012. Cl⁻ concentrations varied between 4-9 mg/L in West Lake and 10-15 mg/L in East Lake from 2006-2010. K⁺ is the least abundant ion in both lakes, with values consistently below 2 mg/L and showing only small annual fluctuations that follow a similar trend to Ca²⁺ and Mg²⁺. Ion concentrations of Ca²⁺ and Mg²⁺ track closely to one another for the study period, ranging between 2-5 mg/L in West Lake and 4-7 mg/L in East Lake. Na⁺ was the second most abundant ion in both lakes from 2006-2010. There is an increasing trend in mean annual concentrations of the most abundant major ions Cl⁻, Na⁺, SO₄²⁻ following the warmest thaw season on record at the CBAWO in 2012. During this period of increase, SO₄²⁻ exceeded Na⁺ as the second most abundant ion in East Lake (c. 2012-2019) and became the most abundant ion in West Lake in 2014 and 2015. SO₄²⁻ continues to be the most abundant ion in the water column (not bottom water) of West Lake for the remainder of the study period (c. 2014-2019). Additionally, the ionic concentrations of all major ions in the bottom water were (mostly) higher than column waters from 2016-2019 to varying degrees in West Lake only. This occurrence was much rarer in East Lake, with Cl⁻ and Na⁺ bottom water concentrations exceeding column waters in 2017 (Figure 3.5). The ratio between bottom-to-column water (B:C) values further emphasizes the differences between dissolved ion concentrations throughout the lake (Figure 3.6).

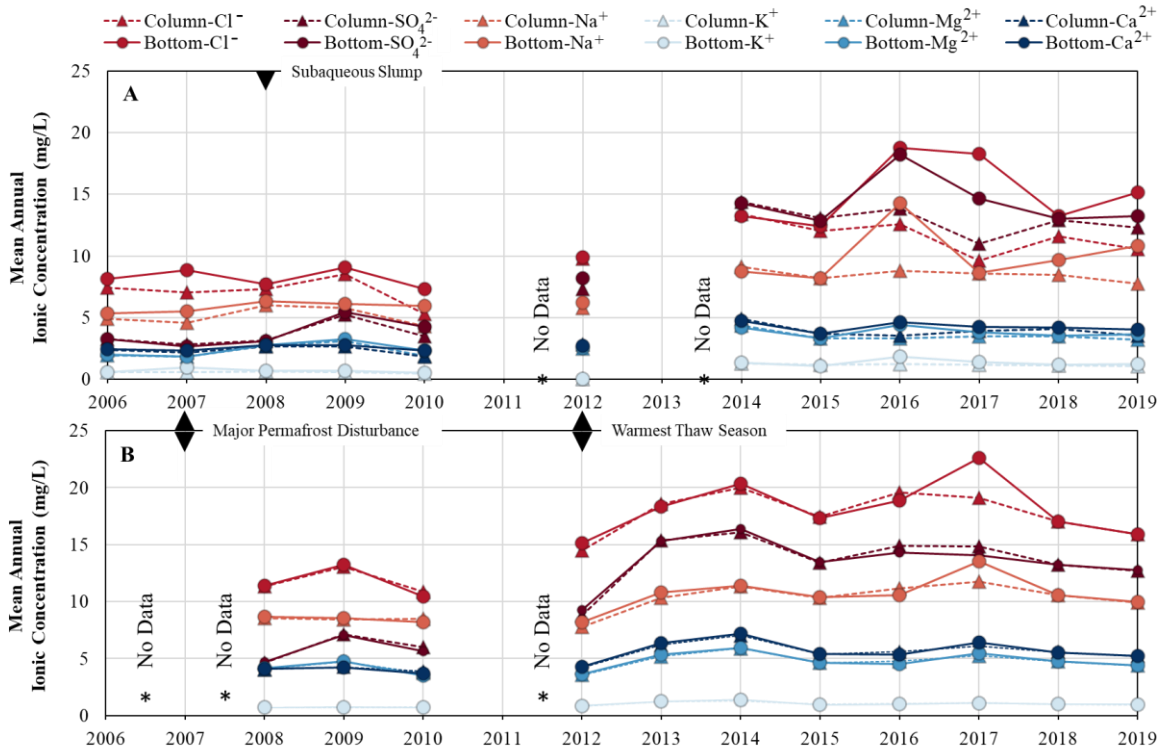


Figure 3.5: Average annual ion concentrations of the column and bottom water in West Lake (A) between 2006-2019 and East Lake (B) between 2008-2019. The plots show an increasing trend in the ionic concentration of major ions for both East and West lakes, in both bottom waters (circles with solid lines) and column waters (triangles with dotted lines). Geochemical data is limited or missing in 2011 in East Lake and West Lake, 2006 and 2007 in East Lake, and 2013 in West Lake (unavailable). Black triangles indicate major events in each lake: major permafrost disturbances resulted in over 100 active layer detachments in 2007. In addition, West Lake experienced a large sub-lacustrine mass movement event causing sustained turbidity in the water column in 2008, and 2012 was the warmest thaw season on record at the Cape Bounty Arctic Watershed Observatory (CBAWO).

Ratios of mean annual B:C water ion concentrations illuminate differences in the abundance of dissolved ions through the water column (Figure 3.6). B:C ratios greater than one indicate enrichment of dissolved ions in bottom waters compared to the column water. West Lake ratios of B:C are between one and two (Figure 3.6 A), whereas ratios of B:C in East Lake are close to one (a 1:1 relationship) (Figure 3.6 B). These ratios in West Lake show enrichment of dissolved ions in the bottom waters compared to the rest of the water column. Conversely, B:C ratios in East Lake are mostly similar, except for a spike in the ratio of B:C for Cl^- and Na^+ in 2017 (also noted above in Figure 3.5). The highest B:C ratio in both lakes was Cl^- (1.90, West; 1.19, East), both in 2017, meaning the bottom water of both lakes was especially enriched in Cl^- at this time.

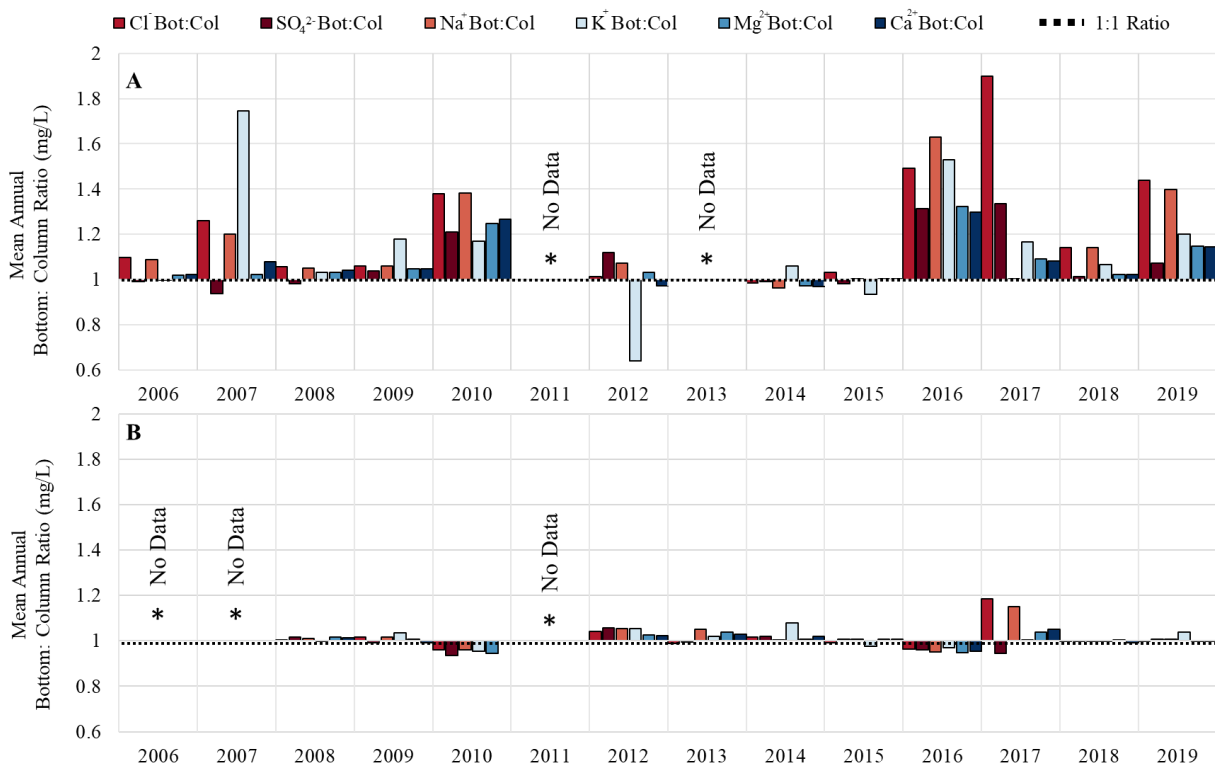


Figure 3.6: Mean annual ion concentration ratios of bottom water to column water (B:C) from 2006 – 2019 in West Lake (A) and East Lake (B). Coloured bars represent B:C ratios, representing mean annual ratios for each major ion. Y-axis represents the ratio outcome, showing enrichment (values > one) or depletion (values < one) of dissolved ions in the bottom water compared to the column water. Values of one indicate the bottom and the column water have equal compositions of a particular ion (1:1 ratio).

Ion ratios of the most abundant ions in the lake $\text{SO}_4^{2-} : \text{Cl}^-$ were plotted against the ratios of SO_4^{2-} to other major cations (Na^+ , Mg^{2+} , Ca^{2+} , K^+) and anions (Cl^-) to compare the abundances of all major ions with SO_4^{2-} throughout the study period (Figure 3.7). Ratios of $\text{SO}_4^{2-} : \text{Cl}^-$ and $\text{SO}_4^{2-} : \text{Na}^+$ have the most similar values (closer to a 1:1 ratio), meaning they are increasing in addition to SO_4^{2-} but not as extensively over the study period. Ratios of SO_4^{2-} to major cations ($\text{SO}_4^{2-} : \text{Na}^+$, $\text{SO}_4^{2-} : \text{Ca}^{2+}$, $\text{SO}_4^{2-} : \text{Mg}^{2+}$, and $\text{SO}_4^{2-} : \text{K}^+$) are much higher (between 1.0 and 15.0), indicating the cations are not increasing nearly as quickly as SO_4^{2-} . In both the water column and bottom water, West Lake becomes increasingly enriched in SO_4^{2-} in all four plots between 2014 and 2019, reaching values close to 1.2 for $\text{SO}_4^{2-} : \text{Cl}^-$ ratios compared to $\text{SO}_4^{2-} : \text{Cl}^-$ ratios in East Lake, which do not surpass 0.9. Major increases in SO_4^{2-} occur as large jumps in grouped years from 2008-2009 and 2012-2013 (Figure 3.7). The years between these large jumps in SO_4^{2-} are organized into three clusters (2006-2008, 2009-2012, and 2013-2019 in Figure 3.7). Following the 2006-2008 grouped cluster, SO_4^{2-} ratio values increasingly become less similar (trend away from the 1:1 ratio) from year to year, both within and between clusters; demonstrating that the ratios of $\text{SO}_4^{2-} : \text{Cl}^-$ became increasingly different from other SO_4^{2-} to ion ratios as the years progressed. These ratios reveal that SO_4^{2-} concentrations were disproportionately increasing faster compared to the other ions in both lakes from 2006-2019. Of the different clustered groupings, the largest increases in SO_4^{2-} occurred within the 2013-2019 cluster in West Lake within West Lakes water column. Between 2013 and 2019, all ions in East Lake bottom and column water stayed close to a 1:1 relationship, where West Lake values have diverged. In West Lake, the differences between $\text{SO}_4^{2-} : \text{Cl}^-$ ratios in the bottom and column water have increased over time. In the 2013-2019 cluster, the ratios of West Lake bottom compared to column water differ by values close to 0.4 compared to the less than 0.2 differences in the 2006-2008 and 2009-2012 clusters. These results represent a time lag between the rapidly increasing water column SO_4^{2-} concentrations relative to bottom water SO_4^{2-} concentrations.

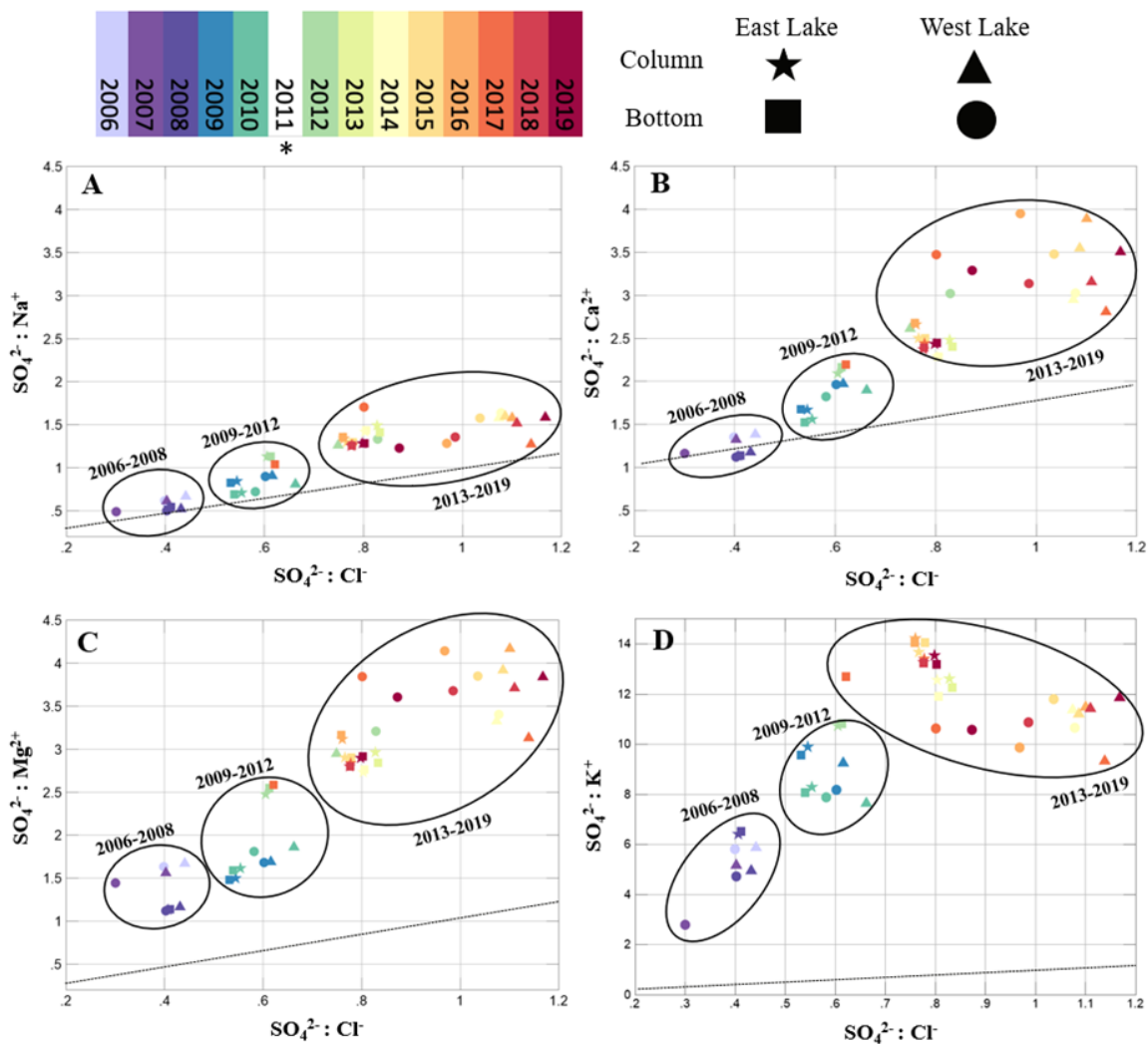


Figure 3.7: Plots A-D display the ratio trend analysis for ion concentrations over time. Mean annual ion concentrations of anion ratios ($\text{SO}_4^{2-} : \text{Cl}^-$ x-axis A-D) and $\text{SO}_4^{2-} : \text{major cations}$ (A: Na^+ , B: Ca^{2+} , C: Mg^{2+} , D: K^+ ; y-axis) are displayed by different types of markers for both West Lake column water (triangles) and bottom water (circles), and East Lake column water (stars) and bottom water (squares). Where shapes for each lake bottom to column region (where B and C water are defined by the regions outlined in Figure 3.2) are close on the plot, this indicates similar ion ratio values in both bottom and column water in that lake. Where they are more dispersed, they are farther from a 1:1 relationship between regions. Dashed lines indicate a 1:1 ratio between SO_4^{2-} -to-cation and -anion ratios. Clustered lake ratios (circled in black) represent years showing similar trends in ion chemistry. Values for K^+ 2012 in West Lake were removed from plot D due to anomalous outliers.

3.5.4 River Ion Concentration Temporal Trends

Total annual river fluxes from East and West Rivers from 2006-2017 demonstrate that SO_4^{2-} is the most abundant ion in both rivers each year (except for East River in 2006) (Figure 3.8). West River shows increased SO_4^{2-} fluxes in 2008, 2012 and 2017, following the three warmest years recorded at the CBAWO. Additionally, multi-year thermal perturbations (a period of consistently above-average air temperatures) and resulting physical disturbances occurred along the tributaries and the banks of West and East rivers between 2007-2012 (increased sediment loads and other continued effects occurred in the catchment) (Beel et al., 2021). These disturbances potentially lead to increasing enrichments of SO_4^{2-} in West Lake following 2006, peaking in 2012 (15.3 Mg), decreasing in 2014 (6.4 Mg) and again increasing in 2017 (12.8 Mg). In comparison, the flux of SO_4^{2-} in East Lake reached peak enrichment (9.8 Mg) in 2008 and proceeded to decrease again after that date. Therefore, where there are SO_4^{2-} increases in rivers, a subsequent increase in the lake SO_4^{2-} composition may be visible.

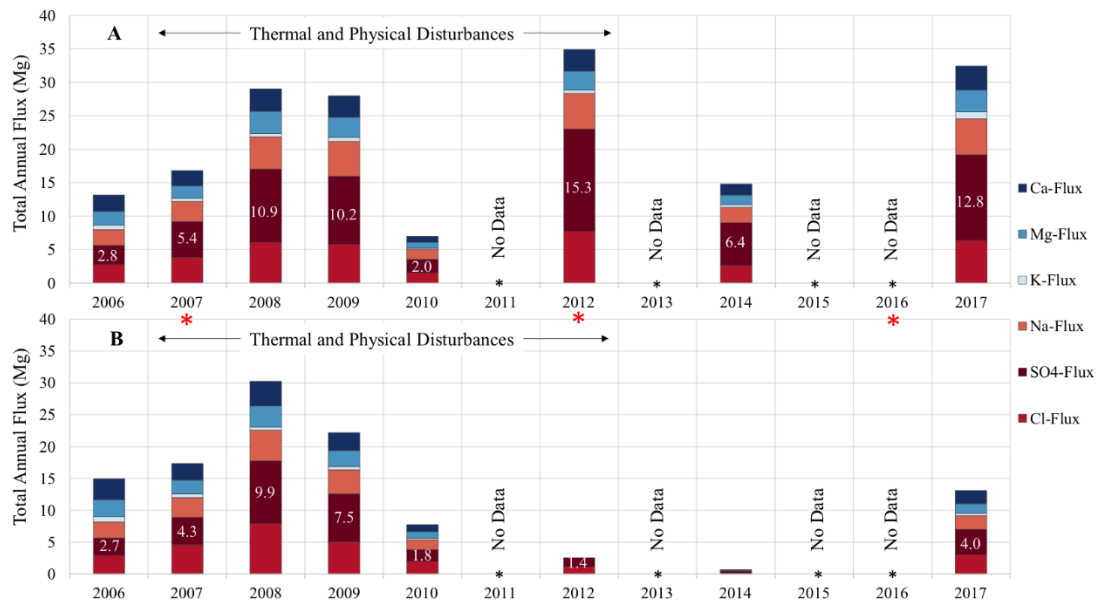


Figure 3.8: Total annual flux (Mg) of major anions (Cl^- , SO_4^{2-}) and cations (Na^+ , Mg^{2+} , Ca^{2+} , K^+) for West River (A) and East River (B) represented as stacked bars from 2006-2017. Data is unavailable for 2011, 2013, 2015 and 2016. Numbers within bars indicate the total annual flux of SO_4^{2-} . An asterisk marks three (red) anomalously warm thaw seasons at the CBAWO, known to result in increased physical disturbances along tributaries in the watershed of each lake (Beel et al., 2021).

3.6 Discussion

This study assesses the chemical changes in over a decade of water column records in two similar High Arctic lakes. The geochemical data presented demonstrates West and East lakes have undergone notable changes in composition over a 10+ year record. West Lake in particular exhibits annually recurring seasonal variation between column and bottom waters. A key component of this work distinguishes the difference between the bottom and column water through analysis of ion ratios, to offer new insights into the EBWC described by others (Harasyn et al., 2017; Lewis et al., 2018). In addition to high SpC in the lake bottom, compositional changes demonstrated by ionic ratios of B:C water in West Lake reveals that the composition of the bottom water is distinctly different from the water column (Figure 3.6). Most notably, the enrichment of SO_4^{2-} in the overlying water column between 2006 and 2019 compared to the bottom water (Figure 3.7), suggesting there is a different source of water replenishing the bottom water compared to the rest of the water column (Mazor, 2004). These trends in SO_4^{2-} establish that the water column has become enriched in SO_4^{2-} at a faster rate compared to the bottom water in just over 10 years, suggesting the source of ions accumulating in the bottom of West Lake is different from the overlying water column.

Column water makes up at least 99% of the total volume of water in East and West Lakes, leaving less than 1% of the entire lake volume existing as bottom water (West Lake: 0.2145 km^3 ; East Lake: 0.02086 km^3 ; EBWC: $0.0005\text{-}0.002 \text{ km}^3$). Given this volume imbalance it is extremely unlikely that bottom waters can influence or control the geochemistry of these lakes and are unlikely to be responsible for the decadal increases in ion concentrations. It is therefore hypothesized that more than one water source controls the geochemical differences in the two zones of the water column. Two mechanisms for these differences are proposed in this High Arctic setting: (1) permafrost degradation; and (2) groundwater seepage, discussed below.

3.6.1 Processes Related to Overall Water Column Trends

The water columns of West and East lake are changing in a manner consistent with increased transfer of ions from the surrounding catchment. Previous studies on the CBAWO West and East lakes have linked increases in SO_4^{2-} ions and specific conductivity in the lakes to the flushing of solutes from the SO_4^{2-} enriched layer below the active layer at the top of the permafrost (Lafrenière & Lamoureux, 2019; Lamhonwah et al., 2017). This zone above the permafrost is known to be high in dissolved solids and has begun to thaw with increasingly warm summer temperatures (Lamhonwah et al., 2017). This region is known as the transient zone and is also where supra-permafrost groundwaters are situated (French, 2018). At the CBAWO, warmer summer temperatures, most notably in 2012, initiated deep seasonal thaw that increased the active layer depth, thereby flushing solute rich water from the active layer into rivers and lakes (Beel et al., 2021). Roberts et al. (2017) observed large increases in average lake water SO_4^{2-} concentrations between 2012 and 2014 at the CBAWO after the warmest consecutive summers on record. Warmer thaw seasons at the CBAWO were also found to initiate greater physical disturbances (i.e., Active Layer Detachments (ALDs)) in both watersheds (2.3 % in West Lake, 1.2 % in East Lake) (Beel et al., 2021). Post-disturbance effects included an increase in sediment load, flux of major dissolved ions, and delivery of dissolved organic carbon into major river channels which ultimately terminate in the CBAWO lakes (Beel et al., 2020). Additionally, increases in SO_4^{2-} have also been correlated to years with late-season summer rainfall events that further initiate flushing of dissolved ions from the seasonally-thawed active layer into the fluvial environment (Lamhonwah et al., 2017). The total annual flux of ions reported here (Figure 3.8 A) show that SO_4^{2-} is the dominant dissolved ion in most years in West and East rivers. The 2012 flux of SO_4^{2-} in West River was 4.4 Mg higher than any other years, after which the largest average annual water column increases in SO_4^{2-} were observed in West Lake (Figure 3.5 A). Combined, these results link the flux of dissolved ions in river water to the accumulation of dissolved ions in the West Lake water column in agreement with previous studies.

After 2012, SO_4^{2-} concentrations increase faster than any other dissolved ions over the duration of this study, with larger increases seen in West Lake than East Lake (Figure 3.7). Previously, Cl^- is the most abundant dissolved ion in the water column, followed by Na^+ in both lakes from 2006-2012, after which SO_4^{2-} becomes the dominant ion in the water column of West Lake (only dominant in both the bottom and column water in 2014 and 2015) (Figure 3.5 A). SO_4^{2-} concentrations also increased in East Lake but did not surpass Cl^- concentrations during the study period (Figure 3.5 B). Although SO_4^{2-} is not the most abundant dissolved ion in East Lake, both lake bottom and water column concentrations increased for two consecutive years (c. 2012-2014) following warmest thaw seasons at the CBAWO. The timing of major SO_4^{2-} enrichments in both lakes were previously found following years with warmer summer temperatures (mean summer temperatures $\sim 1\text{-}2^\circ\text{C}$ warmer) and rainfall events (Lamhonwah et al., 2017; Roberts et al., 2017). In addition, both rivers increase in SO_4^{2-} during this period, where West Lake follows the signature of West River, which is slightly more enriched in SO_4^{2-} in comparison to East River followed by East Lake (Figure 3.9). These increases in SO_4^{2-} concentrations suggest that the water column composition of both lakes has become increasingly influenced over the last ten years by surficial runoff processes and increased dissolved ion fluxes due to permafrost degradation just beneath the active layer (Beel et al., 2021; Lamhonwah et al., 2017). SO_4^{2-} has been found to increase substantially in the soil immediately below the active layer (Lamhonwah et al., 2017). Pre-thaw soil cores collected below the typical maximum active layer depth recorded terrestrial SO_4^{2-} values of 54 Mg/km^2 compared to values of 22 Mg/km^2 from the soil in the active layer (Roberts et al., 2017). This is further evidence indicating SO_4^{2-} enrichments seen in the lakes following the 2012 were sourced from increased solute mobilization and drainage from the active layer and uppermost permafrost (Roberts et al., 2017). This suggests that water column ratios in both lakes reflect changes consistent with the increasing catchment release of dissolved ions because of deepened thawing below the seasonal active layer into the upper permafrost.

Past (2006-2010) chemical compositions of East and West Lakes were similar to mean ocean water chemistry (Harasyn et al., 2017; Roberts et al., 2017). Marine compositions suggest that the lake waters at the CBAWO likely originated from a marine source. This aligns with the history of the lakes which indicates that the land which the lakes are situated on was previously submerged below sea level during the last glacio-isostatic emergence and isolation following the retreat of the Innuitian Ice Sheet (IIS) (Cuven et al., 2011; England, 1999). During this period of submergence, the permafrost retreated due to the warming effect of submergence, and the sea water would have been trapped within sediments and eventually reside within the lakes following re-submergence of the land above sea level (Guimond et al., 2021; Keating et al., 2018). As a result of this history, many coastal lakes in the High Arctic contain highly saline waters (Ouellet et al., 1989; Van Hove et al., 2006). Since their isolation from the sea (c. 1800 years ago) many marine basins such as West and East lakes have freshened because the freshwater inputs from precipitation and snow melt eventually exceed the relic sea water inputs stored in sediments (Van Hove et al., 2006). Compared to the lifetime of these lakes, which were isolated from the sea c.1800 years ago (East Lake, Cuven et al., 2011), the compositional changes in West and East lakes over the last 10 years demonstrate rapid geochemical evolution of their waters, from a composition similar to mean ocean water (cf. lakes Garrow and Sophia, Cornwallis Island) to compositions similar to the mean geochemical composition of the East and West rivers (Figure 3.9). The waters of East and West lakes have therefore shifted away from the geochemical signature of trapped seawater to freshwater in just over a decade (c. 2006-2019). The geochemical trajectory of dissolved ions from West and East rivers also shows a shift from late glacial marine water to increasingly SO_4^{2-} -dominant signatures in the last 10-15 years demonstrating a rapid change in the composition of the water column of these lakes (Figure 3.10). Given the rates of geochemical change observed in the 10+ year record, this suggests that the lakes are experiencing a period of rapid transition, and one could argue that the recent geochemical evolution has been exceptional compared to the lifetime of the lakes.

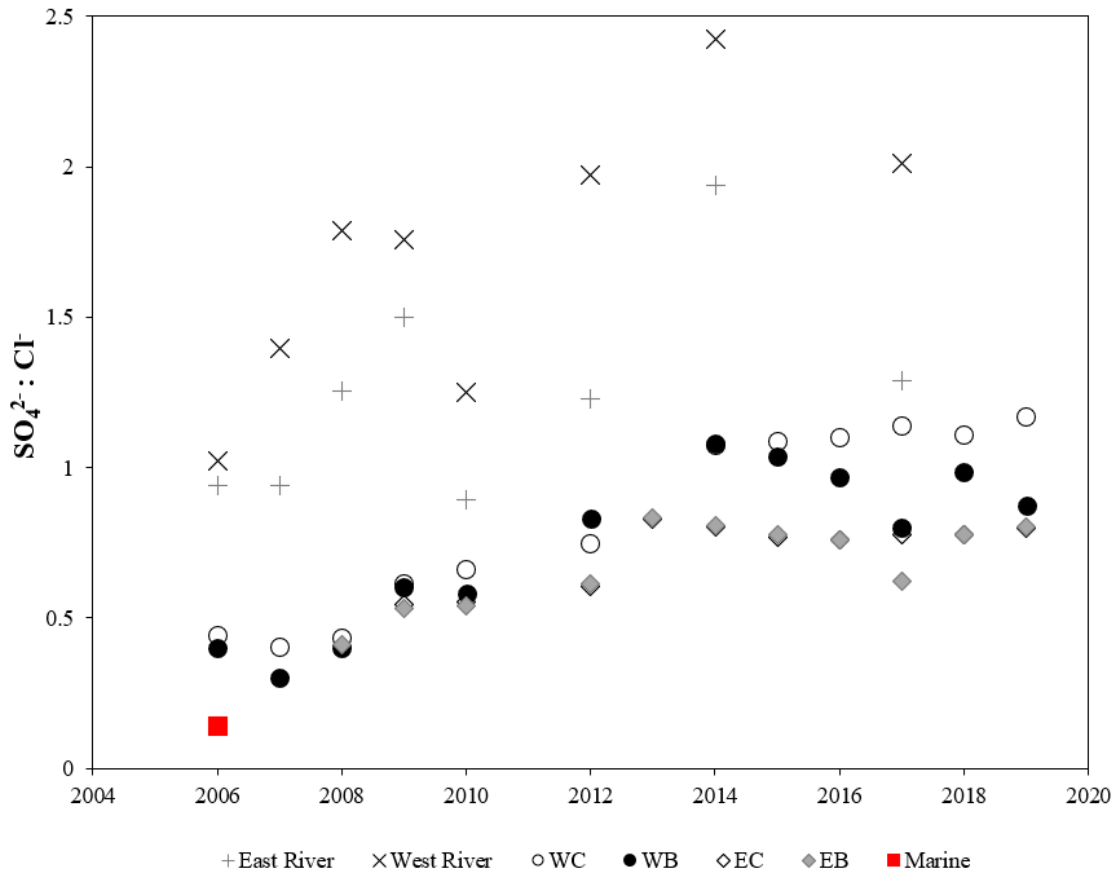


Figure 3.10: Displaying mean annual $\text{SO}_4^{2-} : \text{Cl}^-$ ratios from 2006-2019 for West Lake water column (WC, white circles) and bottom water (WB, black circles), 2008-2019 ratios for East Lake water column (EC, white diamonds) and bottom water (EB, grey diamonds), and annual flux of $\text{SO}_4^{2-} : \text{Cl}^-$ ion ratios from West River (x) and East River (+). Mean $\text{SO}_4^{2-} : \text{Cl}^-$ ratios in seawater (marine, red square) are also shown.

3.6.2 Processes and Origins of Elevated Bottom Water Conductivity

Previous work has shown that the geochemical composition of waters in the bottom five meters of water in West Lake are distinctly different than the overlying water column (Harasyn et al., 2017; Lewis et al., 2018), which correlated with current findings (Figure 3.4). Elevated bottom water conductivity (EBWC), previously defined by Harasyn et al., (2017) and Lewis et al. (2018), is characterized by higher dissolved ions and low dissolved oxygen compared to the overlying water column, separated by a sharp chemocline. CTD casts (Figure 3.3) confirm that EBWC is most prominent in West Lake in late winter (pre-runoff) when the lake surface is still entirely ice covered. This situation contrasts with East Lake, which does not exhibit similar differences in dissolved ion composition and specific conductivity at depth (Figure 3.4). It is possible that the measured differences observed between East and West Lakes are a result of different mixing patterns in the water columns of both lakes. Potential explanations include a later timing of ice-off at West Lake, thereby leaving less time for summer mixing to occur. Sustained high turbidity of the water column (from sub-lacustrine mass movement events; Normandeau et al., 2017) in West Lake may also influence the depth of annual vertical mixing during the melt season in the lake. Either scenario could prevent West Lake from completely overturning, leaving EBWC intact for more than a year and allowing for greater SpC in EBWC in West Lake compared to East Lake.

Although measured changes in the geochemical composition of the West Lake water column suggest a terrestrial source for added solutes, the low bottom water ion ratios with SO_4^{2-} (compared to column water) indicate that EBWC evolves through a different set of processes compared to rapidly increasing SO_4^{2-} concentrations in the overlying water column (Figure 3.7). This further supports the idea that the high SpC and B:C ionic ratios (Figure 3.6) in late winter bottom water of West Lake are a result of increases in dissolved ion inputs to the bottom water originating from a different source compared to the water column at this time. Based upon the fact that EBWC accumulates over winter, the source must be originating from an unfrozen reservoir in the subsurface. Potential sources and mechanisms for the

occurrence of this EBWC in West Lake include (Figure 3.11): (1) diffusion of late glacial lake bottom sediment pore water; (2) lake bottom porewater seepage from a talik surrounding the lake; and/or (3) seepage of intra- or sub-permafrost groundwater into the lake.

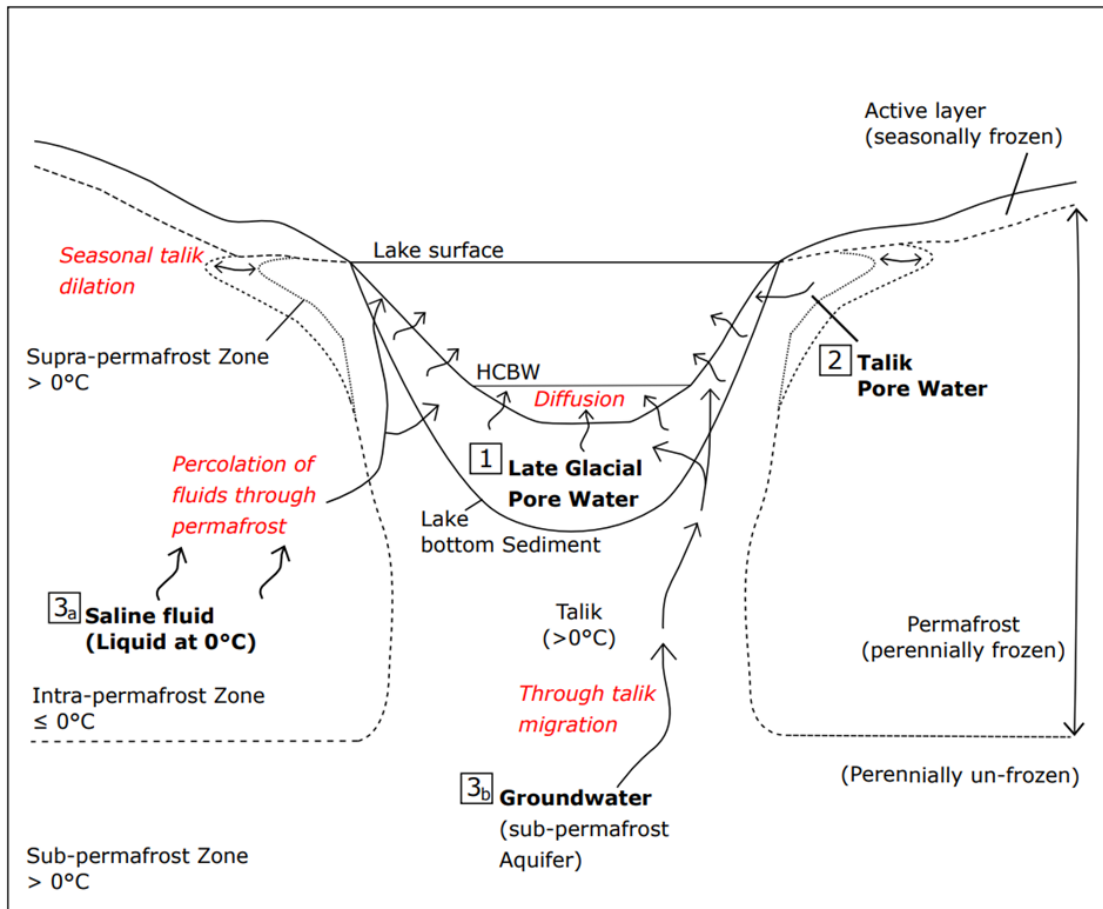


Figure 3.11: Conceptual diagram illustrates three possible mechanisms for compositional differences in elevated conductivity bottom water (EBWC) of West Lake at the Cape Bounty Arctic Watershed Observatory (CBAWO): Scenario 1 – seepage of late glacial pore water; Scenario 2 – seepage of supra-permafrost talik porewater that surrounds the lake but lies below the active layer; Scenario 3 – seepage of intra-permafrost (3a) or sub-permafrost (3b) groundwater via a lake bottom talik.

3.6.2.1 Sediment Pore Water Diffusion

The most likely scenario for the occurrence of EBWC is the diffusion of porewater through the lake bottom (Scenario 1, Figure 3.11). Lake sediment porewaters collect and store the geochemical information of activity within the lake over time; i.e., East and West lakes were filled with marine water before isolation from the sea (Cuven et al., 2011), with evidence of this past marine signature apparent in the similarities in dissolved ion composition of EBWC and marine water, both enriched in Cl^- , SO_4^{2-} , and Na^+ (Figure 3.9). Possible explanations for why changes in EBWC composition lags changes in the overlying water column could be because lake sediment porewaters partially retain a past geochemical marine signature (Cuven et al., 2011) or their composition results from diagenesis of sediments in anoxic conditions (Stiller, 1994). Diffusion of porewaters across the sediment-water interface would create a geochemical gradient both in terms of total dissolved ion concentration and the order of dominant dissolved ions in the lake bottom ($\text{Cl}^- > \text{SO}_4^{2-} > \text{Na}^+$) compared to the overlying water column, which is increasingly dominated by SO_4^{2-} .

Porewater diffusion into the lake bottom can occur as a result of thermal or geochemical disequilibrium between the sediments and the water column or through basin-scale internal wave-generated pressure at the sediment-water interface (Kirillin et al., 2009; Precht & Huettel, 2003). Thermal disequilibrium would result where heat flux-induced diffusion increases lake bottom accumulations of dissolved ions, whereby molecular transfer is initiated by the thermal difference between lake-bottom sediments and the overlying water (Golosov & Ignatieva, 1999). Alternatively, geochemical disequilibrium would occur where lake bottom sediments are enriched in dissolved ions in comparison to the overlying lake bottom water, an upwards advective flux of dissolved ions occurs across the sediment-water interface (Stiller, 1994). Thermal or geochemical diffusion processes are therefore feasible mechanisms following a relatively homogenous water column such as in summer (Figure 3.3). The homogenized water column would create a larger dissolved ion concentration difference between the lake

sediments and bottom water, resulting in subsequent transport of dissolved ions from pore waters into the lake bottom water.

As the EBWC is most prominent in late winter, diffusion across the sediment-water interface would presumably occur over winter when the lake is ice covered. Once ice is established on the lake, warm lake bottom sediments previously heated by convection during the ice-off period (Cortés & MacIntyre, 2020) begin to experience heat exchanges with colder bottom water (Zdorovenova, et al., 2021). The release of heat from bottom sediments over winter has been found to be an important source of heat to the lake bottom water (cf. Chapter 4) with the implication that it could be a contributor to a flux of dissolved ions across the sediment-water interface potentially accumulate in the lake bottom (Bengtsson, 1996; Hesslein, 1980; Stiller, 1994; Welch & Bergmann, 1985; Zdorovenova et al., 2021). In addition, long ice-covered periods in the lake would limit turbulence in the water column, promoting the development of a chemical diffusion gradient just above the sediment-water interface (cf. Chapter 4).

Given the evidence that either a chemical or temperature disequilibrium between the sediment-water interface could initiate a net flux of dissolved ions from porewater to lake bottom water, it is possible that a combination of both processes is contributing to the EBWC at the bottom of West Lake. Compared to the overlying water column in West Lake, the accumulation of EBWC is a slow, small-scale process that is subdued by the rapid geochemical change in the overlying water column from terrestrial and fluvial activity. Therefore, when EBWC is formed in winter, under ice, the overlying column waters are distinct in composition until mixing occurs in the summer; hence, the EBWC is not reflected in the overall composition of the water column. Under Scenario 1 (Figure 3.11), the dissolved ion composition of EBWC reflects ions diffused from underlying porewaters composed of past lake water geochemistry (plus any diagenesis due to anoxia) that is isolated from recent water column changes.

3.6.2.2 Talik Porewater Migration

Porewater sourced from a supra-permafrost talik surrounding the lake could be an alternative source of EBWC (Scenario 2, Figure 3.11). Since the lake is a heat source that prevents freezing of the

surrounding ground, unfrozen subsurface pathways (e.g., lateral taliks) may exist that connect solute-rich supra-permafrost groundwater to the lake (Walvoord & Kurylyk, 2016). The geometry of the talik would depend on a number of factors including depth, geochemistry, and changing surface temperatures. During the thaw season, the talik may expand with warming surface temperatures, causing thermally driven near-surface permafrost thaw, potentially releasing porewaters and delivering solutes via subsurface flow (Lafrenière & Lamoureux, 2013). During freeze-up, supra-permafrost groundwater would be forced towards the lake with contraction of the talik (i.e., regions farthest from the lake would freeze first). Pressure generated at the freezing front would force talik porewater through the pore spaces of sediments, accumulating dissolved ions generated from sediment-water interactions including mineral dissolution. Groundwater undergoing this process would become increasingly enriched with dissolved ions from the surrounding geology with time and migration through the transition zone at the top of the permafrost (Cochand et al., 2019; Lafrenière & Lamoureux, 2013). Deeper seasonal thaw also has the potential to release previously frozen solutes and nutrients and create new pathways for mobilized materials (Lafrenière & Lamoureux, 2019; Roberts et al., 2017)

Previous research elsewhere on Melville Island found the most likely groundwater flow paths into High Arctic lakes are in the littoral zone, where there is less accumulation of fine-grained sediments compared to the lake bottom and therefore easier percolation into lakes (Dugan et al., 2012). This is supported by the fact that groundwater movement towards lakes and rivers is driven by hydrostatic pressure and higher hydraulic conductivity of nearshore sediments (Paquette et al., 2017). When temperatures drop below zero, pore-water remaining in sediment would travel to the zone of least hydrostatic pressure, away from the freezing front within the active layer, driving the migration of solute-rich groundwater to lateral talik zones and thereby moving supra-permafrost groundwater into the lake (Lecher, 2017; Woo, 2012a). In order for this signature to be distinct from the surrounding water, the supra-permafrost groundwater would need to be hydrologically disconnected from the water in the rivers (i.e., by frozen ground). As the geometry of the talik surrounding the lake remains unknown, we are

currently unable to determine if there is a supra-permafrost groundwater source feeding the lakes that is isolated from the SO_4^{2-} rich water released due to deep thaw in the terrestrial surface.

3.6.2.3 Sub-permafrost and intra-permafrost zone groundwater inputs

Sub-permafrost or intra-permafrost groundwater would likely exhibit distinct geochemical signatures compared to surface runoff and shallow subsurface groundwater, which could reach the lake only by connection through a talik. In this scenario, the occurrence of EBWC could therefore originate from groundwater migrating from sub-permafrost or intra-permafrost taliks via through, open, or closed talik formation below West Lake. This seepage would result in the accumulation of EBWC observed in late winter water profiles (Figure 3.3). Such groundwater in permafrost settings usually exhibits higher dissolved ion concentrations than surface waters due to their long residence times and rock-water interactions (Cochand et al., 2019; Schwartz et al., 1981). The northern basin of West Lake is the deepest (34 m) and widest (1-km) region of the lake located near the front of the West River delta. A horizontal talik is suspected to be present beneath the lake given that the lake does not freeze to the bottom and the considerable size of the northern basin. The talik is assumed to be a closed talik but it is also possible that a through talik (extending through the entire depth of the permafrost) may extend to the base of permafrost. A through talik would hypothetically connect surface waters with deep sub-permafrost groundwater, resulting in groundwater exchanges between the subsurface and the lake (Harasyn et al., 2017). A through talik develops beneath a lake where the horizontal dimension is approximately twice the total depth of the permafrost (McGinnis & Jensen, 1971). Considering the ~500 m depth of permafrost at CBAWO (Judge, 1973) it is possible for a through talik to exist under at least a portion of West Lake and a pathway for sub-permafrost groundwater to seep through the littoral regions (Walvoord & Kurylyk, 2016; Woo, 2012a) (Scenario 3B, Figure 3.11).

Alternatively, intra-permafrost groundwater can remain liquid at temperatures below 0 °C if they contain high concentrations of dissolved ions resulting from rock-water interactions that effectively

depress their freezing point (Scenario 3A, Figure 3.11), also known as hydrochemical taliks (French, 2018; W. Pollard et al., 1999; W. H. Pollard, 2005; Zentilli et al., 2019). Underlying Devonian bedrock at the CBAWO is dominated by calcareous sandstones, siltstones, quartzose, and micaceous sandstones with minor amounts of calcareous shale and coal (Christie & McMillan, 1994; Harrison, 1995). This bedrock overlays a salt fold-belt exposed as anhydrite diapirs on northern Melville Island; any groundwater in this setting would contain an abundance of dissolved ions (Harrison, 1995). A potential source of intra-permafrost groundwater could therefore occur within Paleozoic rocks of the Cape Bounty Anticline as highly mineralized waters that percolate through permafrost, effectively expand the volume of the talik beneath the lake and providing a seepage pathway into the lake (French, 2018).

3.6.2.4 The most probable source and mechanism generating the EBWC

Although the results presented here do not rule out the possibility of groundwater seepage from a subsurface talik, current data suggests late glacial lake bottom sediment pore water as the most likely source of EBWC. High concentrations of Cl^- , SO_4^{2-} and Na^{2+} in EBWC are explained through the diffusion of marine-origin dissolved ions deposited during the Holocene and subsequently stored within pore waters of lake bottom sediments. This is supported by observations of increased concentrations of Cl^- compared to SO_4^{2-} in late winter EBWC in West Lake (Figure 3.4) that moves towards the ratio in East Lake, which has a water column ratio with a slightly more marine signature (Harasyn et al., 2017). This replenished EBWC is from a source that is more similar to a marine composition compared to the overlying water column and is distinctly different from the evolving SO_4^{2-} -enriched water column that results from increased permafrost disturbances due to climate warming (Beel et al., 2021; Lafrenière & Lamoureux, 2019b; Roberts et al., 2017), and are shifting towards the composition of the rivers (Figure 3.9). In contrast, the entire composition of the water column of East Lake is slightly more similar to mean ocean water compared to West Lake (Figure 3.10). This would indicate that East Lake may reflect the previous geochemical composition of West Lake before the occurrence of permafrost disturbances in 2007, 2012, and 2017 (Beel et al., 2021).

In comparison, talik porewater (Scenario 2, Figure 3.11) from the supra-permafrost zone is more likely to contain a geochemical signature more similar to river water due to its interactions with the active layer during the thaw season. This supra-permafrost groundwater is located in unfrozen zones just below the active layer and above the permafrost (French, 2018) and is compositionally similar to that of the increasingly SO_4^{2-} enriched water in the catchments flowing from the rivers to the lakes (Roberts et al., 2017) as opposed to the Cl^- dominant signature of the EBWC (Figure 3.10). Groundwater in the supra-permafrost zone mobilizes each year during the thaw season at the CBAWO when the active layer thaws, creating a pathway to the surface (Bolduc et al., 2018), which leads to the conclusion that supra-permafrost groundwater entering the lakes contributes to the chemical evolution of the water column and not EBWC.

It is also possible that sub-permafrost (Scenario 3b, Figure 3.11) or intra-permafrost (Scenario 3a) groundwater migration could contribute to elevated SpC in late winter bottom water in West Lake. However, dissolved ions sourced from deeper groundwater would be expected to deliver water with elevated ionic compositions much higher than what is found in East or West Lake water columns (Johansson et al., 2015; Pollard et al., 1999). Additionally, groundwater moving through anhydrite rich (CaSO_4) formations would contain elevated concentrations of Ca^{2+} and SO_4^{2-} , which are not dominant in the EBWC in West Lake.

The most likely mechanism causing the occurrence of EBWC is therefore the diffusion of dissolved ions (Scenario 1, Figure 3.11), which would occur across the sediment water interface across the bottom of the lake. This diffusion occurs during winter months by thermal and/or chemical differences between lake bottom water and sediment pore water. Upon entry in the lake, this denser groundwater would flow downslope to the lake bottom and could conceptually form EBWC. Although the rate of groundwater inputs is unknown, accumulation would be most notable during the late winter season under still conditions compared to the melt season when the lake mixes and river inflows influence the lake bottom geochemistry. This EBWC accumulation therefore results in the development of a thermocline or

chemocline. Notably, the boundary between EBWC and the water column in West Lake has become shallower in the water column between 2006-2017 (Harasyn et al., 2017), suggesting the source of this bottom water has become more influential in relation to the rest of the water column over time. It is possible that the process responsible for the annual recurrence of EBWC is accelerating, or conversely, because of warming temperatures, EBWC is not as frequently flushed by hyperpycnal flows or diluted through mixing and is therefore accumulating over consecutive years (Lewis et al., 2018).

3.6.3 Environmental Change

The findings of this study emphasize the importance of permafrost thaw as a mechanism for rapid geochemical change in Arctic freshwater lakes, which in this case has flushed out a former marine water signature derived from inherited marine influence in just over a decade due to permafrost degradation and hydrological changes. This has resulted in the previous marine-dominant signatures in both lakes to rapidly shift to geochemical compositions that reflect recently exposed solutes in the deepened active layer that are SO_4^{2-} enriched. The lag in the EBWC signature compared to the column water indicates that the bottom water in West Lake reflects a past marine geochemical signature, preserved as pore water in lake bottom sediments. This would suggest that the lakes possibly have two reservoirs of water: (1) one constituting the majority of a lakes volume (i.e., the water column) that is impacted by rapid environmental change; and (2) a small volume of water (i.e., EBWC) that reflects trapped pore waters representing past water column compositions.

The geochemical trajectory of the changing landscape reflected in these lakes suggests that changing the geochemical compositions of lakes can be used as an indicator for rapid environmental change, as the lakes at the CBAWO are shifting on timescales compatible to those recorded in much smaller Arctic ponds (Smol & Douglas, 2007). However, physical patterns in the water column and lake morphometry can play a large role in annual geochemical dynamics through the water column of a lake. As rapid shifts in lakes geochemistry are occurring presently, it will be increasingly important to

document how biogeochemical dynamics are impacted by changing Arctic freshwater settings to understand how they are impacted.

3.7 Conclusions

The geochemistry of two freshwater lakes at the CBAWO has shown that High Arctic lakes can undergo notable multi-year changes to their composition. Since 2006, dissolved ion concentrations have increased in both West and East lakes, with the most notable changes in the rate and amount of SO_4^{2-} observed in the open water column and in higher conductivity bottom waters (EBWC). Additionally, dissolved ion concentrations observed between 2006-2019 in both lakes demonstrate that both lakes and rivers at the CBAWO are migrating from a geochemical signature similar to seawater towards an increasingly terrestrial-influenced river inflow composition. This indicates a transition in the controls over the geochemical balance in these lakes and a shift in hydrological patterns at the CBAWO due to widespread environmental change. The dominant dissolved ions in river water fluxes for most years is SO_4^{2-} , especially during years with late summer rainfall, suggesting an increased delivery of ions from a deepening active layer is the driver of changing hydrologic inputs to both lakes. Increased freshwater dissolved ion inputs to the lakes thereby transforms the pre-existing seawater signatures and demonstrates the remarkable ability of cold region lake systems, such as West and East lakes, to change rapidly in response to hydrologic changes in the surrounding catchment.

West Lake has demonstrated enriched bottom water and high values of SpC in the bottom five meters of its water column, where East Lake shows more similar B:C ratios. Moreover, results show that changes in EBWC are not necessarily linked to the observed evolution of the overall water column to an increasingly SO_4^{2-} enriched composition. Major dissolved ion concentrations reveal that the bottom waters in West Lake are distinctly different in composition compared to the water column in both lakes. The EBWC in comparison to the water column is not sufficient to alter the geochemical composition of the lakes due to its small volume (< 1 %). However, the higher specific conductivity and ion concentrations in the late-winter bottom waters indicate that a recurring source of dissolved ions increases

their concentration at the bottom of West Lake during the ice-on over winter period. As EBWC ion compositions remain similar to compositions of late glacial marine sourced waters trapped in lake bottom sediments, the likely mechanism for the late winter, under ice accumulation of EBWC in West Lake is diffusion of marine-sourced dissolved ions through lake bottom sediments.

This study is limited temporally to the typical field seasons in late winter and summer melt when the water column casts are collected (i.e., May-August). Therefore, early winter data was not captured in water column casts. Next steps in this project will investigate temporal trends in the lake bottom of West Lake (cf. Chapter 4) to identify patterns in seasonal changes in the bottom water. Temporal data collection should focus on understanding the precise timing of EBWC accumulation, associated temperature and density changes, and better characterization of hydrologic processes causing differences between bottom and column water. Future geochemical work could also investigate if decadal changes are reflected in trace elements, isotopes, and organic compounds to further the characterize the geochemistry of these lakes and narrow down how or if biologic productivity has or will be impacted by this geochemical transition in the CBAWO lakes and rivers.

3.8 References

- Adrian, R., O'Reilly, C. M., Zagarese, H., Baines, S. B., Hessen, D. O., Keller, W., Livingstone, D. M., Sommaruga, R., Straile, D., van Donk, E., Weyhenmeyer, G. A., & Winder, M. (2009). Lakes as sentinels of climate change. *Limnology and Oceanography*, *54*, 2283–2297. https://doi.org/10.4319/lo.2009.54.6_part_2.2283
- Beel, C. R., Heslop, J. K., Orwin, J. F., Pope, M. A., Schevers, A. J., Hung, J. K. Y., Lafrenière, M. J., & Lamoureux, S. F. (2021). Emerging dominance of summer rainfall driving High Arctic terrestrial-aquatic connectivity. *Nature Communications*, *12*(1448). <https://doi.org/10.1038/s41467-021-21759-3>
- Beel, C. R., Lamoureux, S. F., Orwin, J. F., Pope, M. A., Lafrenière, M. J., & Scott, N. A. (2020). Differential impact of thermal and physical permafrost disturbances on High Arctic dissolved and particulate fluvial fluxes. *Scientific Reports*, *10*(1), 1–13. <https://doi.org/10.1038/s41598-020-68824-3>
- Bengtsson, L. (1996). Mixing in ice-covered lakes. *Hydrobiologia*, *322*(1–3), 91–97. <https://doi.org/10.1007/BF00031811>
- Bengtsson, L., & Svensson, T. (1996). Thermal regime of ice covered Swedish lakes. *Nordic Hydrology*, *27*(1–2), 39–56. <https://doi.org/10.2166/nh.1996.0018>
- Biddanda, B. A., Coleman, D. F., Johengen, T. H., Ruberg, S. A., Meadows, G. A., van Sumeren, H. W., Rediske, R. R., & Kendall, S. T. (2006). Exploration of a submerged sinkhole ecosystem in Lake Huron. *Ecosystems*, *9*(5), 828–842. <https://doi.org/10.1007/s10021-005-0057-y>
- Bolduc, C., Lamoureux, S., & Franssen, J. (2018). Thermal and isotopic evidence for surface and subsurface water contributions to baseflow in a high Arctic river. *Hydrological Processes*, *32*(5), 602–616. <https://doi.org/10.1002/hyp.11427>
- Christie, R. L., & McMillan, N. J. (1994). The Geology of Melville Island, Arctic Canada. In *Geological Survey of Canada Bulletin* (Vol. 450). Ministry of Energy, Mines and Resources Canada.
- Cochand, M., Molson, J., & Lemieux, J. M. (2019). Groundwater hydrogeochemistry in permafrost regions. *Permafrost and Periglacial Processes*, *30*(2), 90–103. <https://doi.org/10.1002/ppp.1998>

- Cortés, A., & MacIntyre, S. (2020). Mixing processes in small arctic lakes during spring. *Limnology and Oceanography*, 65(2), 260–288. <https://doi.org/10.1002/lno.11296>
- Cuven, S., Francus, P., & Lamoureux, S. (2011). Mid to Late Holocene hydroclimatic and geochemical records from the varved sediments of East Lake, Cape Bounty, Canadian High Arctic. *Quaternary Science Reviews*, 30(19–20), 2651–2665. <https://doi.org/10.1016/j.quascirev.2011.05.019>
- Dranga, S. A., Hayles, S., & Gajewski, K. (2018). Synthesis of limnological data from lakes and ponds across Arctic and Boreal Canada. *Arctic Science*, 4, 167–185. <https://doi.org/10.1139/as-2017-0039>
- Dugan, H.A. (2010). *Long-term development and recent dynamics of High Arctic coastal basins*. MSc Thesis, Dept. of Geography and Planning, Queen's University, Kingston, ON.
- Dugan, H. A., Gleeson, T., Lamoureux, S. F., & Novakowski, K. (2012). Tracing groundwater discharge in a High Arctic lake using radon-222. *Environ Earth Sci*, 66, 1385–1392. <https://link.springer.com/article/10.1007/s12665-011-1348-6>
- Dugan, H. A., & Lamoureux, S. F. (2011). The chemical development of a hypersaline coastal basin in the High Arctic. *Limnology and Oceanography*, 56(2), 495–507. <https://doi.org/10.4319/lo.2011.56.2.0495>
- England, J. (1999). Coalescent Greenland and Innuitian ice during the Last Glacial Maximum: Revising the Quaternary of the Canadian High Arctic. *Quaternary Science Reviews*, 18(3), 421–456. [https://doi.org/10.1016/S0277-3791\(98\)00070-5](https://doi.org/10.1016/S0277-3791(98)00070-5)
- England, J. H., Furze, M. F. A., & Doupe, J. P. (2009). Revision of the NW Laurentide Ice Sheet: implications for paleoclimate, the northeast extremity of Beringia, and Arctic Ocean sedimentation. *Quaternary Science Reviews*, 28, 1573–1596.
- French, H. M. (2018). *The Periglacial Environment* (4th ed.). John Wiley & Sons Ltd. <https://doi.org/10.2307/j.ctt1w6tb9v.3>
- Golosov, S. D., & Ignatieva, N. v. (1999). Hydrothermodynamic features of mass exchange across the sediment-water interface in shallow lakes. *Hydrobiologia*, 408/409, 153–157. https://doi.org/10.1007/978-94-017-2986-4_16

- Guimond, J. A., Mohammed, A. A., Walvoord, M. A., Bense, V. F., & Kurylyk, B. L. (2021). Saltwater intrusion intensifies coastal permafrost thaw. *Geophysical Research Letters*, 48(19).
<https://doi.org/10.1029/2021GL094776>
- Harasyn, M. L., Lamoureux, S., & Normandeau, A. (2017, October 1-4). *Detecting the presence of localized ground water inputs into High Arctic lakes* [Paper presentation]. GeoOttawa 2017 – 70th Canadian Geotechnical Conference and the 12th CGS/IAH-CNC Groundwater Conference Ottawa, CA.
- Harrison, J. C. (1995). *Melville Island's Salt-Based Fold Belt, Arctic Canada*. Geological Survey of Canada.
- Harvey, F. E., Lee, R., Rudolph, D. L., & Frape, S. K. (1997). Locating groundwater discharge in large lakes using bottom sediment electrical conductivity mapping. *Water Resources Research*, 33(11), 2609–2615.
- Hassol, S. J. (2004). Impacts of a warming arctic. In *Arctic Climate Impact Assessment*. Cambridge University Press. <http://www.acia.uaf.edu>
- Hesslein, R. H. (1980). In situ measurements of pore water diffusion coefficients using tritiated water. *Canadian Journal of Fisheries and Aquatic Sciences*, 37, 545–551.
- Johansson, E., Gustafsson, L. G., Berglund, S., Lindborg, T., Selroos, J. O., Claesson Liljedahl, L., & Destouni, G. (2015). Data evaluation and numerical modeling of hydrological interactions between active layer, lake and talik in a permafrost catchment, Western Greenland. *Journal of Hydrology*, 527, 688–703. <https://doi.org/10.1016/j.jhydrol.2015.05.026>
- Judge, A. (1973). The prediction of permafrost thickness. *Canadian Geotechnical Journal*, 10(1), 313–321.
- Keating, K., Binley, A., Bense, V., van Dam, R. L., & Christiansen, H. H. (2018). Combined geophysical measurements provide evidence for unfrozen water in permafrost in the Adventdalen Valley in Svalbard. *Geophysical Research Letters*, 45(15), 7606–7614.
<https://doi.org/10.1029/2017GL076508>
- Keatley, B. E., Douglas, M. S. V., & Smol, J. P. (2007). Physical and chemical limnological characteristics of lakes and ponds across environmental gradients on Melville Island,

- Nunavut/N.W.T., High Arctic Canada. *Fundamental and Applied Limnology*, 168(4), 355–376.
<https://doi.org/10.1127/1863-9135/2007/0168-0355>
- Kirillin, G., Engelhardt, C., Golosov, S., & Hintze, T. (2009). Basin-scale internal waves in the bottom boundary layer of ice-covered Lake Müggelsee, Germany. *Aquatic Ecology*, 43(3), 641–651.
<https://doi.org/10.1007/s10452-009-9274-3>
- Kokelj, S. V., Zajdlik, B., & Thompson, M. S. (2009). Impacts of thawing permafrost on the chemistry of lakes across the Subarctic boreal-tundra transition, Mackenzie Delta Region, Canada. *Permafrost and Periglacial Processes*, 20, 185–199. <https://doi.org/10.1002/ppp>
- Lafrenière, M. J., & Lamoureux, S. F. (2013). Thermal perturbation and rainfall runoff have greater impact on seasonal solute loads than physical disturbance of the active layer. *Permafrost and Periglacial Processes*, 24(3), 241–251. <https://doi.org/10.1002/ppp.1784>
- Lafrenière, M. J., & Lamoureux, S. F. (2019). Effects of changing permafrost conditions on hydrological processes and fluvial fluxes. *Earth-Science Reviews*, 191, 212–223.
<https://doi.org/10.1016/j.earscirev.2019.02.018>
- Lamhonwah, D., Lafrenière, M. J., Lamoureux, S. F., & Wolfe, B. B. (2017). Multi-year impacts of permafrost disturbance and thermal perturbation on High Arctic stream chemistry. *Arctic Science*, 3(2), 254–276. <https://doi.org/10.1139/as-2016-0024>
- Lamoureux, S. F., & Lafrenière, M. J. (2017). More than just snowmelt: Integrated watershed science for changing climate and permafrost at the Cape Bounty Arctic Watershed Observatory. *WIREs Water*, 5(1). <https://doi.org/10.1002/wat2.1255>
- Lawrence, D. M., & Slater, A. G. (2005). A projection of severe near-surface permafrost degradation during the 21st century. *Geophysical Research Letters*, 32(24), 1–5.
<https://doi.org/10.1029/2005GL025080>
- Lecher, A. L. (2017). Groundwater discharge in the Arctic: A review of studies and implications for biogeochemistry. *Hydrology*, 4(3), 1–16. <https://doi.org/10.3390/hydrology4030041>
- Lewis, T., Lafrenière, M. J., & Lamoureux, S. F. (2012). Hydrochemical and sedimentary responses of paired High Arctic watersheds to unusual climate and permafrost disturbance, Cape Bounty,

- Melville Island, Canada. *Hydrological Processes*, 26(13), 2003–2018.
<https://doi.org/10.1002/hyp.8335>
- Lewis, T., Lamoureux, S. F., Normandeau, A., & Dugan, H. A. (2018). Hyperpycnal flows control the persistence and flushing of hypoxic high conductivity bottom water in a High Arctic lake. *Arctic Science*, 4, 25–41. <https://doi.org/10.1139/as-2017-0022>
- Mazor, E. (2004). Applied chemical and isotopic groundwater hydrology. In *Applied chemical and isotopic groundwater hydrology* (3rd ed.). Marcel Dekker, Inc.
- McGinnis, L. D., & Jensen, T. E. (1971). Permafrost-hydrogeologic regimen in two ice-free valleys, Antarctica, from electrical depth sounding. *Quaternary Research*, 1(3), 389–409. <https://www-sciencedirect-com.proxy.queensu.ca/science/article/pii/0033589471900731>
- Normandeau, A., Lamoureux, S. F., Lajeunesse, P., & Francus, P. (2016). Sediment dynamics in paired High Arctic lakes revealed from high-resolution swath bathymetry and acoustic stratigraphy surveys. *Journal of Geophysical Research: Earth Surface*, 121, 1676–1696.
<https://doi.org/10.1002/2013JF002871>.Received
- Ouellet, M., Dickman, M., Bisson, M., & Pagé, P. (1989). Physico-chemical characteristics and origin of hypersaline meromictic Lake Garro in the Canadian high Arctic. *Hydrobiologia*, 172(1), 215–234. <https://doi.org/10.1007/BF00031624>
- Pagé, P., Ouellet, M., Hillaire-Marcel, C., & Dickman, M. (1984). Isotopic analyses (^{18}O , ^{13}C , ^{14}C) of two meromictic lakes in the Canadian Arctic Archipelago. *Limnology and Oceanography*, 29(3), 564–573. <https://doi.org/10.4319/lo.1984.29.3.0564>
- Paquette, M., Fortier, D., & Vincent, W. F. (2017). Water tracks in the High Arctic: A hydrological network dominated by rapid subsurface flow through patterned ground. *Arctic Science*, 3(2), 334–353. <https://doi.org/10.1139/as-2016-0014>
- Pollard, W. H. (2005). Icing processes associated with high Arctic perennial springs, Axel Heiberg Island, Nunavut, Canada. *Permafrost and Periglacial Processes*, 16(1), 51–68.
<https://doi.org/10.1002/ppp.515>

- Pollard, W., Omelon, C., Andersen, D., & McKay, C. (1999). Perennial spring occurrence in the Expedition Fiord area of western Axel Heiberg Island, Canadian High Arctic. *Canadian Journal of Earth Sciences*, 36, 105–120.
- Precht, E., & Huettel, M. (2003). Advective pore-water exchange driven by surface gravity waves and its ecological implications. *Limnology and Oceanography*, 48(4), 1674–1684.
<https://doi.org/10.4319/lo.2003.48.4.1674>
- Rautio, A., & Korkka-Niemi, K. (2011). Characterization of groundwater-lake water interactions at Pyhäjärvi, a lake in SW Finland. *Boreal Environment Research*, 16(5), 363–380.
- Roberts, K. E., Lamoureux, S. F., Kyser, T. K., Muir, D. C. G., Lafrenière, M. J., Iqaluk, D., Pieńkowski, A. J., & Normandeau, A. (2017). Climate and permafrost effects on the chemistry and ecosystems of High Arctic Lakes. *Scientific Reports*, 7(1), 1–8. <https://doi.org/10.1038/s41598-017-13658-9>
- Schwartz, F. W., Muehlenbachs, K., & Chorley, D. W. (1981). Flow-system controls of the chemical evolution of groundwater. *Journal of Hydrology*, 54, 225–243. [https://doi.org/10.1016/S0167-5648\(08\)70605-1](https://doi.org/10.1016/S0167-5648(08)70605-1)
- Smol, J. P., & Douglas, M. S. V. (2007). From controversy to consensus: Making the case for recent climate change in the Arctic using lake sediments. *Frontiers in Ecology and the Environment*, 5(9), 466–474. <https://doi.org/10.1890/060162>
- Stewart, K. M., & Platford, R. F. (1986). Hypersaline gradients in two Canadian High Arctic lakes. *Canadian Journal of Fisheries and Aquatic Sciences*, 43(9), 1795–1803.
<https://doi.org/10.1139/f86-223>
- Stiller, M. (1994). The chloride content in porewater of Lake Kinneret sediments. *Israel Journal of Earth Sciences*, 43(3–4), 179–185.
- Van Hove, P., Belzile, C., Gibson, J. A. E., & Vincent, W. F. (2006). Coupled landscape-lake evolution in High Arctic Canada. *Canadian Journal of Earth Sciences*, 43(5), 533–546.
<https://doi.org/10.1139/E06-003>
- Vincent, W. F. (2009). Effects of climate change on lakes. In G. E. Likens (Ed.), *Biogeochemistry of Inland Waters: A Derivative of Encyclopedia of Inland Waters*. Elsevier.

- Vincent, W. F., Macintyre, S., Spigel, R. H., & Laurion, I. (2008). The physical limnology of high-latitude lakes. In W. F. Vincent & J. Laybourn-Parry (Eds.), *Polar Lakes and Rivers: Limnology of Arctic and Antarctic Aquatic Ecosystems* (pp. 65–81). Oxford University Press.
<https://doi.org/10.1093/acprof:oso/9780199213887.003.0004>
- Walvoord, M. A., & Kurylyk, B. L. (2016). Hydrologic impacts of thawing permafrost—a review. *Vadose Zone Journal*, 15(6), 20. <https://doi.org/10.2136/vzj2016.01.0010>
- Welch, H. E., & Bergmann, M. A. (1985). Water circulation in small Arctic lakes in winter. *Canadian Journal of Fisheries and Aquatic Sciences*, 42, 506–520. <https://doi.org/10.1139/f85-068>
- Woo, M. (2012). Cold lakes. In *Permafrost Hydrology* (pp. 305–346). Springer-Verlag Berlin Heidelberg.
https://doi.org/10.1007/978-3-642-23462-0_7
- Zdorovennova, G., Terzhevik, A., Palshin, N., Efremova, T., Bogdanov, S., & Zdorovenov, R. (2021). Seasonal change in heat flux at the water-bottom sediment boundary in a small lake. *Journal of Physics: Conference Series*, 2131(3). <https://doi.org/10.1088/1742-6596/2131/3/032080>
- Zentilli, M., Omelon, C. R., Hanley, J., & LeFort, D. (2019). Paleo-hydrothermal predecessor to perennial spring activity in thick permafrost in the Canadian High Arctic, and its relation to deep salt structures: Expedition Fiord, Axel Heiberg Island, Nunavut. *Geofluids*, 2019, 1–33.
<https://doi.org/10.1155/2019/9502904>

Chapter 4

Investigating the physico-chemical response to seasonal changes in a High Arctic monomictic lake at Cape Bounty Arctic Watershed Observatory, Melville Island, Nunavut

4.1 Abstract

This investigation delineated seasonal changes in the lake bottom time series data to identify the mechanisms influencing the physical processes of the lake driving the occurrence and removal of elevated bottom water conductivity (EBWC). Through analysis of 2.5-years of continuous time series data collected in the deepest depression of West Lake (32-m depth), this work reveals temporal changes in the lake bottom specific conductivity (SpC), temperature, and density anomaly. The data revealed two recurring periods of elevated lake bottom SpC (~200-300 $\mu\text{S}/\text{cm}$) displaying quasi-cyclical oscillations (daily amplitudes of ~100 $\mu\text{S}/\text{cm}$) under ice in: (1) late winter (just before the onset of ice melt); and (2) early-winter (following freeze-up). Periodicity in quasi-cyclical oscillations (revealed through wavelet analysis of lake bottom SpC) unveiled two separate processes driving under ice accumulation of EBWC in late and early winter. In late winter, EBWC accumulation occurs through under ice convection initiated by solar heating of the upper water column, where in early-winter EBWC accumulation is driven by subtle under ice circulation, by heat flux from the lake bottom sediments in response to cooling of the bottom water during freeze-up. EBWC accumulation is driven by under ice convection or circulation in the water column, initiating downward currents of denser water (enriched in dissolved ions through pore water diffusion) along the slopes of the lake. Comparatively EBWC is washed out in the melt season following sufficient melt of surficial ice driving complete water column turnover. This work highlights the dynamics of under ice processes and their dependence on the temporal changes in ice phenology.

4.2 Introduction

Identifying processes and cyclical patterns within the water column of High Arctic lakes contributes to a broader understanding of how hydrologic systems are shifting with climate change (Cochand et al., 2019; Vincent et al., 2008). As lakes are the hydrologic sinks in a drainage basin that integrate information from surficial processes operating through atmospheric exchanges and river inputs (Woo, 2012a), they are recognized for their value as sentinels of climate change (Adrian et al., 2009; Mueller et al., 2009; Vincent et al., 2008). High Arctic lakes are most notable for the extended presence of ice cover (9-12 months), which is the product of long periods of little to no solar radiation inputs and persistently low temperatures due to latitude (Vincent, 2009). Ice cover largely controls lake interactions with the atmosphere, impacting solar energy supply, heat content in the water, chemical and biological processes, mixing and stratification, as well as inputs from the terrestrial landscape. Lake processes critical to biogeochemical cycling have been found to occur under-ice in High Arctic lakes (Bégin et al., 2020).

While ice-covered lakes are often considered to be quiescent environments, recent studies reviewed by Kirillin et al. (2012) have found under-ice physico-chemical processes to be dynamic. These dynamics are driven by processes including heat exchange with bottom sediments, wind- or seiche-driven oscillations, and/or convective currents generated by solar radiation at the surface of a lake (Bengtsson, 1996b; Kirillin et al., 2012; MacIntyre et al., 2018; Malm et al., 1998; Welch & Bergmann, 1985). Such processes can initiate circulation within ice-covered lakes that can make significant contributions to the transport of dissolved and suspended particles in the water column (Zdorovenova et al., 2021a).

Ice cover can influence physical, chemical, and biological events in lakes involving both biotic and abiotic processes (Bégin et al., 2020; Cortés & MacIntyre, 2020; Woo, 2012a). Ice duration on lakes in the Northern Hemisphere has become increasingly shorter in the last century and as ice-off dates trend earlier, lakes with historically longer ice cover durations (i.e., High Arctic lakes) will experience the

largest changes to their ecosystem dynamics (Dugan, 2021; Sharma et al., 2019, 2021). Additionally, increasingly deep thaw in the active layer has been shown to increase the delivery of ions (specifically SO_4^{2-}) to lakes, altering the geochemistry of the water column (cf. Chapter 3). Recent studies have also found that increased summer rainfall events are becoming more frequent and intense in High Arctic watersheds, consequentially contributing an increased delivery of solutes to lakes (Lamoureux & Lafrenière, 2017).

The under-ice dynamics of physical processes that occur in the water column of cold-region lakes have been extensively researched (Jansen et al., 2021; Kirillin et al., 2012; MacIntyre et al., 2018; Mortimer & Mackereth, 1958; Vincent et al., 2008; Welch & Bergmann, 1985; Zdrovennova et al., 2021). Year round, comprehensive water column records are generally lacking due to the logistical challenges of working in remote polar regions and difficulty in deploying instruments that can measure and store data over long periods of time in underwater environments. However, improved technologies now allow for near-continuous measurements and collection of data, generating time series datasets that allow for the study of under-ice processes in remote locations such as the High Arctic (Bégin, Tanabe, et al., 2020; MacIntyre et al., 2018).

Analysis of water column ion geochemistry of West Lake ($74^{\circ}89'N$, $109^{\circ}59'W$, unofficially named) at the Cape Bounty Arctic Watershed Observatory (CBAWO), located on the south-central coast of Melville Island, Nunavut, has revealed two reservoirs of water: a main water body (geochemical composition similar to surficial runoff (elevated SO_4^{2-} , < 30 meters depth, $\sim 100 \mu\text{S}/\text{cm}$), and a second, smaller reservoir described as elevated bottom water conductivity (EBWC) with a composition indicative of marine influence representing past water column geochemistry (Cl^- dominant, > 30 meters depth, $\sim 200 \mu\text{S}/\text{cm}$) (cf. Chapter 3). EBWC is defined by elevated SpC compared to the water column, recurring annually through the influx of dissolved ions through lake bottom (Harasyn et al., 2017; Lewis et al., 2018; Roberts et al., 2017) (cf. Chapter 3). This study will: (1) define and determine the degree and extent of physical processes associated with recurring seasonal trends occurring in the lake that contribute to

annually recurring elevated SpC at the lake bottom; and (2) confirm the mechanism (cf. Chapter 3) controlling the influx of elevated SpC in the lake bottom. This information will fill important gaps in our current understanding of trends in the timing of accumulation of EBWC in West Lake by analyzing and interpreting data collected during times when lake water has not typically been sampled or measured in the past, specifically during the ice-covered period.

4.3 Study Area

West Lake is situated in a glacially scoured basin ~2.5 km from the coast of the Arctic Ocean that formed during the retreat of the Innuitian and Laurentide ice sheets to create a convergent contact in the vicinity (England et al., 2009). Following glacial retreat, the land was transgressed by the sea and the basin was a marine embayment with most of the catchment submerged up to c. 80 m asl. Subsequent glacio-isostatic rebound resulted in emergence and isolation of the lake. Analysis of nearby East Lake suggests isolation and freshening of the lake occurred c. 1.8 ka BP (Cuven et al., 2011). After the emergence of the landscape, permafrost aggraded during the Holocene to reach a thickness of 500+ m in the area. The physiography of the region currently consists of gentle slopes and rolling hills covered by unconsolidated late glacial and early Holocene marine sediments overlying Devonian sedimentary bedrock (siltstones and sandstones).

Winters at the CBAWO are cold and dark, where annual solar radiation is close to 0 w/m² between Nov-01 and Feb-01. Mean air temperature is -14°C with maximum ice thickness on the lake reaching 1.8-2.3 meters. Temperatures above 0 °C only occur during the spring-summer “melt season” in June, July, and August with mean seasonal summer air temperatures of 2.7 °C ±1.4 °C (2003-2017). Active layer formation also occurs during the melt season reaching maximum depths between 0.7 and 1.0 m thick in July and early August (Beel et al., 2020). Precipitation is limited with ~160 mm or less annually (Roberts et al. 2017).

West Lake is a cold-monomictic lake, 1.3 km² in area, situated within an 8.0 km² primary watershed. The lake is ~ 35 meters deep, with a mean depth of 15 meters (Harasyn et al., 2017). The lake

is ice-covered for 9-10 months each year with bottom sediments extending to depth of 2-8 meters below the lake bottom (Normandeau et al., 2016) and composed of silt-clay laminated units underlain by marine muds (Cuven et al., 2011). The onset of ice melt, typically beginning in June, initially forms an open water moat around the perimeter of the lake. This moat opens the outlet for water in the lake, and around this time snowmelt begins to flow into the lake primarily through the West River. Runoff is dominated by snowmelt, however rainfall-generated runoff events are becoming more common later in the melt-season (Beel et al., 2021; Lamoureux & Lafrenière, 2017). River discharge reaches peak flow in June then recedes, reaching baseflow in early July through August (Lewis et al., 2018). West Lake overturns once each year in spring-summer as air temperatures warm, and ice melts until the surface of the lake goes ice free sometime between mid-July to early August; however, during colder summers the lake may retain some ice cover (e.g., 2003, 2004 (the coldest thaw season), and more recently in 2013 and 2014 (Lamoureux & Lafrenière, 2017)). By late August air temperatures decline and ice begins to form on the lake surface. In winter snowfall is typically unevenly distributed across the lake due to strong winter winds leaving the northern end of the lake largely free of snow (bare ice) in late winter (Lewis et al., 2018).

Swath bathymetric mapping of the lake bottom revealed that the northern basin is the deepest (34 m) and widest (1-km) region of the lake, located near the front of the West River delta (Figure 4.1) (Normandeau et al., 2016). The authors also showed rill and gully structures along the lake slopes associated with hyperpycnal flows that form during the early snowmelt period when river inflows are denser than the lake water due to high suspended sediment loads (Lewis et al., 2018). These hyperpycnal flows can flush river water down the slopes of the lake into to the deepest regions to displace EBWC, which accumulates over winter (cf. Chapter 3) (Lewis et al., 2018). EBWC develops as a 0.5 to 2.0 m thick zone in the deepest depressions below 30 m depth, making up less than one percent of the entire lake water volume (0.5 m thick, EBWC area is 0.041 km² with a volume of 34,300 m³, and at 2.0 m thick EBWC area is 0.076 km², with a volume of 122,400 m³) (Lewis et al., 2018). Water column profiles show

that the transition between overlying water column and EBWC is gradual, increasing in SpC from ~100 $\mu\text{S}/\text{cm}$ in the water column to $> 200 \mu\text{S}/\text{cm}$ in EBWC (cf. Chapter 3). Although this SpC is insufficient to be considered brackish, groundwater is known to have higher concentrations of dissolved solutes than surface water (Ibanez et al., 2007). Therefore, EBWC was previously considered evidence of groundwater seepage (Dugan & Lamoureux, 2011; Harasyn et al., 2017; Roberts et al., 2017). However, more recent analysis of the geochemistry of EBWC bottom water concluded that EBWC is more likely an accumulation of relict marine water trapped in sediments during past submergence below sea level that now is slowly diffusing into the lake bottom at the sediment water interface (cf. Chapter 3).

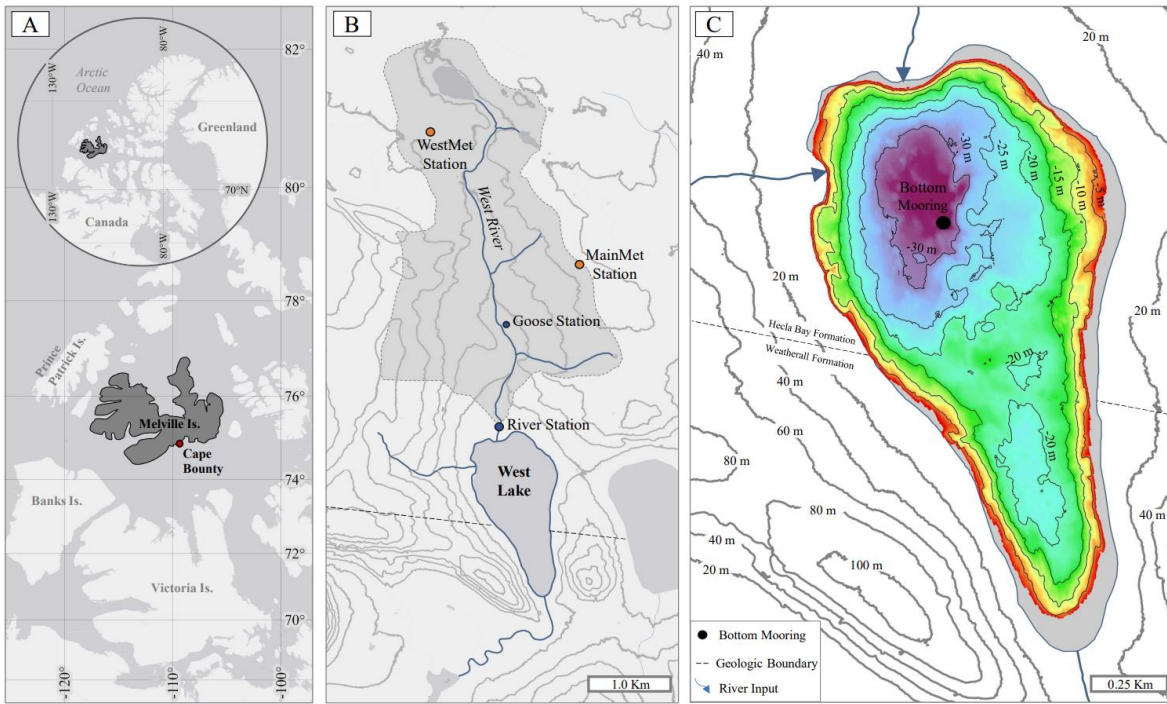


Figure 4.1: Maps of (A) Cape Bounty on Melville Island in the Canadian High Arctic; (B) West Lake watershed at the Cape Bounty Arctic Watershed Observatory (CBAWO); and (C) bathymetric map of West Lake derived from swath bathymetry. The location of the moored CTD logger is visible on map C (solid black circle). The DEM was derived using contours digitized from 1:50 000 NTS 78 F/15. The cell size is 10 m. Shorelines in map A retrieved from Esri, ©OpenStreetMap.

4.4 Methods

4.4.1 Ice Phenology

Ice phenology timing was determined through analysis of time-lapse photography recorded from an automated camera overlooking the northern 80% of the lake surface, capturing images at 30-minute intervals (Appendix B). Ice-on is defined by the date when the lake surface first becomes completely ice covered, and ice-off as the date the lake surface is completely cleared of all ice. At West Lake, trends in ice surface phenology have been collected using time lapse imagery since 2012. The lake was not visible due to obstruction by snow on the lens in time-lapse photos from 2016-Aug-01 to 2016-Oct-01 and 2017-August-08 to 2017-Sept-17; dates of ice-on were therefore determined using mooring temperature data (cf. Section 4.6.3).

4.3.4 Climate

Climate data was collected from two weather stations, Main Met (regional) and West Met stations located near the CBAWO (Figure 4.1). Local air temperature and rainfall were collected hourly from West Met station, and hourly solar radiation was measured 2.8-km from the lake at Main Met station. Additionally, soil temperature data was collected around West Lake to determine the timing of freeze-up and thaw in the active layer. Dates of active layer freeze-up and thaw were determined from soil temperature measurements collected from Lower Goose Station at the CBAWO (Figure 4.1) (Appendix D; Rahman, 2021).

4.3.3 Fluvial Inputs

West River discharge (m^3/s) and suspended sediment concentration (SSC, mg/L) data was collected from a hydrometric station located 0.2 km from the West Lake inlet on the main river channel (Figure 4.1 B). River water 500 mL samples was obtained every three hours using an ISCO 3700C

automatic pump sampler. SSC was determined by filtering through pre-weighed 1.0 µm glass fibre filters that were subsequently freeze-dried and reweighed.

4.4.2 Lake Mooring

An RBR XR-420 CTD datalogger (the “mooring”) was deployed on June 6, 2016, in the deepest depression at the northern end of the lake (Figure 4.1 C), anchored to the lakebed at a fixed depth of 32 m, and attached to a buoyant rope and float for later retrieval from the surface on August 5th, 2018 (Figure 4.2). The mooring was programmed to measure specific conductivity (SpC (µS/cm), corrected at 25°C, $\sigma = 1 \mu\text{S/cm}$), temperature ($\sigma = 0.001^\circ\text{C}$), and density anomaly (kg/cm^3) at 15-minute intervals. SpC is derived from the expected atmospheric pressure and temperature of the water calculated using the Standard Methods for the Examination of Water and Wastewater (Clesceri et al., 1999). The equation for deriving SpC (k_s) from raw conductivity (k_m) measured at a given temperature (t) is (Boehrer and Shultze, 2008):

$$k_s = \frac{k_m}{1 + 0.0191(t - 25)}$$

Density measurements are valuable in limnological studies as an indication of the stability of the water column (Boehrer & Schultze, 2009). This study uses density anomaly which is the departure from the density of pure water ($\sim 1 \text{ g/cm}^3$ at 4°C). At 4°C water contracts to its lowest volume reaching its maximum density ($T_{MD} = \sim 4^\circ\text{C}$). As water warms or cools from the T_{MD} it expands, and its density decreases. Since both temperature and dissolved solutes contribute to density differences in water, they are used to calculate density in fresh water. Density is calculated based on UNESCO Technical paper in Marine Science # 44, using a correction to the density measurements based on an estimated pressure and density for fresh water (Fofonoff & Millard, 1983). Depth measurements were analysed to confirm the mooring did not shift its position due to the possibility of lake ice freezing to the retrieval rope and subsequently dragging the mooring during ice melt periods.

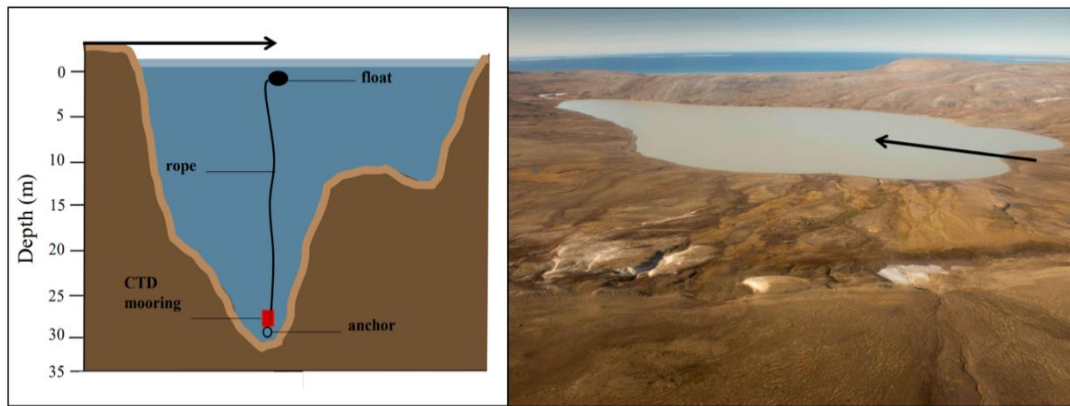


Figure 4.2: The placement of the CTD (red box – panel A) moored in the deepest depression of West Lake located approximately 0.5-km off the north shore of the lake (location offshore marked with an arrow – panel A and B). The mooring is anchored to the lake bottom (black circle) and tied to a rope (black line) accessible with a float from the water surface (black oval). Lake image taken August 2015 during ice-off conditions (photo credit: S. Lamoureux).

4.3.5 Wavelet Analysis

Wavelet and cross-coherence analyses were used to identify patterns such as periodicity in the mooring records for SpC, temperature and density. Wavelet analysis is used to analyze time-variant changes in spectral power within a time series (Torrence & Compo, 1998). WaveletComp, an R package developed by Rösch and Schmidbauer, (2018) for continuous wavelet-based analysis of univariate and bivariate time series was used for the analyses. It uses Fast Fourier Transform algorithms following the methodology by Terrance and Compo (1998) to evaluate the Morlet wavelet transform of a time series (x_t):

$$Wave(\tau, s) = \sum_t x_t \frac{1}{\sqrt{s}} \psi * \left(\frac{t-\tau}{s} \right)$$

The analysis decomposes a time series into time-frequency space to determine both the dominant modes of cyclical variability as well as the variation of these dominant modes in time. The ‘analyze.wavelet’ function was used to generate images showing: (i) the average power and phase for selected periods; and (ii) time/period image of phases. Cross-coherence analysis compares the phase of two separate time series. The ‘analyze.coherency’ function was used to plot a time (x-axis), and period (y-axis) image of cross-wavelet power. SpC, temperature and density wavelet signals were subsequently compared with the 24-hour wavelet signal for solar radiation. Statistical significance tests (p-value) were determined from generated simulations operating on the null hypothesis that there is no correlation between periodicities (i.e., joint periodicity) of two separate wavelet series (i.e., SpC, temperature, or density anomaly with solar radiation). Where joint periodicity is present between two wavelet series, cross-coherence results will reflect this, and additionally will also indicate if the data are in phase with one another during a given period.

4.5 Results

4.5.1 Surface Ice Phenology

Figure 4.3 shows temporal trends for ice phenology for West Lake from 2012-2019. In each year of this study (2016-2018), time-lapse imagery shows thaw beginning at the shoreline in early- to mid-June, eventually causing the ice pan to become mobile (when sufficient melt around the perimeter of the shoreline allows the ice pan to detach from the land) (Appendix B). The mobile ice pan begins to break apart ('ice breakup') as it travels across the lake surface and temperatures warm (Figure 4.3). In all three melt seasons, time-lapse imagery shows the ice pan completely melts and the lake is ice free by mid-August ('ice-off'). The mean ice-free period from 2013-2018 was 45 days, with ice-free periods ranging from 62 days in 2016, 39 days in 2017, and 28 days in 2018. In addition to 2016 being the longest ice-free period, it also began much earlier (Aug-01-2016) compared to 2017 (Aug-18-2018) and 2018 (Aug-07-2017). By late September to early October, the ice begins to form again on the surface of the lake. The active layer typically freezes around the same date the lake surface freezes over (Figure 4.3), where the mean freeze-up date for West Lake is Sept-21, followed by the mean freeze-up date for the active layer on Sept-23 (Figure 4.3). After this initial freeze-up of the ice surface the lake remains completely frozen until the following melt season.

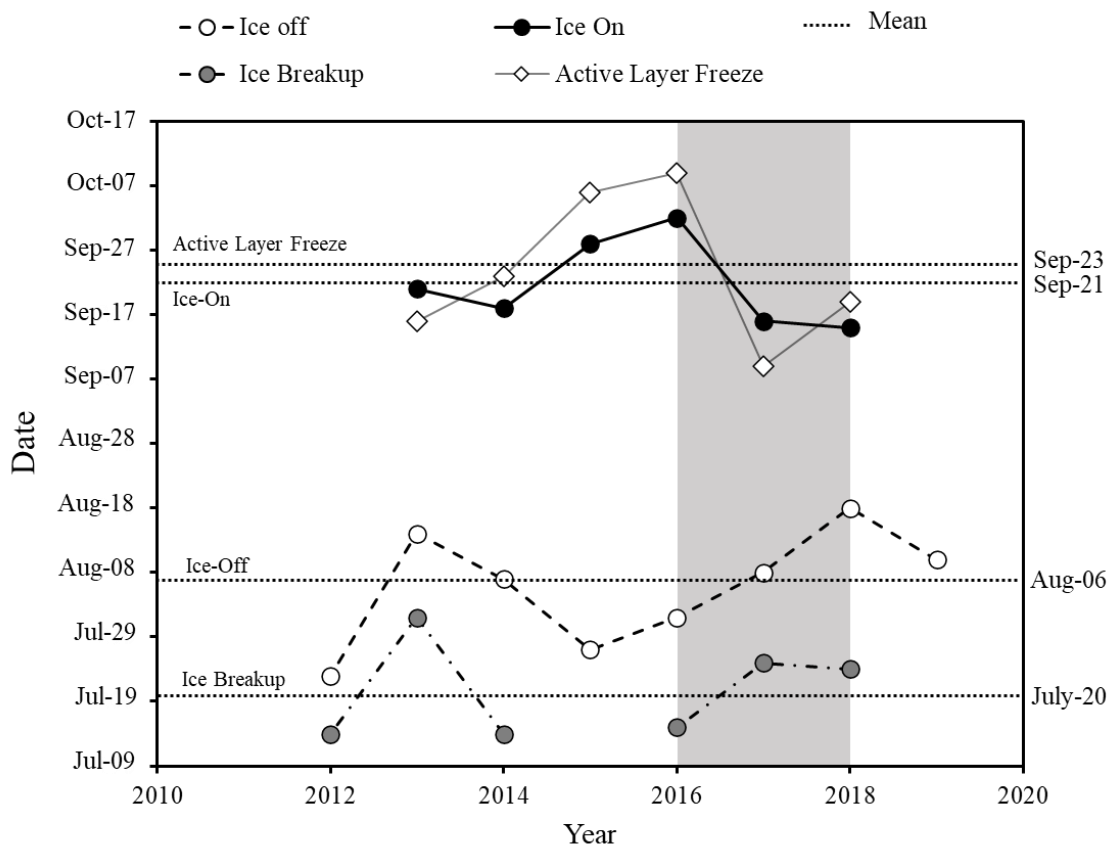


Figure 4.3: Temporal trends in surface ice phenology and active layer (AL) freeze up near West Lake between 2012 and 2019. Onset dates where the water is completely clear of ice (ice-off), completely frozen (ice-on), breakup of the ice pan (breakup date), and complete freeze up of the AL occur between July 13 and October 8. Lake ice phenology dates were acquired by visual interpretation of automated time-lapse imagery overlooking the northern portion of West Lake (ice-on dates for 2017 unavailable, determined from lake-bottom temperature signature). The study interval is shaded in grey.

4.5.2 Hydrometeorology

4.5.2.1 Air Temperature and Precipitation

Seasonal air temperatures at Cape Bounty rise and fall in conjunction with solar radiation (Figure 4.4 A-B). For example, daily surface temperatures begin to warm in spring in response to heat provided by increasing solar radiation in late March; by August, air temperatures begin to decline with a steady decrease in solar radiation. Table 1 provides a summary of monthly temperature and rainfall data from 2016-2018. During the study period the mean annual air temperature was -13.4°C , with 2016 being the warmest year and 2018 the coldest (Table 4.1 A). Precipitation, as rainfall, occurs only during late spring and summer when temperatures exceed 0°C (Table 4.1 B) with peak rainfall events occurring between June and mid-August. For the three years of the study 2018 had the highest total annual rainfall with 82.4 mm, followed by 2016 with 72.6 mm, and 2017 with the lowest total of 41.2 mm.

Table 4.1: (A) Mean daily air temperature ($\sigma = 0.1$ °C) and rainfall (B) were collected from West Met meteorological station at CBAWO. Mean monthly air temperature and total precipitation values are shown for winter (December, January, February), spring (March, April, May), summer (June, July, August), autumn (September, October, November) between 2016 and 2018. Annual maximum (red) and minimum (blue) annual air temperatures are highlighted.

A	Temperature (°C)		
Month	2016	2017	2018
Jan	-26.9	-30.9	-25.5
Feb	-28.4	-30.7	-29.9
March	-27.1	-31.8	-32.2
April	-22.3	-21.2	-21.8
May	-7.1	-8.3	-10.3
June	2.4	-0.5	0.8
July	5.5	4.5	3.8
Aug	2.1	1.6	0.9
Sept	-3.2	-5.8	-6.3
Oct	-12.2	-15.2	-12.4
Nov	-18.3	-21.3	-25.4
Dec	-26.0	-24.5	-29.1
Mean Annual (Max, Min)	-13.4 (+11.0, -36.22)	-15.3 (+11.2, -47.33)	-15.5 (+9.86, -37.8)
B	Rainfall (mm)		
Month	2016	2017	2018
Jan	0.0	0.0	0.0
Feb	0.0	0.0	0.0
March	0.0	0.0	0.0
April	0.0	0.0	0.0
May	1.0	1.6	0.0
June	14.0	2.6	10.6
July	37.2	11.6	34.6
Aug	19.0	25.0	31.6
Sept	1.4	0.4	5.4
Oct	0.0	0.0	0.0
Nov	0.0	0.0	0.0
Dec	0.0	0.0	0.0
Total Annual	72.6	41.2	82.2

4.5.2.2 West River Discharge and Suspended Sediment Load

Figure 4.4 C shows hydrometric data from the West River station for 2016 and 2017. Water flow in West River generally begins shortly after air temperatures rise above 0°C, with maximum discharge occurring in both years as thaw on the terrestrial surface begins in June. High discharge rates are closely followed by a high SSC (Figure 4.4 C). Peak discharge occurs 12 days earlier in June 2016 (June-13; 2.47 m³/s) compared to June 2017 (June-25; 3.36 m³/s). Following peak discharge, peak SSC values lagged 3 days behind peak discharge in 2016 (June-16; 633.63 mg/L SSC) compared to an 11-day lag in 2017 (July-03; 1531.58 mg/L SSC). Discharge and SSC data was not analyzed for 2018 because the lake bottom mooring was removed before the 2018 melt season began.

4.5.3 Water Column Conditions

Measurements of SpC, temperature and density from the mooring, which all vary over the course of the study period (Figure 4.4 C); i.e., SpC values ranged between 30-289 µS/cm, water temperature between 0.2-3.7 °C, and density anomaly from 0.02-0.16 kg/m³. SpC show periods of higher values that rapidly oscillate over time in the thaw seasons and shortly after ice-on, which contrasts with other periods of relatively quiescent, yet increasing values during the ice-on periods. Temperatures are lowest during ice-on periods, increasing during the thaw season reaching maximum and minimum values while the lake is ice free. Density anomalies reflect both periods of higher values with rapid oscillations during the thaw seasons and following ice-on, with comparatively quiescent increases under ice, with gradual increases and decreases during the late thaw and ice-free season.

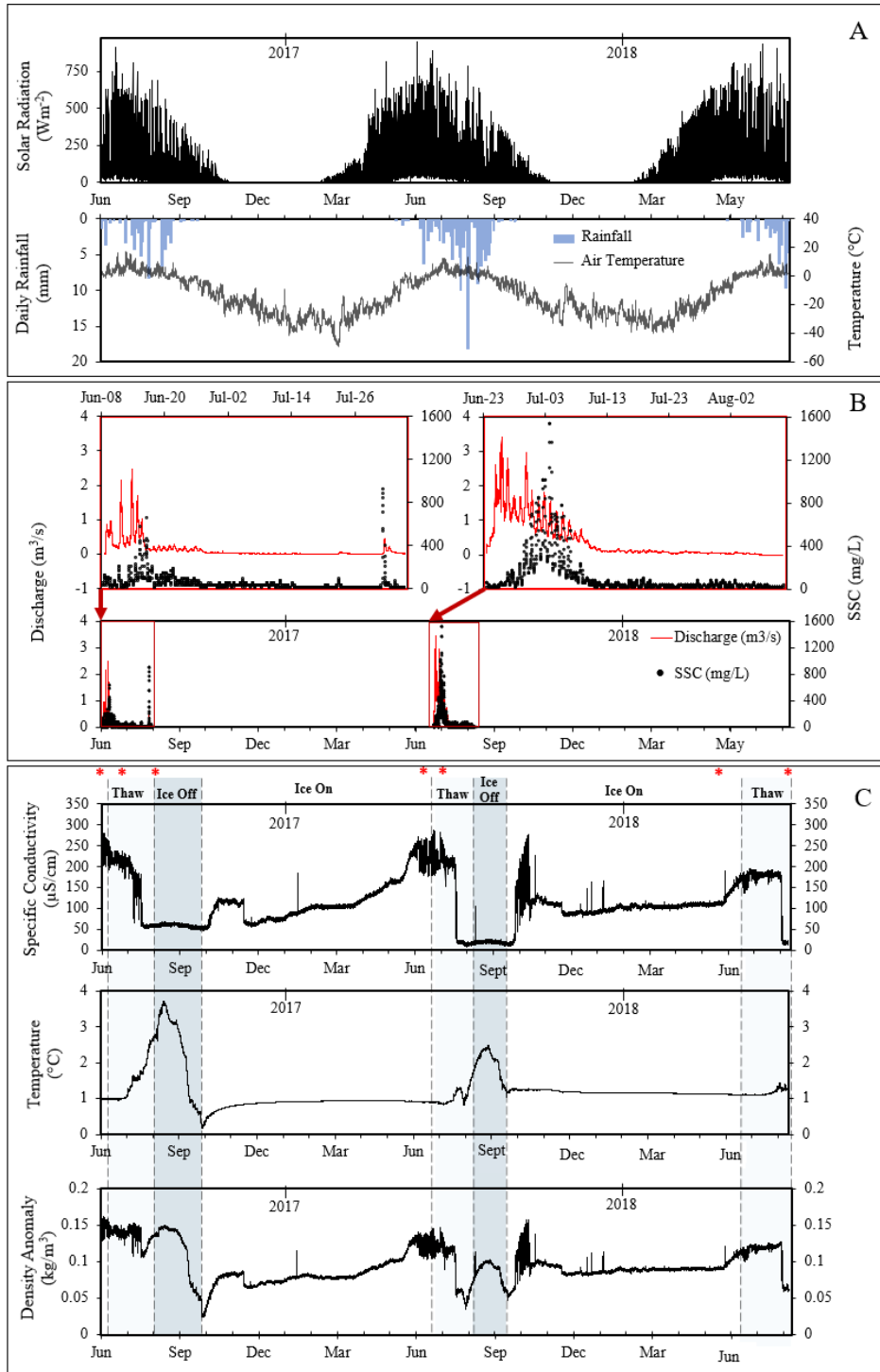


Figure 4.4: Terrestrial and lake data collected at the CBAWO during the study period: (A) Solar radiation (W/m^2) (Main Met meteorological station), mean daily air temperature ($^{\circ}C$) and total daily rainfall (mm) (West Met meteorological station); (B) river discharge (m^3/s) and suspended sediment concentration (SSC) (mg/L) (West River station); (C) and lake-bottom (mooring at 32 m depth) specific conductivity (SpC) (mS/cm), temperature ($^{\circ}C$), and density anomaly (kg/m^3).

Water column casts collected in spring and summer between 2016-2018 display temperature and SpC values (Figure 4.5) comparable to the values collected from the bottom mooring (Figure 4.4 C). Water temperatures ranged from 0°C to 3.7 °C depending upon time of measurement. Average water temperature at the bottom of West Lake was 1.2 °C during the study period. Lake bottom temperature fluctuated annually between a low of 0.17 °C and a high of 3.7 °C (Figure 4.4 C). The warmest annual water column temperatures were recorded during summer in 2016 (3.7 °C), 2017 (2.5 °C) and 2018 (1.3 °C) and remained constant through the water column (water column casts were not collected during the ice-free period in 2017.) Conversely, in May, water column temperatures were slightly lower near the surface beneath lake ice (shallower than ~5 m depth) and increased gradually in the bottom 15 m of the lake with differences of less than 1 °C.

SpC values were constant through the water column when the lake was ice-free, measuring ~86 µS/cm and ~123 µS/cm, in August 2016 and 2018, respectively. However, late-winter casts show SpC increases in the bottom five metres of the water column. This is an example of increases in SpC previously identified as the EBWC zone by Harasyn et al. (2017) and Lewis et al., (2018) and defined as a distinctly different region from the water column (cf. Chapter 3).

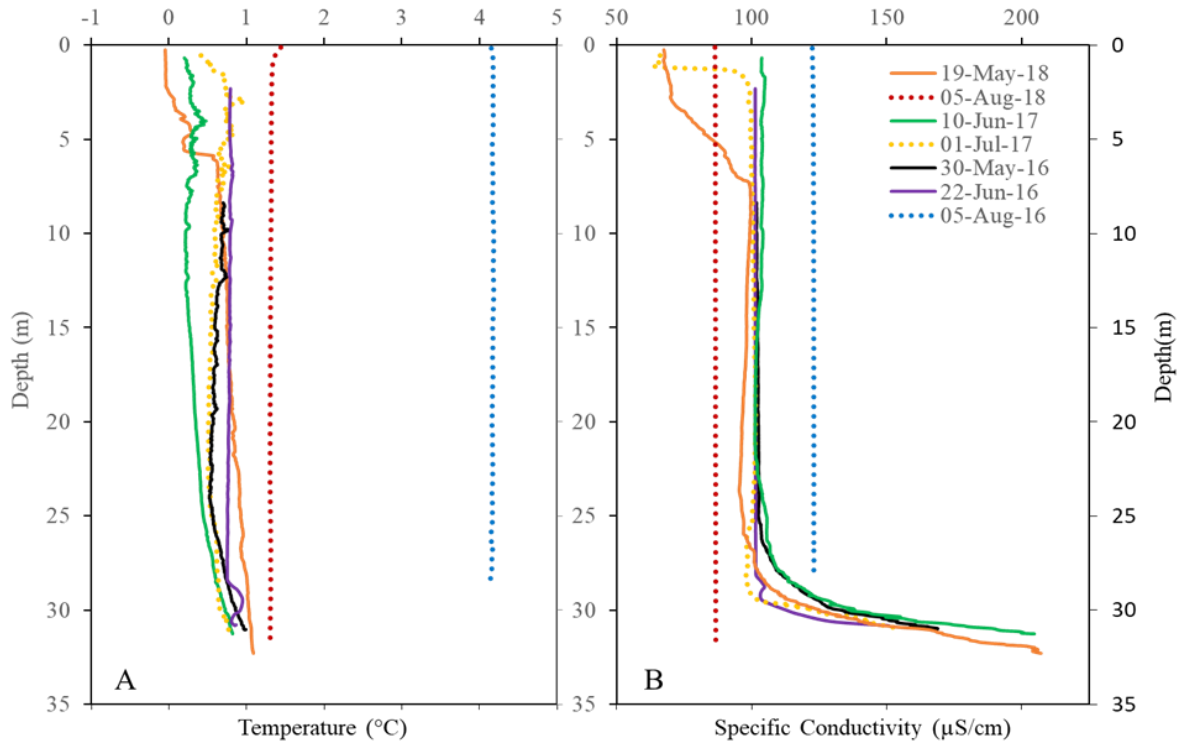


Figure 4.5: Profiles of (A) temperature and (B) specific conductivity collected in spring (solid lines – May, June) and summer (dotted lines – July, August) in 2016, 2017, and 2018 from a mid-lake station in West Lake.

4.5.4 Lake Mooring Patterns

Notable events (e.g., peak SSC, ice breakup, etc.) recur annually in conjunction with measured changes in SpC, temperature, and density anomaly for the entire study period (Figure 4.6). Seasonal patterns identified in the full year of lake bottom data recorded in 2017 are also visible in 2017 (June-December) and 2018 (January-August) partial years (Figure 4.6). Patterns identified in SpC, temperature and density vary and are compared to the timing of key events occurring on the terrestrial surface (i.e., peak SSC, the start of ice breakup (i.e., the ice pan begins to travel around the lake), complete ice-on and -off, and active layer freeze-up) outlined individually in the following sections.

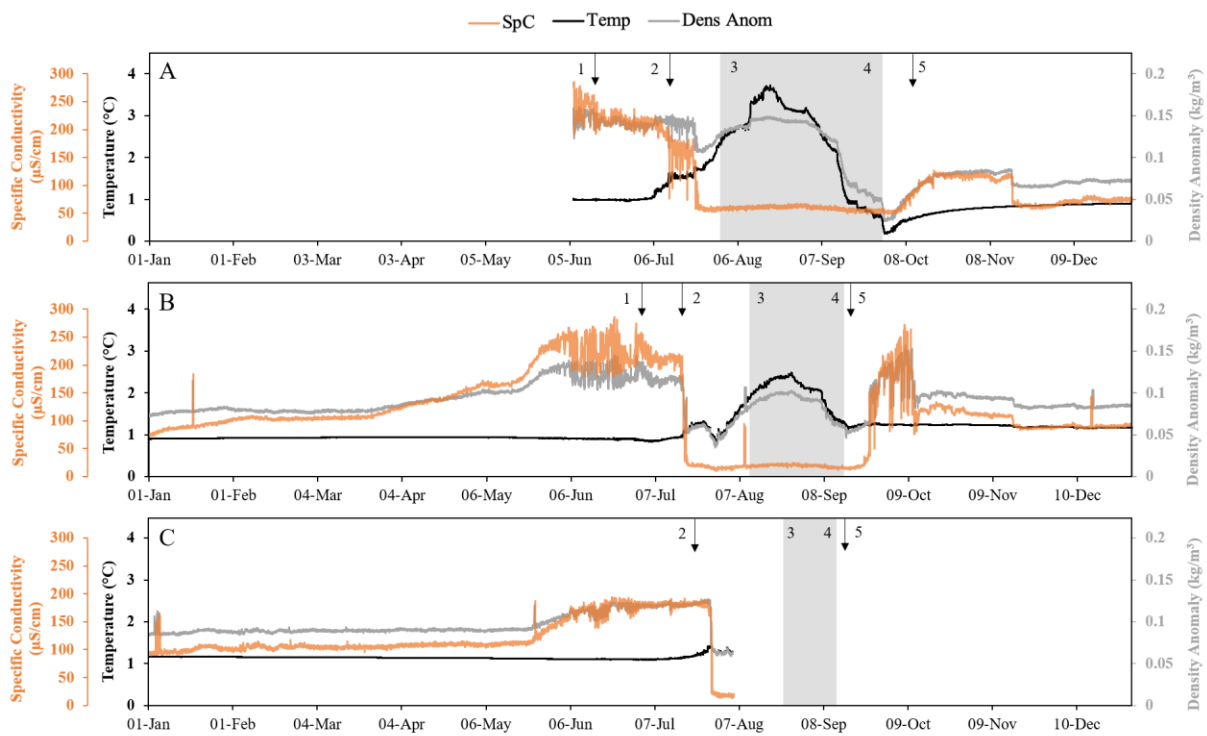


Figure 4.6: Annual patterns in the lake bottom specific conductivity, temperature, and density collected by a lake-bottom mooring in 2016 (A), 2017 (B), and 2018 (C). Repetition of annual lake bottom patterns from the full year of 2017 data are visible in the partial years of 2016 and 2018. Numbered arrows mark key dates of: (1) peak SSC; (2) date of ice pan detachment from the land; (3) complete ice-off; (4) complete ice-on; and (5) active layer freeze-up at Lower Goose Station (Rahman, 2021). Ice-free periods shaded in grey. SSC data not available for 2018.

4.5.4.1 Bottom Specific Conductivity

May-June

The mooring record begins in June 2016 (Figure 4.6 A) recording some of the highest SpC values in the lake through the entire mooring period. The following two years of data display high annual SpC values, in addition to visible changes in the pattern of lake bottom SpC where gradual over winter increases in SpC begin to accelerate rapidly (becoming steeper) in late May 2017. In addition, cyclical variations in the data are visible (Appendix C). Oscillations are quasi-cyclical, where the amplitude increases from $28.4 \mu\text{S cm}^{-1} \text{ day}^{-1}$ in late May to $105 \mu\text{S cm}^{-1} \text{ day}^{-1}$ by late June of 2017 (Figure 4.6 B). Quasi-cyclical oscillations in lake bottom SpC occur between May-25 and July-01 in 2017. Oscillations are similarly visible in 2018 between May-23 to July-01 but with less extreme variations in oscillations (Figure 4.6 C). In 2016, the start of these oscillations in lake bottom SpC occurred before the start of data collection, however, the data collected reveal 2016 oscillations end on June-16 (Figure 4.6 A), earlier than the other two years. Oscillations in 2017 show more consistent and greater daily amplitudes in comparison to data available in 2016 and 2018. In each study year, peak annual SpC values (values between $200\text{-}300 \mu\text{S/cm}$) and daily amplitudes ($\sim 100 \mu\text{S cm}^{-1} \text{ day}^{-1}$) occur during this late winter period. Quasi-cyclical oscillations begin to dissipate in early July 2016 and 2017, and in late July 2018, where the daily variation in SpC becomes more irregular and the trend of lake bottom SpC values begin to decrease.

June-September:

Around the time that the river reaches peak SSC, lake bottom SpC begins to decrease gradually, and the amplitude of daily oscillations become more irregular, decreasing from the late winter peaks (Figure 4.6 A-B, 1). By mid- to late July, SpC decreases to the lowest values in the time span of hours following the detachment of ice from the land where the ice pan becomes visibly mobile (Figure 4.6 A-C, 2). In 2017, values drop from $160 \mu\text{S/cm}$ to $30 \mu\text{S/cm}$ on July-17, in 2016 from $140 \mu\text{S/cm}$ to $70 \mu\text{S/cm}$ on July-21, and in 2018 from $180 \mu\text{S/cm}$ to $30 \mu\text{S/cm}$ on July-28. Following this decrease in lake bottom SpC, the lake becomes ice-free (Figure 4.6 A-C, 3) and lake bottom SpC shows slight gradual increases

until late August (Aug-25-2017 and Aug-28-2016) which then change to a gradual decreasing trend continuing until the complete freeze over of the lake in late September (Figure 4.6 A-C, 4), followed by the complete freeze-up of the active layer (Figure 4.6 A-C, 5).

September-May:

By October, the SpC begins to increase for approximately two weeks in both 2017 (15 days) and 2016 (12 days). In 2017 values peak at 276 $\mu\text{S}/\text{cm}$ on 10-Oct-2017 (Figure 4.6). In 2017 these increases are accompanied by oscillations with irregular variations in high and low values. Although this increasing SpC is evident in 2016, oscillations are not present, and values are lower, rising from 50 $\mu\text{S}/\text{cm}$ on 04-Oct-16, to 127 $\mu\text{S}/\text{cm}$ on 18-Oct-16, with some irregular drops, although less abrupt compared to the 2017 data. These increases in SpC are followed by a period of consistency over winter (Nov-1-2016 to May-25-2017) and 2017 (Nov-17-2017 to May-23-2018) where the magnitude of oscillatory variations in SpC are typically $< 5 \mu\text{S}/\text{cm}$ with only sporadic larger daily fluctuations close to $\sim 50 \mu\text{S}/\text{cm}$. Larger fluctuations occur over several hours and are visible in both December 2017 and January 2018, with only one instance in January 2017. This quiescent period in the data ends in mid- to late May each year, when daily fluctuations gradually become larger and values begin to increase more rapidly (Figure 4.6 B-C).

4.5.4.2 Bottom Temperature

May-August:

In both years, beginning in May, lake bottom temperatures begin to decrease displaying irregular daily fluctuations increasing in amplitude until early July. Lake bottom water temperature is constant in June showing small daily fluctuations with peak amplitudes fluctuating between 0.04 $^{\circ}\text{C}/\text{day}$ in June 2017 and 0.02 $^{\circ}\text{C}/\text{day}$ in June 2018. In early July, in the days following peak SSC river discharge temperatures begin to increase from just above to 0 $^{\circ}\text{C}$ closer to the T_{MD} . (Figure 4.6 A-C, 1). Increasing temperatures continue until they reach annual maximum values by mid-August during the ice-free period in the lake (Figure 4.6 A-C, 3-4). Lake bottom temperatures were quicker to warm in 2016, reaching a maximum of 3.7 $^{\circ}\text{C}$ on Aug-18 compared to 2017 temperatures which reached a maximum of 2.5 $^{\circ}\text{C}$ on Aug-26.

August-November:

Lake bottom temperatures steadily decline from mid-August into September. In 2016 the temperature decreased from a high of 3.7 °C to 0.17 °C on 30-Sept, whereas in 2017 the temperature decreased from 2.5 °C to 1.03 °C on 17-Sept. On the same date as complete ice-on, lake temperatures stop declining and begin to rebound (Figure 4.6 A-C, 4). Within hours of reaching minimum temperatures the water slowly warms for approximately two weeks (increasing to 0.6 °C in 2016, and to 1.3 °C in 2017).

November-May:

After the period of lake bottom warming following ice-on (Figure 4.6 A-C, 4), the two winter sampling periods (Nov 2016 – May 17 and Nov 2017 – May 18) demonstrate diverging temperature trends. In winter 2016-17, lake bottom temperatures increase slightly from 0.8 °C to 0.9°C, however, in winter 2017-18 the lake bottom temperatures cool irregularly from 1.2 °C to 1.1°C.

4.5.4.3 Bottom Density Anomaly

Over the sampling period, the density anomaly of the water in the lake varied between values of 0.15 kg/cm³ and 0.025 kg/cm³. Density anomaly reflects patterns visible in both temperature and specific conductivity; the dominant control on water density (i.e., SpC or temperature) varies throughout the study period depending on which is dominant at any specific time (Boehrer and Shultze, 2009). In general, the density anomaly reflects SpC during the late winter and autumn seasons demonstrating prominent periods of increasing SpC in the lake bottom. Additionally, in the winter (Nov-May), an almost identical gradual increasing trend is visible in density anomaly and SpC data (Figure 4.6 A-C).

4.5.4.4 Wavelet Analysis of Bottom Data

Wavelet analysis of the lake bottom data revealed strong periodicity in SpC, oscillating on a 24-hour cycle between May-30-2017 and July-01-2017 (Figure 4.7A). This daily periodicity is strongest and consistent in late winter of 2017. Periodicity also occurred in the fall between Oct-01-2017 and Oct-12-

2017, however with more irregular occurrences between 12- and 24-hours. Wavelet analysis of lake bottom temperature did not return any discernable periodicity in the data (Figure 4.7 B) where wavelet analysis of lake bottom density anomaly showed similar diel cyclicity as SpC during the late winter period (Figure 4.7 C). Wavelet power spectra for both SpC and density anomaly show the most consistent 24-hour periodicity occurred in the late winter, and a shorter more sporadic period of cyclicity following the ice-on period in the fall (Figure 4.8).

24-hour periodicity in the data was further investigated through cross-coherence analysis between late winter and autumn solar radiation and lake bottom SpC periodicity wavelet functions (Appendix C). Over the full year of data in 2017, SpC and solar radiation were in phase in late winter, with solar radiation leading by approximately three hours ($1/8$ (or $\pi/8$) of a cycle) (Figure 4.9). Autumn (after the ice surface completely freezes) quasi-cyclical oscillations that occur in lake bottom SpC between late September and mid-October do not demonstrate the coherence with the 24-hour cyclicity visible in solar radiation; alternatively, their periodicity changes during this time, ranging between 0.25 and 4 days (Figure 4.8 B).

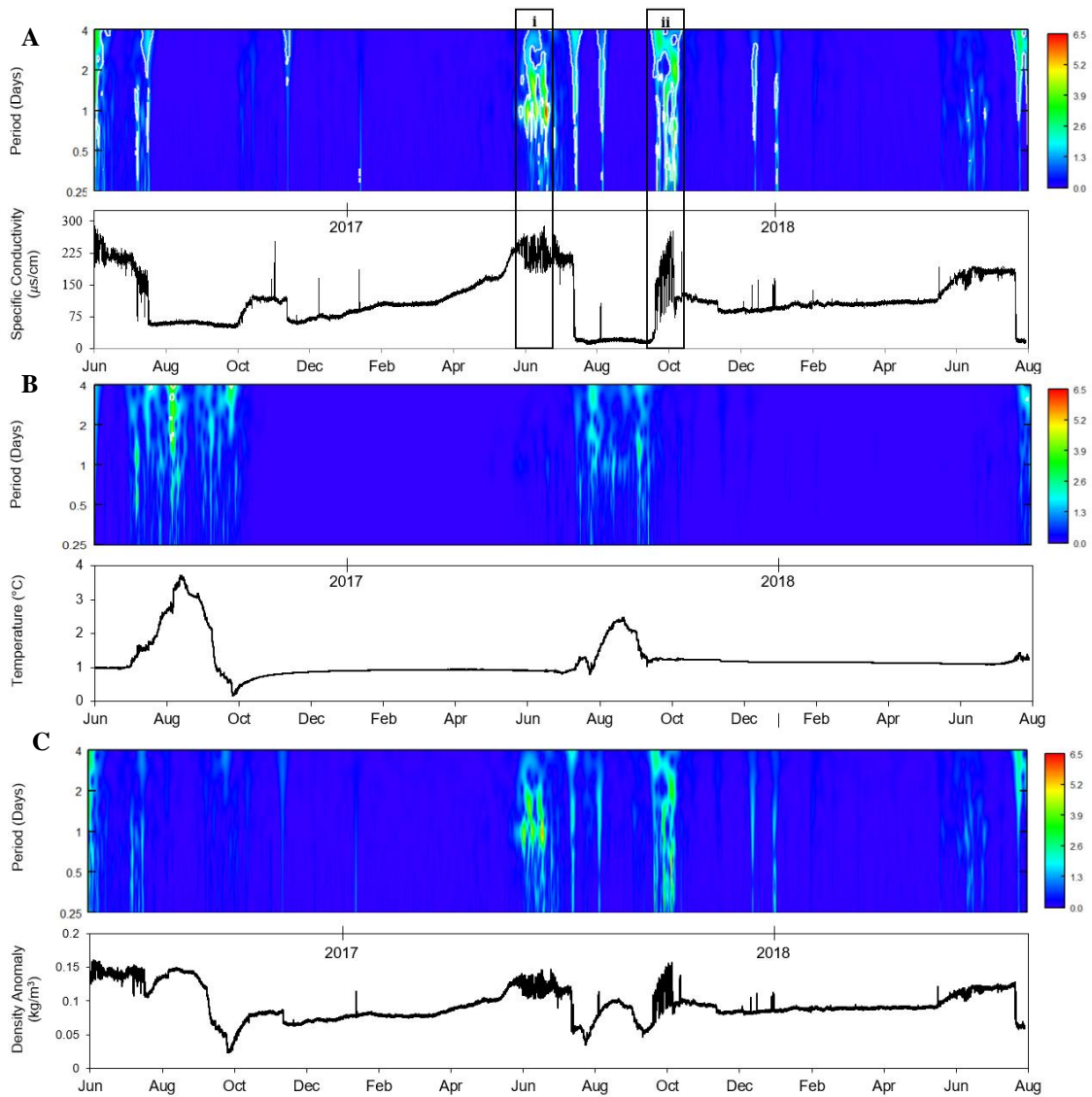


Figure 4.7: The wavelet power spectrum for the West Lake bottom specific conductivity data (A), temperature (B), and density anomaly (C). The spectrum ranges from the strongest signal (6.5 = red) to the weakest signal (0.0 = blue). White lines mark the areas where the p-value is less than 0.1 (rejecting the null hypothesis; there is no periodicity is not present) indicating that there is significant periodicity in the data.

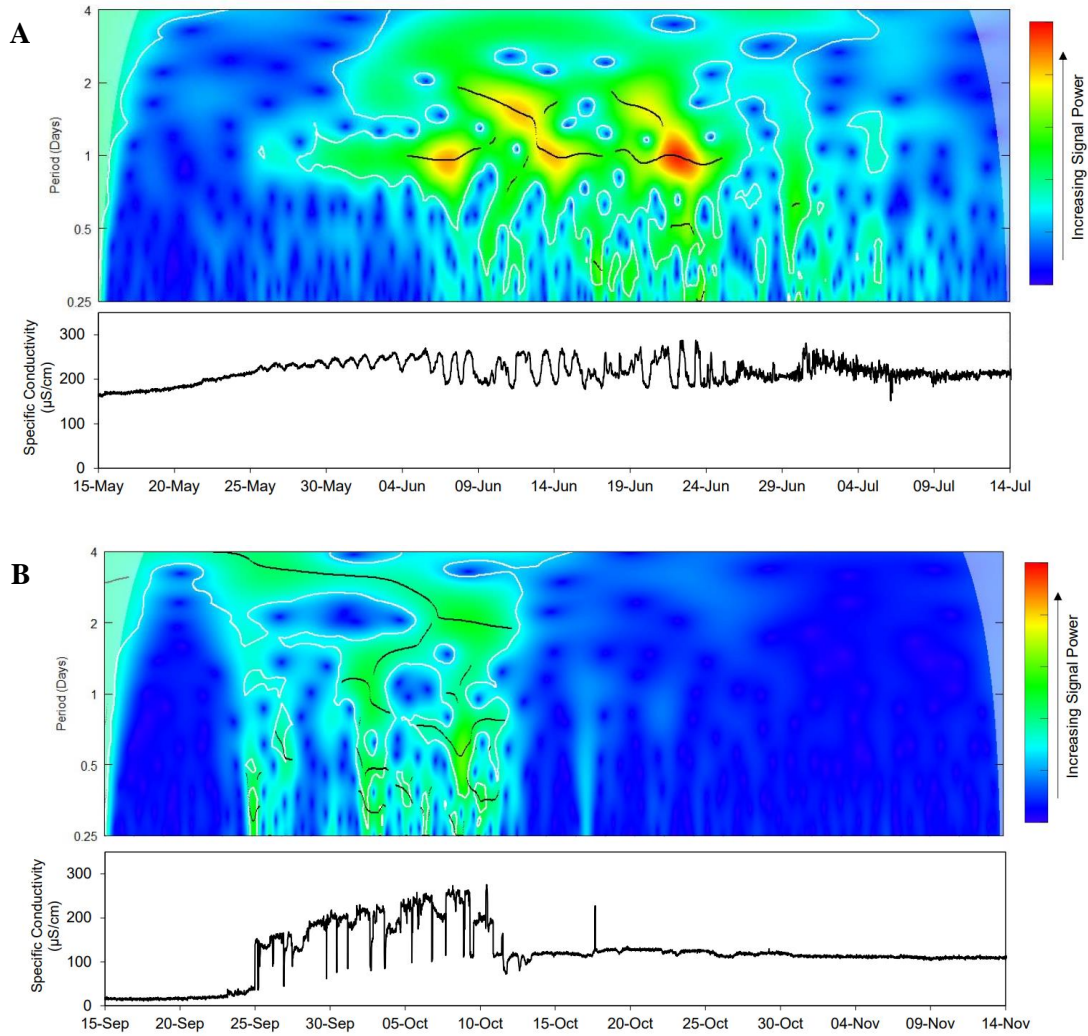


Figure 4.8: Wavelet power spectrum for 2017 lake bottom SpC data displaying oscillations found in Phase 1: Late winter (A) and Phase 3: Early winter (B) phases (see Section 4.6 Discussion for descriptions). Shaded areas indicate the cone of influence, where data within is considered non-significant due to a series of edge effects. The spectrum ranges from the strongest signal (6.5 = red) to the weakest signal (0.0 = blue). White lines mark the areas where the p-value is less than 0.1 (rejecting the null hypothesis; there is no periodicity is not present) indicating that there is significant periodicity in the data. Black lines indicate the ridge of maximum power.

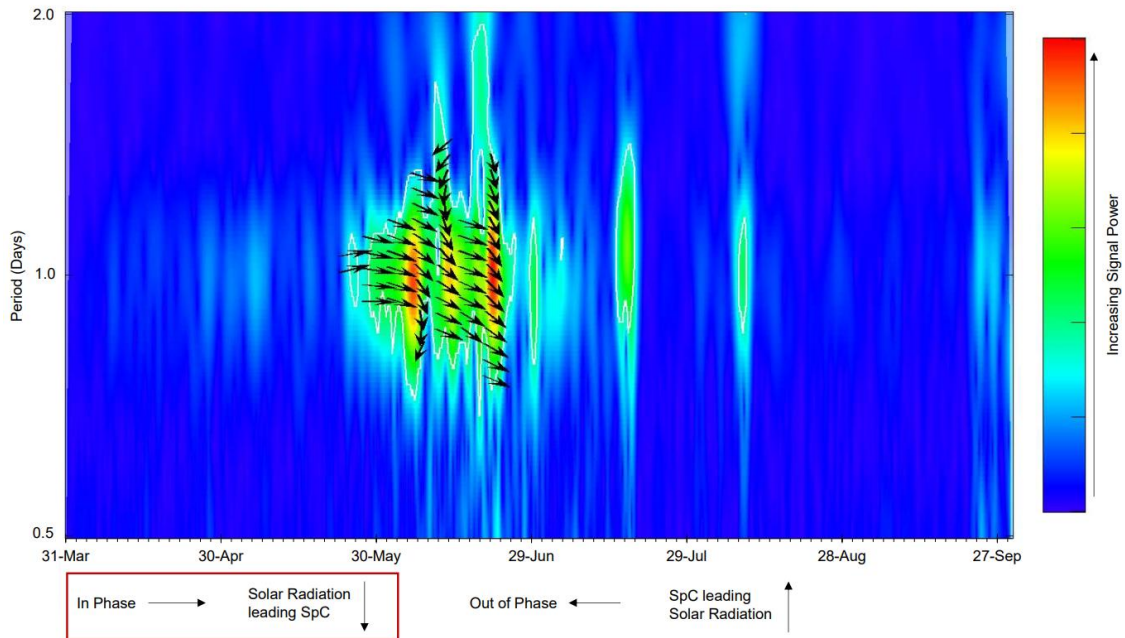


Figure 4.9: Displaying the cross-coherence spectrum of solar radiation (y) and lake bottom specific conductivity (SpC) (x) between March 31, 2017, and Sept. 30, 2017. The spectrum ranges from the strongest signal (6.5 = red) to the weakest signal (0.0 = blue). White lines mark the areas where the p-value is less than 0.1, (null hypothesis is rejected; periodicity is not present) indicating that there is significant periodicity in the data. Arrows indicate the phase difference between the x and y signals. Where horizontal arrows are pointing right (left) this indicates an in-phase (anti-phase) relationship; vertical/diagonal arrows indicate one signal leads/lags the other by a specific time interval denoted by the angle of the arrow.

4.6 Discussion

The zone of EBWC in West Lake has been identified as a geochemically distinct region, separate from the overlying water column, and likely resulting from the diffusion of marine-sourced porewaters across the sediment-water interface (cf. Chapter 3). This work investigates EBWC further through analyzing the temporal occurrence of EBWC using a time series data record of bottom water SpC, temperature, and density anomaly in the EBWC zone (~32 m depth) between June 2016 and August 2018. Over the 2.5-year sampling period, four distinct recurring phases are identified (Figure 4.10). As SpC is the most striking indicator of differences between the water column and bottom water, it has been the focus of this analysis. The four phases are as follows:

Phase 1: Late Winter (late May to late June)

Phase 2: Spring-Summer (late June to late September)

Phase 3: Early Winter (late September to late October)

Phase 4: Mid-Winter (late October to late May)

Note that some phases are cyclical (i.e., Phases 1 and 3) while others are not (i.e., Phases 2 and 4). This following section discusses the patterns found in the data and how they are related to the evolution of EBWC.

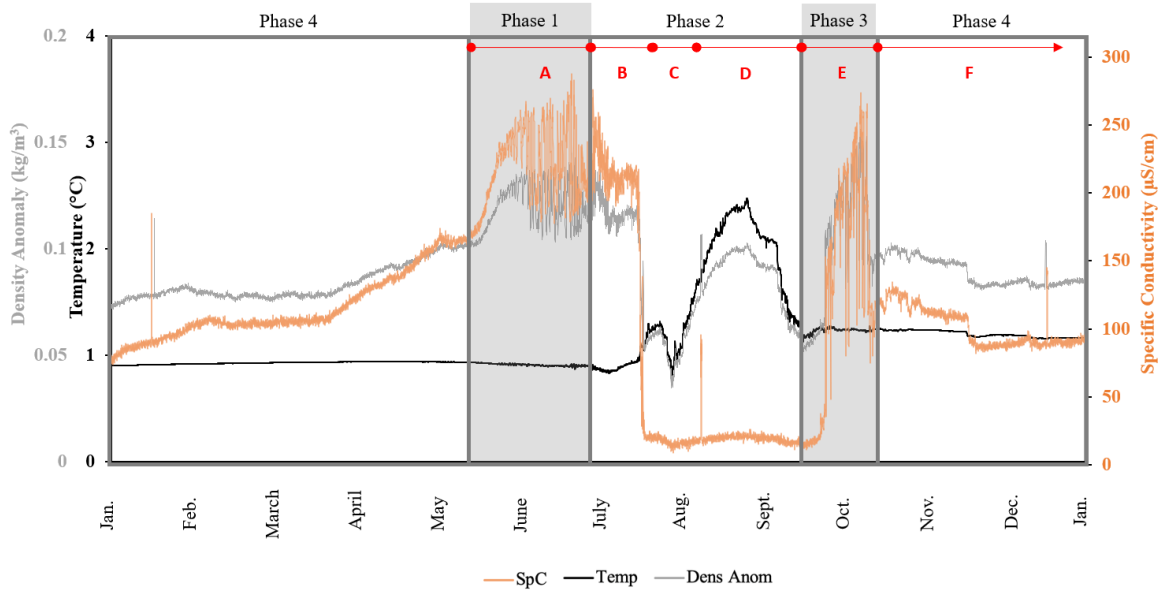


Figure 4.10: Displaying the entire year of 2017 West Lake bottom specific conductivity (orange), temperature (black), and density anomaly (grey) collected at the CBAWO. 2017 data is divided into phases (1-4) based on seasonal changes reflected in meteorological data, lake bottom data, and hydrologic data from the terrestrial surface. Grey boxes mark the periods of cyclical cycles in the data. Periods where terrestrial mechanisms are the dominant control impacting the lake bottom water are indicated (red lines): (A) Soar Radiation (May 15, 2017-July 3, 2017); (B) following peak suspended sediment concentration inputs (July 3, 2017-July 15, 2017) from West River; (C) the period of lake ice breakup following the detachment of ice from the land (July 15-2017-Aug. 8-2017); (D) ice-free period (Aug. 8, 2017- Sept. 17, 2017); and (E) ice-on complete and the response of the lake bottom (Sept. 17, 2017-Oct. 10, 2017), and (F) the majority of the winter period (indicated by the red line with an arrow; Oct 12, 2017-May 15, 2017).

4.6.1 Phase 1: Late Winter

Phase 1 is broadly defined by increasing lake bottom SpC. Time series data reveals that EBWC, previously identified through lake bottom casts (Figure 4.5), is not only most pronounced during late winter (accelerating increases beginning in mid- to late May, e.g., May-15-2017), but also reveals the mechanism causing the increases. An investigation of quasi-cyclical oscillations in the data using wavelet analysis indicates diel (24-hour) periodicity beginning in late May (May-25-2017 and May-23-2018) in the lake bottom SpC (Figure 4.8 A). Diel periodicity in bottom water SpC points to the influence of solar radiation as the main driver controlling the late winter increases of SpC. The coherence spectrum confirms this association, demonstrating a strong correlation between the periodicity in solar radiation and lake bottom SpC. Solar radiation and SpC are in phase with one another, with SpC lagging 3-hours behind solar radiation (Figure 4.9). This suggests three hours is the length of time it takes for the solar radiation signal to reach the lake bottom.

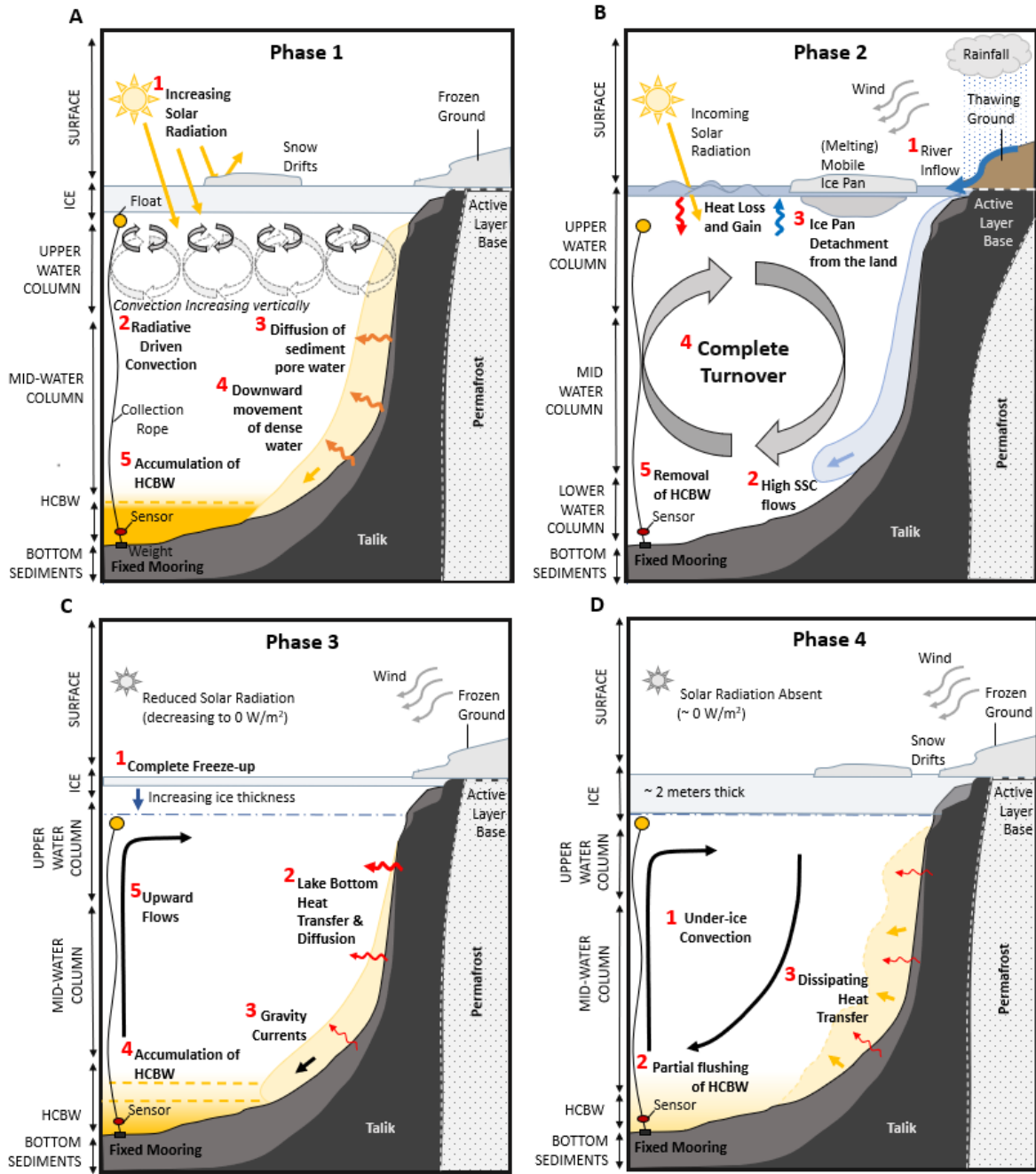
The influence of solar radiation on physical processes within ice-covered lakes has been reported in many studies (Bengtsson, 1996a; Cortés & MacIntyre, 2020; Kirillin et al., 2012; Yang et al., 2017; Zdrovennova et al., 2021a; Zdrovennova et al., 2021b). The period of solar influence is understood to consist of energetic and dynamic processes under-ice driven by the penetration of solar radiation through the ice surface (Kirillin et al., 2012; Matthews & Heaney, 1987). Solar radiation causes heating of the water column, initiating under-ice circulation known as radiatively-driven convection (RDC) (Jansen et al., 2021). Initial late-winter heating of the upper water column results in a subsequent sinking of this warmer and heavier water. Combined with the fresher cooler water released with melting of ice, this produces a thin convective mixed layer beneath the ice surface (Bengtsson, 1996a; Jansen et al., 2021; Kirillin et al., 2018). Convection in the upper water column occurs first and generates movement of warming water beneath the ice surface towards littoral areas (Jansen et al., 2021; Kirillin et al., 2012). The initiation of the convective mixed layer is visible in water column temperature casts where temperatures at the surface are slightly

warmer between 2-5 m depth below near-freezing temperatures at the ice-water interface (Figure 4.5 A; May 19, 2018). As the intensity of solar radiation increases, the convectively mixed layer extends deeper vertically within the water column (Kirillin et al., 2018). Dense bottom water will limit the vertical extent of the convectively mixed water column (CMWC), preventing it from reaching the lake bottom (Jansen et al., 2021; Kirillin et al., 2012).

During this period of solar heating, temperatures in the lake bottom gradually decrease (Figure 4.6). Other studies have found that temperatures increase in the lake bottom during a time of RDC due to the circulation of warmer (solar-heated) surface water down to the lake bottom (Cortés & MacIntyre, 2020; Kirillin et al., 2012; Yang et al., 2017; Zdrovennova et al., 2021a). However, in the bottom water at West Lake, temperatures do not begin to increase until early July, 2-months after diel increases in SpC were occurring in the lake (Figure 4.8) Therefore, a late winter temperature decrease in West Lake suggests that the convective mixing does not reach the denser EBWC. Alternatively, the RDC only disturbs the EBWC, causing turbulence at the interface between the EBWC-CMWC. Additionally, the wavelet analysis did not reveal diel cyclicality in the temperature data as it did for SpC oscillations (Figure 4.7 B). The lack of spectral characteristics in the decreasing temperatures in EBWC indicates that the lake bottom temperature is cooling independently of the diurnal cycles. Therefore, increases in SpC are influenced by processes beneath the lake as the lake is still ice-covered when lake bottom SpC increases, and temperatures begin cooling. Findings from Chapter 3 suggest the source of dissolved ions in late winter EBWC is sediment pore-water diffusion. Diffusion can occur where there is a chemical or thermal gradient at the sediment-water interface anywhere along the lake slopes and littoral regions (Jansen et al., 2021). Rapid convection driven by solar heating is likely responsible for increasing SpC in EBWC, driving the downward movement of denser high dissolved ions accumulated along the lake slopes (Figure 4.11 A) (Cortés & MacIntyre, 2020; Kirillin et al., 2012; Zdrovennova et al., 2021a).

RDC creates turbulence at the gradient between the CMWC and EBWC, causing the influx of dissolved solutes on a diel cycle. By late June, the intensity of solar radiation increases in conjunction with

the intensity of diel oscillations in SpC. Long internal waves generated by RDC disrupt the interface between the EBWC-CMWC, which the stationary mooring records as oscillations with diel periodicity in the SpC data. Kirillin et al. (2009) found a similar effect in the bottom of a boundary layer of an ice-covered lake in Müggelsee, Germany, where basin-scale internal waves were associated with oscillations in the lower stratified region of the water column. In West Lake, the most apparent diel periodicity in SpC occurred in late June (Figure 4.8 B). At this time, the gradient between the EBWC and the water column would presumably be very sharp, as the chemocline has been developing with little disruption all winter. As the intensity of solar radiation increases (closer to the annual solar maximum), each daily influx of heat becomes more influential, making the disruption to the EBWC more apparent and resulting in more notable diel periodicity in the mooring data (Figure 4.8). Variability in the magnitude of oscillations due to decreases in the intensity of daily solar radiation that makes it through the ice surface are likely due to snow accumulation and cloud cover (Bengtsson, 1996b; Kirillin et al., 2012). For example, the striking oscillations seen in 2017 are not as apparent in 2018 SpC data due to more frequent cloud cover in 2018, observed in both the solar radiation data and the time-lapse imagery (Appendix C).



*Diagrams are not to scale

Figure 4.11: Schematic diagram illustrating the mechanisms influencing the physical processes driving the occurrence of elevated bottom water conductivity EBWC in West Lake. Panels depict the occurrences through out the water column of the lake during each season: (A) Phase 1- late winter, (B) Phase 2 - spring-summer, (C) Phase 3 - early winter, and (D) Phase 4 - mid-winter.

4.6.2 Phase 2: Spring-Summer

EBWC is flushed from the lake bottom during Phase 2, the melt season. Mean daily air temperatures increase (>0 °C), initiating the melting of snow and lake ice, and active layer thaw (Figure 4.6). Melt and thaw enables mass and energy exchanges between the lake, the atmosphere, and the surrounding landscape that was previously inhibited due to lake ice freezing to the land in winter (i.e., fluvial inputs and outputs, and meteorological changes).

The influence of river inflow on bottom water is evident as diel cyclicality in the SpC lake bottom data is followed by a pattern of irregularity after West River reaches peak SSC flow on July-03-2017 (Figure 4.6 A-B, 2). Lewis et al. (2018) found that river inflows at West Lake will reach the bottom of the lake when peak SSC makes them denser than the rest of the water column (Lewis et al., 2018). Dense gravity flows are known as hyperpycnal flows, which sink and flow downwards along the slopes of the lake and (Mulder & Syvitski, 1995). According to Lewis et al. (2018) the velocity of a hyperpycnal flow is between 6.0×10^{-3} m/s and 4.4×10^{-3} m/s, meaning it would take approximately two hours for the flows to reach the lake bottom. However, during the period of peak SSC flows the lake ice is still attached to the land and is at least a partial barrier to inflows. In previous years where persistent hyperpycnal flows occur, the zone of EBWC is eventually removed (Lewis et al., 2018). This is shown by a rapid drop in lake bottom SpC in July of all three study years (July-21-2016, July-17-2017, July-28-2018) (Figure 4.6). The flushing of EBWC occurs 21 days after peak SSC in 2016 (peak SSC: June-16, EBWC flushed: July-03) and 14 days after peak SSC in 2017 (peak SSC: July-03, EBWC flushed July-17). The delay between peak SSC and flushing of the bottom water occurs due to the ice pan on the lake surface preventing the direct flow of the river inputs to the lake bottom.

The separation of the ice from the land surface on July-15-2017 occurs just days before the overturn of the entire water column on July-18-2017, represented by an abrupt drop in Lake bottom SpC (Figure 4.6 A-C). Given the timing of events, it is likely that the detachment of the ice pan from the land surface triggers the complete turnover of the water column and flushing of EBWC. This pattern recurs in

all three years where bottom water flushing is preceded by high SSC inputs and the movement of ice away from the land surface. When ice separates from the land surface, an influx of melt water (from the river and ice) collecting in the moat around the perimeter of the ice surface is released into the water column, resulting in the complete flushing of EBWC and overturn of the water column.

Following the removal of EBWC, it is realistic to assume that lake bottom diffusion could continue to occur during the ice-off period. However, accumulation of ions is not recorded due to greater disturbances in the water column when the lake is ice free (Vincent et al., 2008). The formation of EBWC is subtle (cf. Chapter 3) and accumulation that is measured during long quiescent periods (i.e., mid- to late-winter) cannot occur during the melt season due to river flushing, convective mixing, or wind-induced turbulence in the water column while the lake surface is ice free.

In the latter half of the ice-free period, temperatures in the lake bottom begin to cool in response to cooling air temperatures. Heat loss occurs at the surface of the lake due to the temperature difference between the water and the colder overlying air causing radiative and sensible heat loss to the atmosphere (Kirillin et al., 2012). Convective cooling through the entire water column continues until eventually ice begins to form on the surface of the lake (Zdrovennova et al., 2021b).

4.6.3 Phase 3: Early Winter

Phase 3 begins with the formation of stable ice cover on the surface of the lake (Figure 4.6 A-C, 4). In response to the formation of ice, the water column stabilizes as cooling dissipates, and the lake becomes increasingly insulated as ice cover thickens (Zdrovennova et al., 2021b). In response to freeze-up, temperatures warm from 0°C to closer to the T_{MD} in all three years (Figure 4.6 A-C). The sudden rise in lake bottom temperatures is indicative of a positive flux of heat from warmer lake bottom sediments that were previously heated during the ice-off period. Bottom sediments are heated by convection, driving exchanges between sediments (cooler at this time), and circulating warmer water heated at the surface (Cortés & MacIntyre, 2020; Kirillin et al., 2012; Woo, 2012a). As water in the lake begins to cool this exchange at the sediment-water interface reverses from the summer, where warmer lake-bottom

sediments are cooled through the convection of stored heat to the colder bottom water (Golosov & Kirillin, 2010; Zdrovennova et al., 2021b). This mechanism is reflected in the prominent drop and rebound in lake bottom temperature observed before and after complete freeze over of the lake surface in both 2016 and 2017 after ice-on (Figure 4.6 A-B, 4).

Following the warming temperatures lake bottom SpC increases rapidly. As lake bottom water temperature is increasing with SpC, this suggests there is a common mechanism controlling these two variables. Elevated SpC may be linked to heat exchanges at the sediment-water interface as thermal gradients at the sediment water interface have the potential to transport dissolved solutes from sediment porewaters into lake bottom waters (Hesslein, 1980). This suggests the source of Phase 3 EBWC could be derived from the slow flux of porewater from the lake bottom sediments. Greater disparities between the temperature of colder the bottom water and warmer sediment would result in stronger heat flux and greater ion transfer into the lake bottom water, resulting in the accumulation of EBWC (Terzhevik et al., 2009). This temperature difference is determined by the extent of summer heating of lake bottom sediments and cooling of lake water before ice-on (cf. Section 4.6.4).

The accumulation of EBWC could also result from the diffusion by ionic gradients across the sediment-water interface whereby dissolved solutes are transferred from sediments to lake bottom waters by molecular diffusion. Molecular diffusion occurs where sediment pore water contains high concentrations of dissolved solutes compared to the bottom water (Lerman & Brunskill, 1971; Stiller, 1994). During the ice-free period, 2017 lake bottom SpC values were lower in comparison to 2016 values, leaving a greater disparity between dissolved ions at the sediment-water interface and pore waters, which would result in a greater flux of ions as shown as increases in the SpC data during Phase 3 in 2017 (Figure 4.10 E). It is therefore possible that Phase 3 EBWC accumulation is driven by the contribution of dissolved ions from pore water seepage in addition to post ice-on temperature disparities between the bottom sediments and water column temperature. Alternatively, studies of lake bottom increases in SpC have also suggested that density increases could result from microbial respiration at the sediment-water

interface (which produces solutes), or solute ejection from the ice during formation (i.e., cryo-concentration) (Jansen et al., 2021; MacIntyre et al., 2018; Mortimer & Mackereth, 1958). However, we do not have sufficient evidence in this study to confirm if microbial activity or cryo-concentration is contributing to the accumulation of EBWC in Phase 3.

As heat flux from the bottom sediments continues to warm the lake bottom water closer to T_{MD} , warmer denser water would flow down the lake slope creating a subtle thermal disparity between the overlying water column and the bottom water in the deepest depressions of the lake (Huttula et al., 2010; Jakkila et al., 2009). The accumulation of warmer, denser, and more conductive bottom water near the sediment-water interface would form a weak thermal gradient between the EBWC and the overlying water column. This is known as thermal reverse stratification and has been found to occur under ice-covered Arctic lakes, where colder, less dense water overlies warmer but denser water below (MacIntyre et al., 2018). Where the gradient is shallow the sensor of the mooring will detect a less defined signal compared to the clear diel signal detected in phase 1 (Figure 4.12). The accumulation of dissolved ions with warmer, denser water in the deepest depressions of the lake is potentially a key stabilizing element that permits the establishment of EBWC.

The movement of denser water down the lake slopes causes the oscillations observed in the bottom water during this time. However, given that the periodicity in Phase 3 is between 0.25 and 4 days, the mechanism behind the oscillations measured in Phase 3 EBWC is certainly different than the diel periodicity visible in Phase 1 (Figure 4.8 B). Phase 3 oscillations are not related to solar radiation as they do not exhibit diel cyclicity, and solar insolation is much lower in September and October compared to May and June (Figure 4.4 A). Additionally, snow and ice cover are increasing during this time, reducing the effects of any remaining solar heating of the water column (Jewson et al., 2009; Yang et al., 2017) (Figure 4.8 B). Zdrovennova et al., (2021b) have described under ice oscillations in early winter to have occasional “jump-like changes” similar to those visible in Phase 3, with periodicity on a scale of minutes to close to a day (Kirillin et al., 2012; Zdrovennova et al., 2021b). The periodicity of 0.25 to 4 days

could be caused by advection of heat from the littoral zone to the deepest parts of the lake or basin scale waves (seiches) formed from oscillations generated by variations in wind or atmospheric pressure acting on the surface of the lake ice (Bengtsson, 1996a; Huttula et al., 2010; Kirillin et al., 2009, 2012; MacIntyre et al., 2018; Malm, 1998; Petrov et al., 2007; Rahm, 1985). The morphometry of a lake will be a major determinant of the circulation patterns in the water, impacting the periodicity recorded in a stationary bottom mooring (Boyce et al., 1989; Kirillin et al., 2012).

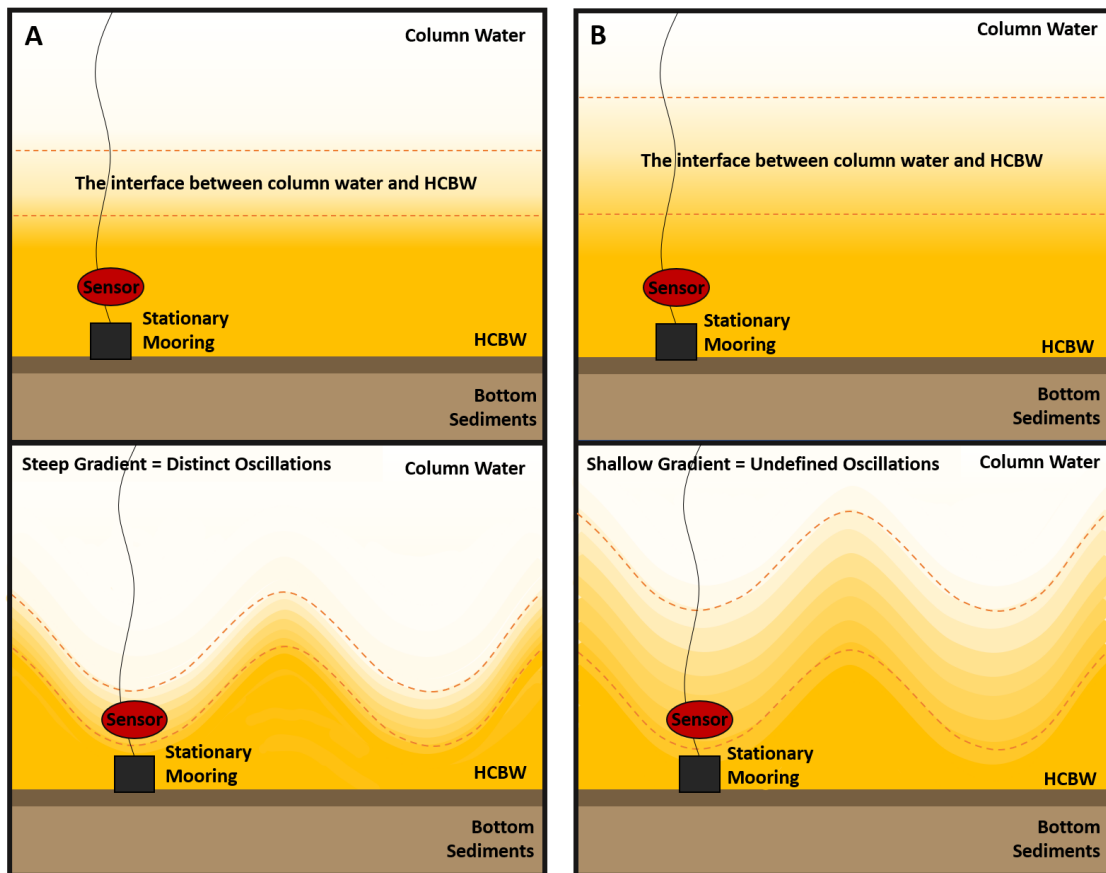


Figure 4.12: A schematic depicting the stationary lake bottom mooring in West Lake during (A) Phase 1: late May to late June and (B) Phase 3: mid-September to mid-October. The images in each panel represent the interface between the water column and the elevated bottom water conductivity (EBWC) in the absence of oscillations (top) and with oscillations present (bottom). The steep gradient (A) between the water column and EBWC would result in more distinct oscillations than the shallow gradient (B), which would display less defined, more gradual changes in SpC recorded by the mooring.

4.6.4 Phase 4: Mid-Winter

Temperature-driven porewater heat exchanges can continue through the entire ice-covered period, where the amount of heat directed from the bottom sediments into the water is greatest in the initial winter period and gradually diminishes as heat accumulated in bottom sediments is depleted (Terzhevik et al., 2009; Zdrovennova et al., 2021b). The amount of heat released is dependent on the amount of heat accumulated over summer (Golosov & Kirillin, 2010; Huttula et al., 2010; Jansen et al., 2021). This process occurs until water and sediment temperatures reach equilibrium, suggesting that the period immediately after ice-on would be when the greatest influx of ions is measured in the lake (Figure 4.10 E).

Phase 4 begins when lake bottom SpC begins to stabilize from irregular oscillations, observed in November 2016-17 and 2017-18. The exact cause of stabilization is not clear; one potential explanation is partial flushing of EBWC due to an overturning convective circulation (Jansen et al., 2021) caused by upward movement in the water column to balance downslope gravity currents as described in Phase 3. Following the stabilization of the bottom water SpC signature, the water column shifts to a quiescent under-ice period.

In winter 2016-17, lake bottom temperatures gradually warmed until the onset of late winter SpC increases (see Phase 1). However, in winter 2017-18, temperatures display a gradual cooling trend over winter, interrupted by steep irregular periods of decline (Nov-17-2017; Dec-09-2017; Jan-13-2018; Feb-04-2018). A continued increase in lake bottom temperatures over winter is likely an indication of continued heat flux from the bottom sediments. In contrast, gradual winter cooling in the lake bottom is an indication of a negative heat flux from the bottom sediments suggesting that the summer heat radiating from the sediments has been completely exhausted through radiative heat transfer (Kirillin et al., 2012). Greater increases in lake bottom temperature in winter 2016-17 are a result of greater differences between temperatures in the lake bottom sediments and bottom waters following complete ice-on. Cooler lake

bottom temperatures occur with later ice-on dates as more heat can be lost from the lake to the atmosphere. Ice-on was complete later in 2016 (Oct-01-2016) compared to 2017 (Sept-17-2017), resulting in cooler lake bottom temperatures at ice-on. Additionally, ice-free conditions were more favourable for heat exchanges at the sediment-water interface and greater warming was visible over winter 2016-17 compared to winter 2017-18. Lake bottom sediments were likely warmer during ice-on in 2016 because summer (ice-free) lake bottom temperatures were warmer in 2016 (3.6 °C) compared to 2017 (2.5 °C). Although the temperature of the sediments was not recorded, warmer summer bottom water temperatures should result in greater heat storage in lake bottom sediments (Terzhevik et al., 2009). The larger differences between the cold water column and warmer lake bottom sediments results in a greater increase in lake bottom temperatures during the ice-on period (MacIntyre et al., 2018).

Temperature trends vary between the two years, which contrasts with trends in SpC that increase in both years. This suggests that there is still slow accumulation of dissolved solutes in the lake bottom over winter. Furthermore, SpC increases were greater in winter 2016-17 compared to winter 2017-18. This could be correlated to the greater lake bottom heat flux over winter 2016-17 which may contribute to increases in solute delivery over winter. Greater heat flux would result in greater balancing upward currents which would drive under-ice circulation and the slow movement of dissolved ions along the bottom slopes at this time (Figure 4.11 D). Under-ice circulation caused by heat exchange at the sediment water interface has been found to contribute to the transport of shallow lake bottom dissolved solutes downslope, where they accumulate in the deepest areas (Kirillin et al., 2012; MacIntyre et al., 2018).

In ice-covered lakes, sediment heat fluxes are a major driver of under-ice circulation (Terzhevik et al., 2009; Welch & Bergmann, 1985). Over winter circulation has been observed in many previous studies on ice covered lakes (Bengtsson, 1996; Kirillin et al., 2012; Malm, 1998; Rahm, 1985; Welch & Bergmann, 1985; Zdrovennova et al., 2021b), with many factors influencing the size, pattern and number of cells circulating in a lake during this period (Bengtsson, 1996). In Arctic ice-covered lakes, circulation occurs where water gains heat along the lake slopes at the sediment-water interface, becoming

denser as it warms closer to the T_{MD} to sink to deeper basins in the lake (MacIntyre et al., 2018). Eventually, the lake reaches an equilibrium state of circulation whereby shoreward currents balance downward currents, resulting in stable under-ice circulation of lake water (Bengtsson, 1996; Malm, 1998; Welch & Bergmann, 1985). Welch and Bergman (1985) used tracer dyes to record over winter convection in Char Lake (~ 30 m deep) on Cornwallis Island and discovered it takes ~ 10 hours for solutes at the surface to reach the lake bottom. Similar convection in West Lake would result in ongoing slow gravity drainage down slopes to the lake bottom, collecting solutes transferred from sediments. Welch and Bergmann (1985) also noted a “filling-up” of denser solute-enriched water that is eventually displaced by lake circulation through the winter. This description resembles the accumulation of EBWC overwinter; however, accumulated solutes are not displaced over winter in West Lake (Figure 4.10). This suggests any movement of solutes to the bottom water would be driven by the release of heat from lake bottom sediments creating a lake bottom gradient between the EBWC and water column that is strong enough to withstand the under-ice convection discussed by Welch and Bergmann (1985).

Over-winter circulation is more subtle than the dynamic RDC, which overtakes winter circulation when the intensity of solar radiation begins warming the lake (Phase 1; cf. Section 4.6.1). Convective mixing due to solar heating appears in SpC data in April of 2017 and 2018 in West Lake data (at the end of Phase 4) where the rate of change in lake bottom SpC begins to increase exponentially with time. Once this process begins, any subtle over-winter circulation is presumably overcome by the stronger convection generated by solar heating (Zdorovenova et al., 2021a). By the end of the winter, lake bottom water is much warmer, denser and has higher dissolved solutes, creating a thermo-chemocline strong enough to prevent under-ice convection over winter and even RDC from washing away accumulating EBWC. The depth of this thermocline would be determined by the extent of warming at the lake bottom and the volume of denser EBWC. As more solutes are delivered to the lake bottom the volume of EBWC would expand non-linearly, as the lake bottom area increases as this layer gets deeper. A constant flux of dissolved ions would result in a diminishing change in SpC as the EBWC increases in volume. This is

visible in lake bottom data over winter where eventually the lake reaches a stable state; bottom water conditions reflect this through a reduction in irregular oscillations (Mid-November; cf. interactive SpC plot in Appendix C) with SpC, temperature, and density anomaly becoming increasingly stable towards the end of Phase 4 (April-May). This stability could be a result of a deepening thermo-chemocline with an increase in the volume of EBWC. Stability continues until the main driver of under-ice convection shifts and water column circulation is influenced by RDC (Phase 1).

4.7 Conclusion

This study identified the mechanisms driving physical changes in West Lake that are responsible for temporal changes in the timing and occurrence of EBWC. Lake bottom SpC and temperature data can be subdivided into four phases to reflect the response of annually-recurring physical processes in the lake bottom that are correlated to the duration and timing of ice cover on the lake. The data displayed repeated patterns in the fluctuation of EBWC over the 2.5-year study period, revealing two recurring periods of EBWC accumulation separated by periods of bottom water flushing.

These two main periods of EBWC accumulation are identified through large increases in SpC: late winter (Phase 1) and following complete ice-on (Phase 3). Quasi-cyclical oscillations visible in both periods of increasing SpC provide further evidence of the mechanisms driving physical processes in the lake during EBWC accumulation. There are two main mechanisms initiating the accumulation of EBWC under ice: (1) Phase 1, RDC generated through heat provided to the water column by solar radiation causing increases in the delivery of ions to the bottom water, and (2) Phase 3, under-ice convective gravity currents are driven by the release of heat through the lake bottom sediments and the water column following ice-on. In both phases, the increase in SpC results from convection-driven delivery of ions diffused through the sediment-water interface to the deepest regions in the lake. EBWC is completely flushed out during the melt season corresponding to the lowest annual lake bottom SpC values (Phase 2) and flushed to a lesser extent over winter (Phase 4).

Peak SpC values in the lake bottom varied from year to year. Quantification of seasonal SpC could indicate the impact that EBWC might have on biogeochemical cycling in the lake, and how this would change with future warming. Summer temperatures, which determine the extent of the thermal gradient between the lake bottom sediments and water, control the amount of heat transferred to the lake following ice-on (i.e., more summer warming of lake bottom sediments results in greater heat transferred following ice-on). Future work should specifically collect water column casts and chemical samples during Phase 3 to compare bottom water conditions to the overlying water column to confirm what drives increasing SpC during this time. The findings of this study emphasize the importance of the timing of lacustrine sampling, and how critical it is to compare seasonal changes in lake parameters and physical processes. As temperatures warm and hydrologic systems in High Arctic regions change, year-round observations will be critical to understanding how patterns of freeze and thaw are shifting and ultimately affecting the physical processes and the chemical composition of High Arctic lake systems.

4.8 References

- Adrian, R., O'Reilly, C. M., Zagarese, H., Baines, S. B., Hessen, D. O., Keller, W., Livingstone, D. M., Sommaruga, R., Straile, D., van Donk, E., Weyhenmeyer, G. A., & Winder, M. (2009). Lakes as sentinels of climate change. *Limnology and Oceanography*, *54*, 2283–2297.
https://doi.org/10.4319/lo.2009.54.6_part_2.2283
- Beel, C. R., Heslop, J. K., Orwin, J. F., Pope, M. A., Schevers, A. J., Hung, J. K. Y., Lafrenière, M. J., & Lamoureux, S. F. (2021). Emerging dominance of summer rainfall driving High Arctic terrestrial-aquatic connectivity. *Nature Communications*, *12*(1448). <https://doi.org/10.1038/s41467-021-21759-3>
- Beel, C. R., Lamoureux, S. F., Orwin, J. F., Pope, M. A., Lafrenière, M. J., & Scott, N. A. (2020). Differential impact of thermal and physical permafrost disturbances on High Arctic dissolved and particulate fluvial fluxes. *Scientific Reports*, *10*(1), 1–13. <https://doi.org/10.1038/s41598-020-68824-3>
- Bégin, P. N., Tanabe, Y., Kumagai, M., Culley, A. I., Paquette, M., Sarrazin, D., Uchida, M., & Vincent, W. F. (2020). Extreme warming and regime shift toward amplified variability in a far northern lake. *Limnology and Oceanography*, *July*. <https://doi.org/10.1002/lno.11546>
- Bengtsson, L. (1996a). Mixing in ice-covered lakes. *Hydrobiologia*, *322*(1–3), 91–97.
<https://doi.org/10.1007/BF00031811>
- Boehrer, B., & Schultze, M. (2008). Stratification of lakes. *Reviews of Geophysics*, *46*(2), 1–27.
<https://doi.org/10.1029/2006RG000210>
- Boehrer, B., & Schultze, M. (2009). Density Stratification and Stability. *Reviews of Geophysics*, *46*(2), 583–593. <https://doi.org/10.1029/2006RG000210>
- Boyce, F. M., Donelan, M. A., Hamblin, P. F., Murthy, C. R., & Simons, T. J. (1989). Thermal structure and circulation in the great lakes. *Atmosphere-Ocean*, *27*(4), 607–642.
<https://doi.org/10.1080/07055900.1989.9649358>
- Clesceri, L. S., Greenberg, A. E., & Eaton, A. D. (1999). *Standard Methods for the Examination of Water and Wastewater* (20th ed.). L. S. Clesceri, A. E. Greenberg, & A. D. Eaton, (Eds.). American Public Health Association.

- Cochand, M., Molson, J., & Lemieux, J. M. (2019). Groundwater hydrogeochemistry in permafrost regions. *Permafrost and Periglacial Processes*, 30(2), 90–103. <https://doi.org/10.1002/ppp.1998>
- Cortés, A., & MacIntyre, S. (2020). Mixing processes in small arctic lakes during spring. *Limnology and Oceanography*, 65(2), 260–288. <https://doi.org/10.1002/lno.11296>
- Cuven, S., Francus, P., & Lamoureux, S. (2011). Mid to late Holocene hydroclimatic and geochemical records from the varved sediments of East Lake, Cape Bounty, Canadian High Arctic. *Quaternary Science Reviews*, 30(19–20), 2651–2665. <https://doi.org/10.1016/j.quascirev.2011.05.019>
- Dugan, H. A. (2021). A comparison of ecological memory of lake ice-off in eight north-temperate lakes. *Journal of Geophysical Research: Biogeosciences*, 126(6). <https://doi.org/10.1029/2020JG006232>
- Dugan, H. A., & Lamoureux, S. F. (2011). The chemical development of a hypersaline coastal basin in the High Arctic. *Limnology and Oceanography*, 56(2), 495–507. <https://doi.org/10.4319/lno.2011.56.2.0495>
- England, J. H., Furze, M. F. A., & Doupe, J. P. (2009). Revision of the NW Laurentide Ice Sheet: implications for paleoclimate, in the north east extremity of Beringia, and Arctic Ocean sedimentation. *Quaternary Science Reviews*, 28, 1573–1596.
- Fofonoff, N. P., & Millard, R. C. Jr. (1983). *Algorithms for computation of fundamental properties of seawater*. UNESCO.
- Golosov, S., & Kirillin, G. (2010). A parameterized model of heat storage by lake sediments. *Environmental Modelling and Software*, 25(6), 793–801. <https://doi.org/10.1016/j.envsoft.2010.01.002>
- Harasyn, M. L., Lamoureux, S., & Normandeau, A. (2017, October 1-4). *Detecting the presence of localized ground water inputs into High Arctic lakes* [Paper presentation]. GeoOttawa 2017 – 70th Canadian Geotechnical Conference and the 12th CGS/IAH-CNC Groundwater Conference Ottawa, CA.
- Hesslein, R. H. (1980). In situ measurements of pore water diffusion coefficients using tritiated water. *Canadian Journal of Fisheries and Aquatic Sciences*, 37, 545–551.

- Huttula, T., Pulkkanen, M., Arkhipov, B., Leppäranta, M., Solbakov, V., Shirasawa, K., & Salonen, K. (2010). Modelling circulation in an ice-covered lake. *Estonian Journal of Earth Sciences*, *59*(4), 298–309. <https://doi.org/10.3176/earth.2010.4.06>
- Ibanez, J. G., Hernandez-Esparza, M., Doria-Serrano, C., Fregoso-Infante, A., & Singh, M. M. (2007). *Environmental Chemistry: Fundamentals*. Springer. <https://doi.org/10.1007/978-0-387-31435-8>
- Jakkila, J., Leppäranta, M., Kawamura, T., Shirasawa, K., & Salonen, K. (2009). Radiation transfer and heat budget during the ice season in Lake Pääjärvi, Finland. *Aquatic Ecology*, *43*(3), 681–692. <https://doi.org/10.1007/s10452-009-9275-2>
- Jansen, J., MacIntyre, S., Barrett, D. C., Chin, Y. P., Cortés, A., Forrest, A. L., Hrycik, A. R., Martin, R., McMeans, B. C., Rautio, M., & Schwefel, R. (2021). Winter limnology: How do hydrodynamics and biogeochemistry shape ecosystems under ice? *Journal of Geophysical Research: Biogeosciences*, *126*(6). <https://doi.org/10.1029/2020JG006237>
- Jewson, D. H., Granin, N. G., Zhdanov, A. A., & Gnatovsky, R. Y. (2009). Effect of snow depth on under-ice irradiance and growth of *Aulacoseira baicalensis* in Lake Baikal. *Aquatic Ecology*, *43*(3), 673–679. <https://doi.org/10.1007/s10452-009-9267-2>
- Kirillin, G., Aslamov, I., Leppäranta, M., & Lindgren, E. (2018). Turbulent mixing and heat fluxes under lake ice: the role of seiche oscillations. *Hydrology and Earth System Sciences*, *22*, 6493–6504, <https://doi.org/10.5194/hess-2018-376>
- Kirillin, G., Engelhardt, C., Golosov, S., & Hintze, T. (2009). Basin-scale internal waves in the bottom boundary layer of ice-covered Lake Müggelsee, Germany. *Aquatic Ecology*, *43*(3), 641–651. <https://doi.org/10.1007/s10452-009-9274-3>
- Kirillin, G., Leppäranta, M., Terzhevik, A., Granin, N., Bernhardt, J., Engelhardt, C., Efremova, T., Golosov, S., Palshin, N., Sherstyankin, P., Zdorovenova, G., & Zdorovenov, R. (2012). Physics of seasonally ice-covered lakes: A review. *Aquatic Sciences*, *74*(4), 659–682. <https://doi.org/10.1007/s00027-012-0279-y>
- Lamoureux, S. F., & Lafrenière, M. J. (2017). More than just snowmelt: Integrated watershed science for changing climate and permafrost at the Cape Bounty Arctic Watershed Observatory. *WIREs Water*, *5*(1). <https://doi.org/10.1002/wat2.1255>

- Lerman, A., & Brunskill, G. J. (1971). Migration of major constituents from lake sediments into lake water and its bearing on lake water composition. *Limnology and Oceanography*, *16*(6), 880–890.
- Lewis, T., Lamoureux, S. F., Normandeau, A., & Dugan, H. A. (2018). Hyperpycnal flows control the persistence and flushing of hypoxic high conductivity bottom water in a High Arctic lake. *Arctic Science*, *4*, 25–41. <https://doi.org/10.1139/as-2017-0022>
- MacIntyre, S., Cortés, A., & Sadro, S. (2018). Sediment respiration drives circulation and production of CO₂ in ice-covered Alaskan Arctic lakes. *Limnology and Oceanography Letters*, *3*(3), 302–310. <https://doi.org/10.1002/lol2.10083>
- Malm, J. (1998). Bottom buoyancy layer in an ice-covered lake. *Water Resources Research*, *34*(11), 2981–2993. <https://doi.org/10.1029/98WR01904>
- Malm, J., Bengtsson, L., Terzhevik, A., Boyarinov, P., Glinsky, A., Palshin, N., & Petrov, M. (1998). Field study on currents in a shallow, ice-covered lake. *Limnology and Oceanography*, *43*(7), 1669–1679. <https://doi.org/10.4319/lo.1998.43.7.1669>
- Matthews, P. C., & Heaney, S. I. (1987). Solar heating and its influence on mixing in ice-covered lakes. *Freshwater Biology*, *18*(1), 135–149. <https://doi.org/10.1111/j.1365-2427.1987.tb01302.x>
- Mortimer, C. H., & Mackereth, F. J. H. (1958). Convection and its consequences in ice-covered lakes. *Verhandlungen des Internationalen Verein Limnologie*, *13*(2), 923–932. <https://doi.org/10.1080/03680770.1956.11895490>
- Mueller, D. R., van Hove, P., Antoniadou, D., Jeffries, M. O., & Vincent, W. F. (2009). High Arctic lakes as sentinel ecosystems: Cascading regime shifts in climate, ice cover, and mixing. *Limnology and Oceanography*, *54*(6 part 2), 2371–2385. https://doi.org/10.4319/lo.2009.54.6_part_2.2371
- Mulder, T., & Syvitski, J. P. M. (1995). Turbidity currents generated at river mouths during exceptional discharges to the world oceans. *The Journal of Geology*, *103*(3), 285–299. <https://www.jstor.org/stable/30071222>
- Normandeau, A., Lamoureux, S. F., Lajeunesse, P., & Francus, P. (2016). Sediment dynamics in paired High Arctic lakes revealed from high-resolution swath bathymetry and acoustic stratigraphy surveys. *Journal of Geophysical Research: Earth Surface*, *121*, 1676–1696. <https://doi.org/10.1002/2013JF002871>.Received

- Petrov, M. P., Terzhevik, A. Y., Zdorovenov, R. E., & Zdorovenova, G. E. (2007). Motion of water in an ice-covered shallow lake. *Water Resources*, 34(2), 113–122.
<https://doi.org/10.1134/S0097807807020017>
- Rahm, L. (1985). The thermally forced circulation in a small, ice-covered lake. *Limnology and Oceanography*, 30(5), 1122–1128.
- Rahman, T. B. (2021). *The role of land cover classes and rainfall events on the active layer thermal regime in the High Arctic*. MSc Thesis, Dept. of Geography and Planning, Queen's University, Kingston, ON.
- Roberts, K. E., Lamoureux, S. F., Kyser, T. K., Muir, D. C. G., Lafrenière, M. J., Iqaluk, D., Pieńkowski, A. J., & Normandeau, A. (2017). Climate and permafrost effects on the chemistry and ecosystems of High Arctic Lakes. *Scientific Reports*, 7(1), 1–8. <https://doi.org/10.1038/s41598-017-13658-9>
- Rösch, A., & Schmidbauer, H. (2018). *WaveletComp 1.1: A guided tour through the R package*.
https://www.researchgate.net/publication/323836523_WaveletComp_11_A_guided_tour_through_the_R_package
- Sharma, S., Blagrove, K., Magnuson, J. J., O'Reilly, C. M., Oliver, S., Batt, R. D., Magee, M. R., Straile, D., Weyhenmeyer, G. A., Winslow, L., & Woolway, R. I. (2019). Widespread loss of lake ice around the Northern Hemisphere in a warming world. *Nature Climate Change*, 9(3), 227–231.
<https://doi.org/10.1038/s41558-018-0393-5>
- Sharma, S., Richardson, D. C., Woolway, R. I., Imrit, M. A., Bouffard, D., Blagrove, K., Daly, J., Filazzola, A., Granin, N., Korhonen, J., Magnuson, J., Marszelewski, W., Matsuzaki, S. I. S., Perry, W., Robertson, D. M., Rudstam, L. G., Weyhenmeyer, G. A., & Yao, H. (2021). Loss of ice cover, shifting phenology, and more extreme events in northern hemisphere lakes. *Journal of Geophysical Research: Biogeosciences*, 126(10). <https://doi.org/10.1029/2021JG006348>
- Stiller, M. (1994). The chloride content in porewater of Lake Kinneret sediments. *Israel Journal of Earth Sciences*, 43(3–4), 179–185.
- Terzhevik, A., Golosov, S., Palshin, N., Mitrokhov, A., Zdorovenov, R., Zdorovenova, G., Kirillin, G., Shipunova, E., & Zverev, I. (2009). Some features of the thermal and dissolved oxygen structure in boreal, shallow ice-covered Lake Vendyurskoe, Russia. *Aquatic Ecology*, 43(3), 617–627.
<https://doi.org/10.1007/s10452-009-9288-x>

- Torrence, C., & Compo, G. P. (1998). A practical guide to wavelet analysis. *Bulletin of the American Meteorological Society*, 79(1), 61–78.
https://psl.noaa.gov/people/gilbert.p.compo/Torrence_compo1998.pdf
- Vincent, W. F. (2009). Effects of climate change on lakes. In Gene. E. Likens (Ed.), *Biogeochemistry of Inland Waters: A Derivative of Encyclopedia of Inland Waters*. Elsevier.
- Vincent, W. F., Macintyre, S., Spigel, R. H., & Laurion, I. (2008). The physical limnology of high-latitude lakes. In W. F. Vincent & J. Laybourn-Parry (Eds.), *Polar Lakes and Rivers: Limnology of Arctic and Antarctic Aquatic Ecosystems* (pp. 65–81). Oxford University Press.
<https://doi.org/10.1093/acprof:oso/9780199213887.003.0004>
- Welch, H. E., & Bergmann, M. A. (1985). Water circulation in small Arctic lakes in winter. *Canadian Journal of Fisheries and Aquatic Sciences*, 42, 506–520. <https://doi.org/10.1139/f85-068>
- Woo, M. (2012). Cold lakes. In *Permafrost Hydrology* (pp. 305–346). Springer-Verlag Berlin Heidelberg.
https://doi.org/10.1007/978-3-642-23462-0_7
- Yang, B., Young, J., Brown, L., & Wells, M. (2017). High-frequency observations of temperature and dissolved oxygen reveal under-ice convection in a large lake. *Geophysical Research Letters*, 44(24), 12,218–12,226. <https://doi.org/10.1002/2017GL075373>
- Zdrovennova, G., Palshin, N., Golosov, S., Efremova, T., Belashev, B., Bogdanov, S., Fedorova, I., Zverev, I., Zdrovennov, R., & Terzhevik, A. (2021a). Dissolved oxygen in a shallow ice-covered lake in winter: Effect of changes in light, thermal and ice regimes. *Water (Switzerland)*, 13(17).
<https://doi.org/10.3390/w13172435>
- Zdrovennova, G., Terzhevik, A., Palshin, N., Efremova, T., Bogdanov, S., & Zdrovennov, R. (2021b). Seasonal change in heat flux at the water-bottom sediment boundary in a small lake. *Journal of Physics: Conference Series*, 2131(3). <https://doi.org/10.1088/1742-6596/2131/3/032080>

Chapter 5

Conclusions and Future Work

5.1 Conclusions

Multiple studies have noted the occurrence of EBWC in West Lake at the CBAWO (Dugan, 2010; Harasyn, 2017; Lewis et al., 2018). Through an investigation of the water column geochemistry of East and West lakes at the CBAWO, this study concludes that there are two water reservoirs in these lakes: (1) the main water column and (2) the sediment porewater-derived EBWC.

The geochemistry of the water columns of West and East lakes show rapid responses to catchment changes over time, resulting in unprecedented increases in SO_4^{2-} concentrations in these waters. Ratios of major dissolved ions reveal that the concentration of SO_4^{2-} in the water columns is increasing disproportionately compared to other major dissolved ions. This confirms previous findings that observed an enrichment of SO_4^{2-} in underflows released from the active layer due to increasingly warm summer temperatures (Lafrenière & Lamoureux, 2019; Lamhonwah et al., 2017).

In contrast, sediment pore water at EBWC constitutes only a small volume of water within the lakes that reflects past water column compositions (cf. Chapter 3). Furthermore, recurring EBWC in West Lake does not demonstrate the same geochemical evolution as the water column and is distinctly different in ionic composition (Cl^- dominant). This suggests there is a different mechanism controlling the input of EBWC compared to the input of water in the remainder of the water column. Three possible sources of water have been identified: (1) lake bottom sediment pore water diffusion; (2) supra-permafrost groundwater seepage; or (3) intra- or sub-permafrost groundwater migration and seepage into the lake via a lake bottom talik. Geochemical analysis confirms that the chemical composition of EBWC in West Lake is similar to that of late glacial marine sourced water and ‘lags’ behind changes observed in the water column (cf. Chapter 3), suggesting that trapped late-glacial marine sediment pore water is the

source of EBWC. Under specific lake conditions, sediment pore water accumulates as EBWC through diffusion at the sediment-water interface.

A lake bottom mooring in West Lake identified the mechanisms responsible for the recurrence of HCWB (cf. Chapter 4). Processes in the water column are defined by four distinct phases in the physical structure of the water column: Phase 1: late winter, Phase 2: spring-summer, Phase 3: early winter, Phase 4: mid-winter. Each phase is defined by a distinct mechanism causing changes in the lake and is linked to the accumulation and dissipation of EBWC. The data revealed two phases of EBWC accumulation that are both regulated by under-ice processes, including: (1) radiation-driven convection (Phase 1: late winter); and (2) density-driven convection (Phase 3: early winter). Both processes are well understood to operate in ice-covered lakes and are known to deliver solutes from the slopes of a lake at the sediment-water interface, increasing the concentration of dissolved ions in the lake bottom (Cortés & MacIntyre, 2020; Jansen et al., 2021; Kirillin et al., 2012). This enrichment occurs due to the diffusion of sediment pore water either due to a chemical or thermal gradient along the sediment-water interface. Some form of diffusion is suspected to occur continuously in the lake bottom, but accumulation is only visible when the lake is ice covered and undisturbed by terrestrial processes.

During the spring-summer (Phase 2) and mid-winter (Phase 4) seasons, complete or partial flushing of EBWC occurs. Complete flushing of EBWC occurs in summer with water column turnover, but only partially over winter due to strengthening of under-ice convection. During the thaw period, when ice is melting at the lake surface, interactions with the terrestrial landscape (i.e., river inputs, precipitation, and wind) create turbulence in the water column, overpowering any subtle diffusion that may be occurring in the lake bottom.

5.2 Impact of Lake Size and Morphology on Biology

Under-ice processes of sediment heat flux and RDC are both specific to ice-covered lakes (Jansen et al., 2021; Kirillin et al., 2012). As processes related to the accumulation of EBWC are driven by ice

cover, the findings in this study are applicable to all ice-covered lakes with lake bottom sediments that could support diffusion of sediment pore water.

Although the volume of EBWC does not impact the overall composition of the water column in West Lake, it could potentially have a greater influence on lakes of smaller size as it would occupy a greater percentage of overall lake volume. In addition, the morphometry of a lake would have a large control on the distribution of density flows. Lake morphometry has been shown to impact the path of density currents, which would impact where denser water ultimately settles in a lake (Cortés & MacIntyre, 2020). In West Lake, rills and gullies are visible in the bathymetry of the lake bottom (Normandeau et al., 2016) and would presumably funnel any denser water diffused through the lake bottom to the deepest region in the lake where the EBWC is found. A fill-and-spill model (along the lake bottom bathymetry) can be applied here, where denser water accumulating in shallow depressions in the lake could fill up and spill into other regions of the lake. Complex bathymetry could impact the distribution and timing of the flux of density currents (i.e., heat and solutes) at depth in a lake, where denser water overflows the boundaries of shallow basins to deeper ones (Cortés & MacIntyre, 2020; Jansen et al., 2021).

Turnover and water column circulation deliver oxygen and nutrients to the lake bottom, however, the presence of a quiescent EBWC separated from the overlying water column may prevent oxygen from reaching the lake bottom to form anoxic zones (MacIntyre et al., 2018). The extent of an anoxic zone would be determined by the volume of EBWC, lake size, and morphology. If EBWC occupies a larger portion of the lakes volume, it would have a greater impact on the biological populations in the lake bottom. At the CBAWO, known biota that include amphipod populations and juvenile Char use anoxic-EBWC zones to protect them from predation. Therefore, a reduction in the occurrence of EBWC in the lake bottom would in turn put stress on these organisms.

5.3 Future Work

This research is important for use as part of a future understanding of cold-monomictic lake processes. Both lakes have demonstrated a rapid shift in lake geochemistry in response to thawing permafrost. Additionally, the lake bottom mooring dataset from West Lake has proven that long-term monitoring in the lake is a useful resource in delineating how the water column conditions change seasonally. The rapid daily changes observed in the EBWC of West Lake emphasizes that lake hydrodynamics can shift the water column conditions within minutes. Future work should consider the importance of the timing, collection, and location of measurements collected for limnologic research with a focus on filling knowledge gaps in under-ice processes. The CBAWO is specifically lacking in early-winter water column samples, which this work has highlighted as an active period of EBWC accumulation in the lake bottom. As circulation and mixing of regimes have implications for biogeochemical cycling in lakes, changes to these patterns could impact aquatic life and water quality. It is becoming increasingly important to gain an understanding of baseline conditions in a lake to detect rapid changes occurring in High Arctic landscapes. Not only will lakes be directly impacted by the effects of climate change, but as integrators of their catchments processes, they will be important indicators of ongoing environmental changes to the landscapes in which they reside.

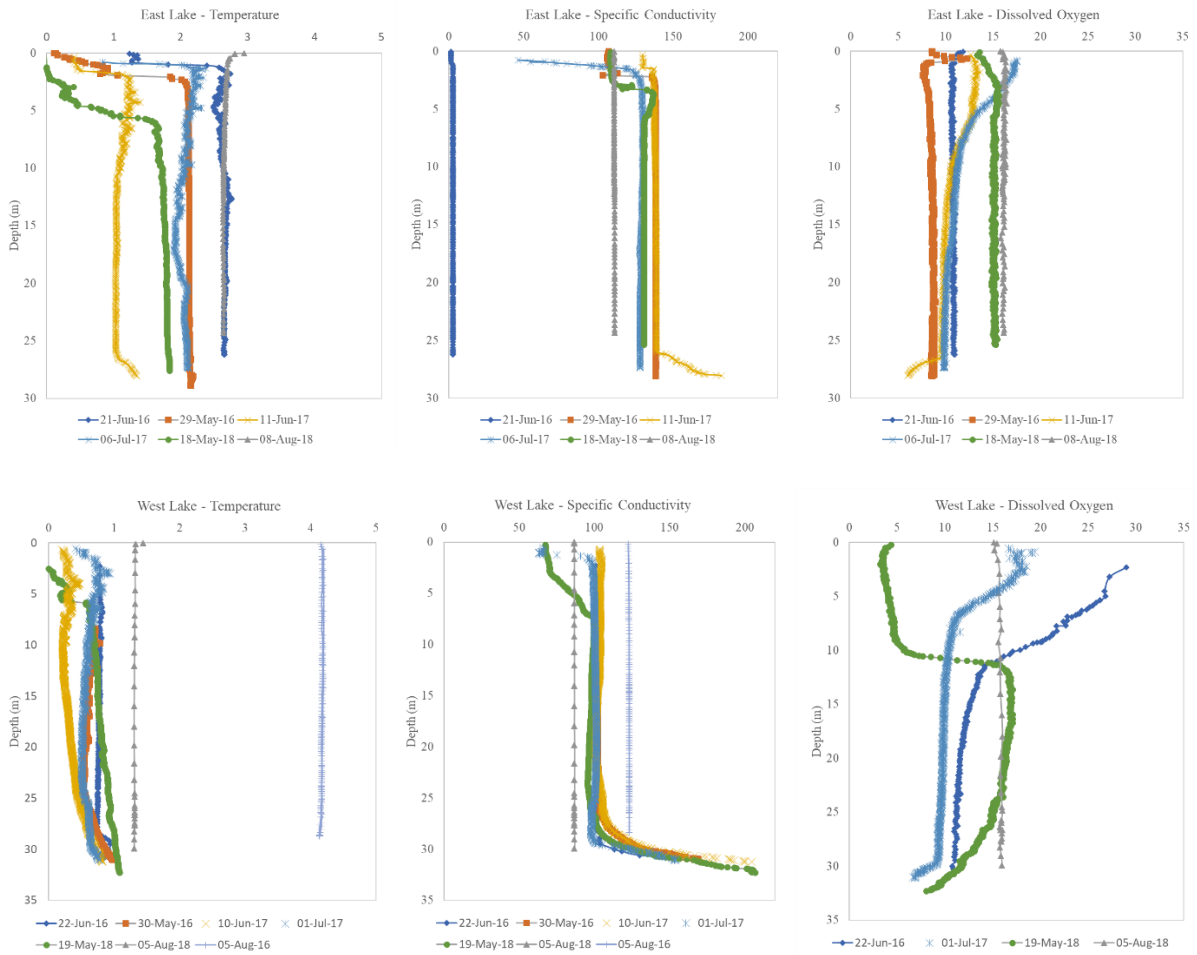
5.4 References

- Cortés, A., & MacIntyre, S. (2020). Mixing processes in small arctic lakes during spring. *Limnology and Oceanography*, 65(2), 260–288. <https://doi.org/10.1002/lno.11296>
- Dugan, H.A. (2010). *Long-term development and recent dynamics of High Arctic coastal basins*. MSc Thesis, Dept. of Geography and Planning, Queen's University, Kingston, ON.
- Harasyn, M. L. (2017). *Detecting the Presence of Localized Groundwater Inputs into High Arctic Lakes*. BSc Thesis, Dept. of Geography and Planning, Queen's University, Kingston, ON.
- Jansen, J., MacIntyre, S., Barrett, D. C., Chin, Y. P., Cortés, A., Forrest, A. L., Hrycik, A. R., Martin, R., McMeans, B. C., Rautio, M., & Schwefel, R. (2021). Winter limnology: How do hydrodynamics and biogeochemistry shape ecosystems under ice? *Journal of Geophysical Research: Biogeosciences*, 126(6). <https://doi.org/10.1029/2020JG006237>
- Kirillin, G., Leppäranta, M., Terzhevik, A., Granin, N., Bernhardt, J., Engelhardt, C., Efremova, T., Golosov, S., Palshin, N., Sherstyankin, P., Zdorovenova, G., & Zdorovenov, R. (2012). Physics of seasonally ice-covered lakes: A review. *Aquatic Sciences*, 74(4), 659–682. <https://doi.org/10.1007/s00027-012-0279-y>
- Lafrenière, M. J., & Lamoureux, S. F. (2019). Effects of changing permafrost conditions on hydrological processes and fluvial fluxes. *Earth-Science Reviews*, 191, 212–223. <https://doi.org/10.1016/j.earscirev.2019.02.018>
- Lamhonwah, D., Lafrenière, M. J., Lamoureux, S. F., & Wolfe, B. B. (2017). Multi-year impacts of permafrost disturbance and thermal perturbation on High Arctic stream chemistry. *Arctic Science*, 3(2), 254–276. <https://doi.org/10.1139/as-2016-0024>
- Lewis, T., Lamoureux, S. F., Normandeau, A., & Dugan, H. A. (2018). Hyperpycnal flows control the persistence and flushing of hypoxic high conductivity bottom water in a High Arctic lake. *Arctic Science*, 4, 25–41. <https://doi.org/10.1139/as-2017-0022>
- MacIntyre, S., Cortés, A., & Sadro, S. (2018). Sediment respiration drives circulation and production of CO₂ in ice-covered Alaskan arctic lakes. *Limnology and Oceanography Letters*, 3(3), 302–310. <https://doi.org/10.1002/lol2.10083>

Normandeau, A., Lamoureux, S. F., Lajeunesse, P., & Francus, P. (2016). Sediment dynamics in paired High Arctic lakes revealed from high-resolution swath bathymetry and acoustic stratigraphy surveys. *Journal of Geophysical Research: Earth Surface*, *121*, 1676–1696.
<https://doi.org/10.1002/2013JF002871>.

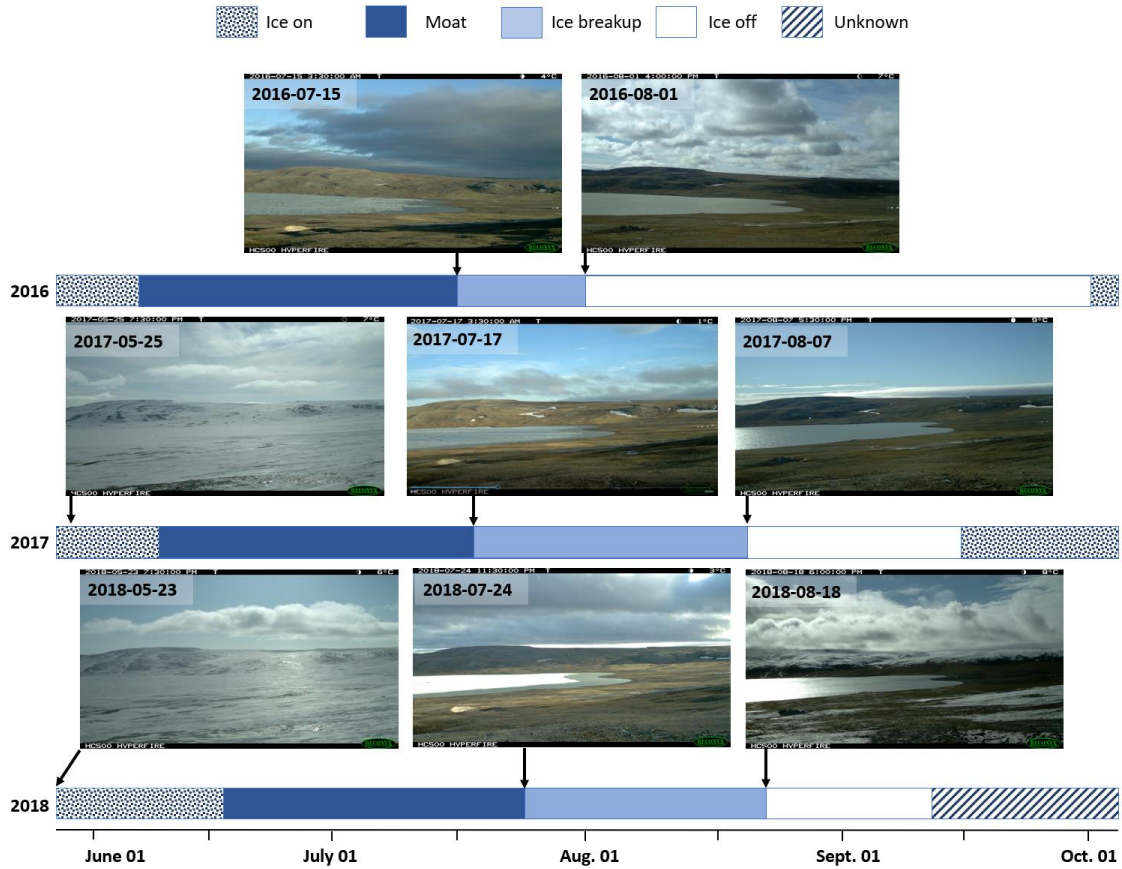
Appendix A

Water Column Casts



Displaying water column casts collected in May-August between 2016 and 2018.

Appendix B Lake Phenology



Lake ice phenology visible through screen shots of time lapse imagery taken between 2016 and 2018 of the northern basin of West Lake. Periods of ice-on and -off, moat formation around the ice pan, ice breakup (detachment of the ice pan from the land to complete ice melt) are indicated on a time scale for each year. Unknown periods are indicated for 2018 as snow coverage on the camera did not provide a clear view of the lake.

Appendix C

Linked Data

Links to accessory data.		
	Description	Link to Data
Timelapse Video	The timelapse of images collected between 2016-2018 viewing the northern basin of West Lake.	Available through the Department of Geography and Planning
Interactive Mooring Data	Interactive plot created using R to view the lake bottom mooring data for specific conductivity (SpC), temperature, and density anomaly.	Available through the Department of Geography and Planning
R Code	Code for the wavelet and cross coherence analysis.	Available through the Department of Geography and Planning

Appendix D

Active Layer Data

Active layer station data collected near West Lake (Rahman, 2021).									
Station Name	LG (Lower Goose)			PLAT A (Plateau A)			PLAT B (Plateau B)		
	2016	2017	2018	2016	2017	2018	2016	2017	2018
Start of thaw (date) (date of first 0°C temp at 5 cm depth)	2016- 06-12	2017- 06-29	2018- 06-14	2016- 06-06	2017- 06-14	2018- 06-06	2016- 06-08	2017- 06-15	2018- 06-12
Maximum thaw depth (cm)	n/a	71	64	82	71	68	78	69	65
Duration of thawing (days)	n/a	63.0	59.7	72.6	60.6	64.5	73.9	58.8	62.5
Start of Bottom-up freezing (last date of deepest temperature)	n/a	2017- 08-31	2018- 08-13	2016- 08-18	2017- 08-14	2018- 08-10	2016- 08-21	2017- 08-13	2018- 08-14
Start of TD freezing (date when 5 cm (for LG), 15 cm (PLAT A and B) reaches 0°C for first time in autumn)	2016- 09-15	2017- 09-08	2018- 09-10	2016- 09-08	2017- 09-06	2018- 09-09	2016- 09-07	2017- 09-06	2018- 09-07
Date of complete freeze	2016- 10-08	2017- 09-19	2018- 09-19	2016- 09-15	2017- 09-08	2018- 09-10	2016- 09-15	2017- 09-09	2018- 09-10